The Role of mRNA Turnover in Ageing of *Caenorhabditis Elegans*

—

Novel Tools for Microscopic 3D Imaging

By

Matthias Rieckher

A Thesis submitted for the Degree of

Doctor of Philosophy

Πανεπιστημιο Κρητης
University of Crete

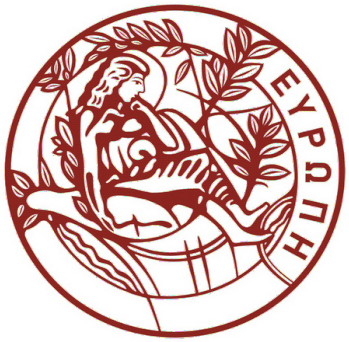

Heraklion • Greece

Department of Biology,
University of Crete

June, 2013

...for my parents.

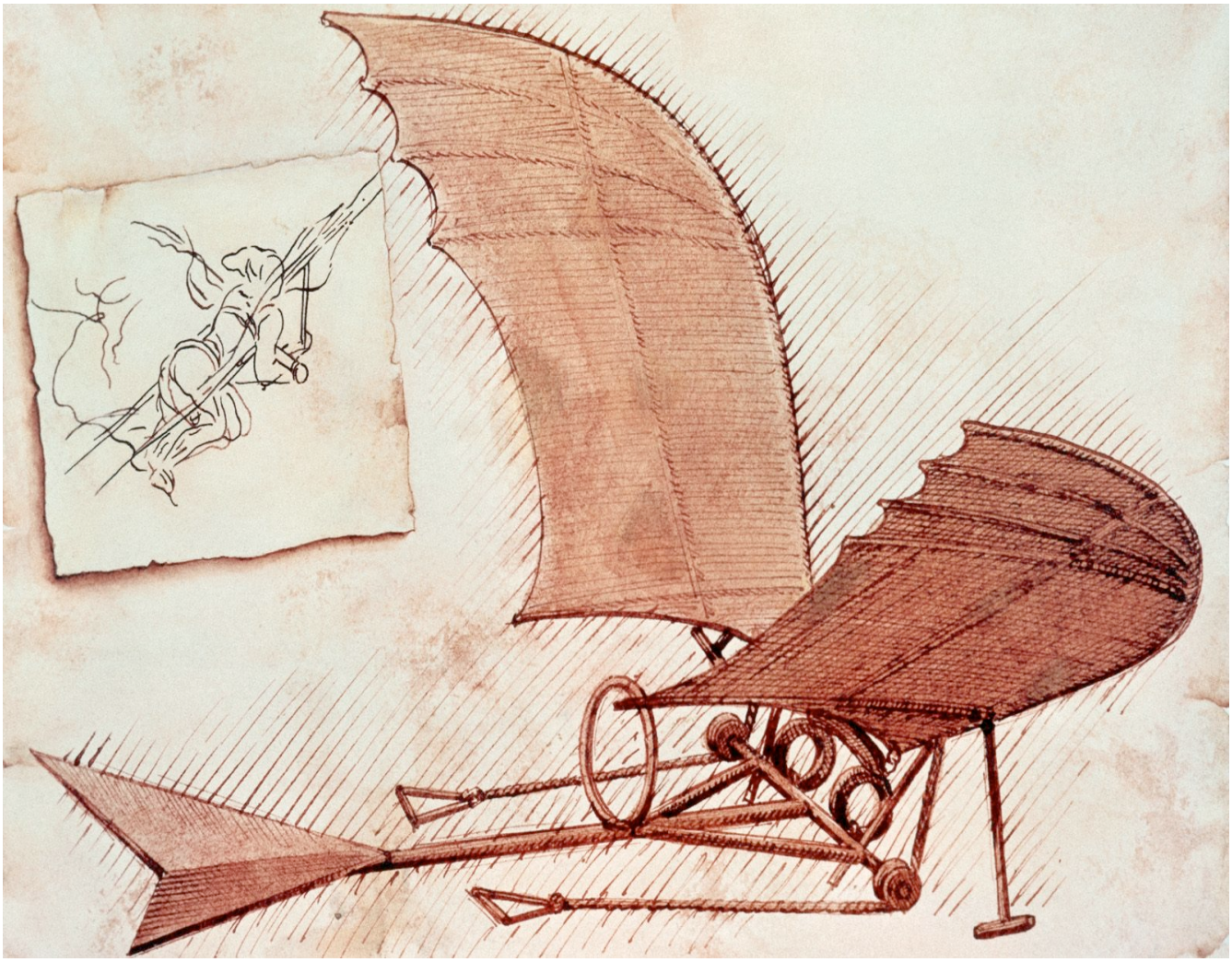

The ornithopter (1485),
Leonardo da Vinci

"The knowledge of all things is possible."
- Leonardo da Vinci

Acknowledgements

Firstly, I thank my supervisor Nektarios Tavernarakis for hosting me in his lab, for his guidance, patience, constant enthusiasm for advice, and support. It was specifically his groundbreaking work on neurodegeneration in C. elegans and his reputation that attracted me to his lab in Crete. His style as advisor, lab manager and skilled author is exemplary and will forever influence my career as a scientist. Further, I thank my collaborator, advisor and friend Jorge Ripoll for the unexpected possibility to explore the interdisciplinary field of 3D imaging of biological samples. Jorge's practical support was specifically important for me, and his highly motivated and passionate way of scientific work left a permanent encouraging impression on me.

My gratitude goes to my three-member committee, who next to Nektarios, are Aristides Eliopoulos and Xristos Delidakis. Both supplied me with extremely valuable and influential advice for my work. Further, I thank my seven-member committee, completed by Kriton Kalantidis, George Garinis, Domna Karagogeos and Tassos Economou for evaluating my work critically and giving advice for my future career.

The members and friends of the Tavernarakis lab I want to thank for their constant support, scientific exchange and the exceptionally positive collegial atmosphere. I specifically highlight the personal and professional support of Maria Markaki who, at all times, generously provided help and advice. I thank Angela Pasparaki, heart and soul of the daily life in the lab, a source of reliability and constant support. Thanks to Nikos Kourtis, Daphne Bazopoulou, Kostas Palikaras, Markella Katidou, Chrysa Samara, Giannis Voglis and Kostoula Troulinaki for joining the journey towards the PhD. I wish them all the best for their future career. Thank you Artemis Andreou, Evgenia Megalou, Vassiliki Nikoletopoulou, Eirini Lionaki, Marta Artal-Sanz and Manos Kyriakakis for passing on their experience, knowledge and support. Finally, I wish courage to the new graduate students in the lab, Andrea Princz, Dionysia Petratou, Ioanna Daskalaki and Nikos Charmpilas, and all the best on their way to success in the PhD. Also I thank Giannis Zacharakis and Athanasios Zacharopoulos for ongoing collaboration.

I am dearly grateful to my friends, who were with me over the years here in Crete, for lots of fun times and relaxing hours at and outside work. Schmutzi, who has constantly verschmutzt das ganze Haus and her sons, the little monsters EDC-3, DCAP-1, DCAP-2, HSF-1 and SKN-1 (R.I.P.), for making my life more colorful during the weekends. Gogo for many conversations, Nikos for big games on the pitch and at Yedi Kule, Vathsa and Joe for relaxed days at the beach, Rhiannon for all the cakes, Annette and Clemens for their heartwarming and parental care. Thanks to my friends in Germany, Tobi, Kristel, Matze, Tati, Uli, Kerstin, Pete und Holger for supportively staying in touch over the years.

My loving gratitude goes to Rena. Her serene support and amorous care are beyond words. I express my straightest gratitude to my family for their continuous mental and practical support. It is needless to say that the adventure of Master and PhD studies away from home, at times, is a difficult task. I thank my sister Andrea, her husband Tilman, my nephew Joshua and my niece Anika for their interest in my work, fun times in Crete, and during holidays back home. The same thanks go to my brother Frederik and his fiancée Morgaine. Their Cretan cats will mess up their flat in Germany for a long time to come. Especially I thank my parents, Lieselotte and Ulrich, who were regularly visiting me in Crete and supporting me emotionally through the unavoidably appearing tough times. Being adventurous travellers, they now know each and every corner in Crete, a place that I will always feel tied to and call my second home, wherever the road may lead.

Summary

Alterations of general or specific mRNA levels are a universal manifestation of the ageing process (Cookson, 2011). During their existence, mRNAs are constantly decorated by dynamically changing factors, which form messenger ribonucleoprotein (mRNP) complexes and determine the fate of an mRNA. Mechanisms that control mRNA turnover in the cytoplasm have been described in great detail but whether they might be involved in the regulation of ageing is unknown (Anderson and Kedersha, 2009; Decker and Parker, 2012). Bulk mRNA decay in eukaryotes is initiated by irreversible shortening of the poly(A)-tail, subsequent decapping and final 5' to 3' degradation (Houseley and Tollervey, 2009). We present compelling evidence that EDC-3, a highly conserved modulator of decapping, is a novel determinant of ageing in *C. elegans*. Decapping has been shown to regulate protein synthesis by competing with the mechanism of translation initiation. Congruently, we find that EDC-3 regulates protein synthesis and lifespan in interaction with the previously described translation initiation factor IFE-2, an isoform of the human eIF4E, which has a conserved role in the control of ageing. We demonstrate that EDC-3 and IFE-2 mediated regulation of *C. elegans* lifespan happens specifically in neuronal tissue and governs neural integrity. Further, we show that loss of EDC-3 protects from oxidative and heat induced stress and that lifespan extension depends on the activity of Nrf-like xenobiotic-response factor SKN-1 and heat shock response factor HSF-1. Also, longevity upon loss of EDC-3 triggers a ROS induced hormesis response that depends on SKN-1 activity.

Most mRNPs accumulate in distinct cellular foci termed processing bodies (P-bodies) or stress granules, which store mRNAs stalled in modes of degradation or translation initiation (Sheth and Parker, 2003, reviewed in Decker and Parker, 2012; Franks and Lykke-Andersen, 2008). Decapping factors, including EDC-3, are part of P-bodies, while IFE-2 localizes to stress granules in *C. elegans*. We establish an increased formation of P-bodies and stress granules and their co-localization upon specific stress insults and during age in the nematode, thereby defining them as biomarkers of ageing. It is unknown, whether mRNP granule formation is cause or consequence of mRNA decay and stress response (Eulalio et al., 2007). We demonstrate, that loss of SKN-1 contributes to an increased formation of P-bodies upon oxidative stress. Curiously, down-regulation of HSF-1 prevents P-body assembly specifically upon heat stress and causes age-related granulation of IFE-2. These results implicate that mRNP aggregation is a transcriptionally controlled process that contributes to maintenance of cellular stress response and ageing.

Unexpectedly, we find that HSF-1 suppresses transcription, stability and nuclear granulation of IFE-2 during ageing. These granules co-localize with components of P-bodies at the nuclear envelope, which also have been shown to be involved in transcription regulation in the nucleus (summarized in Reines, 2012). Excitingly, we observe decreased localization of IFE-2 in the nucleus, upon depletion of EDC-3. Our findings suggest that HSF-1 modulates IFE-2 function and localization during ageing, and that IFE-2 also serves as nuclear mRNP export factor in *C. elegans*. Thus, IFE-2 likely mediates the effects of the heat stress response on both mRNA translation and degradation to influence ageing.

Contents

Introduction

The ageing model *Caenorhabditis elegans*

General facts about the model organism *C. elegans*

Simple model organisms are becoming increasingly important for investigating principal biochemical and molecular mechanisms during development. *Caenorhabditis elegans* (*C. elegans*) has been instrumental in deciphering the molecular underpinnings of senescent decline during ageing (Olsen, 2006). *C. elegans* possesses relatively simple anatomy. The total number of cells of the animal is 959, including 302 neurons that form a simple nervous system. The cell lineage in development of the nematode is fully deciphered and a complete lineage tree is available (see http://www.wormatlas.org/, Sulston et al., 1983). During development 131 cells undergo programmed cell death (Ellis, 1986). This makes *C. elegans* a powerful tool for investigating developmental biology (Bargmann and Avery, 1995).

C. elegans goes through a short life cycle and likewise, has a short mean life span. The nematode develops from the fertilized egg to a self-fertilizing adult hermaphrodite within 3.5 days by undergoing four larval stages (L1 to L4). Due to food starvation or harsh environmental conditions the developing larva can enter a so-called, dauer stage before completing the L1 stage, which increases the mean life span for more than 5 months. Favorable food conditions allow the animal to reenter the normal life cycle as an L4 larva. After entering the adult stage an approximately three day reproductive period follows, during which the animal lays about 300 eggs. *C. elegans* lives around 20 days, of which the last two weeks are characterized by a decline in locomotion, food pumping and recognizable tissue degeneration, revealing typical symptoms of ageing (Collins et al., 2008).

Another important advantage of the nematode is its transparency, which makes microscopy far easier, permitting every cell division throughout development to be tracked. The simple nervous system is well documented, all neurons are mapped and an almost complete wiring diagram has been created (see http://www.wormatlas.org/, Hall and Russell, 1991). Specific behaviors, such as locomotion, chemo- or thermotaxis, as well as learning and memory, can be experimentally associated with the relevant neuron(s) (Mori, 1999). The detailed characterization of its nervous system renders *C. elegans* particularly suited for the study of neurodegeneration and ageing (Murakami, 2007). A low percentage of male nematodes (about 0.1 % of the progeny) is generated by hermaphrodites during self fertilization. These males enable genetic crosses that allow easy construction of double or multiple mutants (Riddle et al., 1997).

Particularly advantageous is the easy maintenance in the laboratory. *C. elegans* feeds on bacteria (usually *Escherichia coli* strain OP50), which are grown either on solid agar plates or in liquid culture medium, and grows best at a temperature of 20°C (Brenner, 1974). The culturing temperature affects development timing: *C. elegans* grows about 30% slower at 16°C compared to 20°C, making it convenient to time experimental procedures. The nematode can be cultured on large scale.

The *C. elegans* genome has been fully sequenced and annotated (Waterston and Sulston, 1995). Physical maps of the genome based on the use of cosmids and yeast artificial chromosomes (YACs) have been created (Coulson et al., 1991). The *C. elegans* genome is organized in 5 autosomes plus the sex chromosome X (sequence database: http://www.wormbase.org/). Approximately 20.000 open reading frames (ORFs) for the

nematode have been predicted (Blumenthal et al., 2002). Additionally, detailed protein interaction networks have been modeled (Walhout et al., 2000). The availability of fully charted genomes allows the implementation of large-scale, genome-wide genetic and molecular methodologies such as double stranded RNA mediated interference (dsRNAi) (Mello and Conte, 2004). In *C. elegans* high-throughput RNAi screens against all 20.000 ORFs have been published (Simmer et al., 2003). High-throughput screens have been proven advantageous to identify large numbers of genes implicated in the control of ageing (Hertweck et al., 2003). The use of dsRNAi in the nervous system of the nematode has been less successful so far, but can be offset by the use of special hypersensitive mutants or the introduction of double-stranded hairpin RNAs (dshRNAs) through microinjection (Schmitz et al., 2007; Tavernarakis et al., 2000).

C. elegans is genetically malleable. The most straightforward method of creating mutants is random mutagenesis through the use of the chemical Ethyl methanesulfonate (EMS). Mutants for almost every gene are available or can be ordered. Animals carrying multiple mutations can be constructed and efficient genetic mapping is possible, by utilizing precise single nucleotide polymorphism (SNP) maps (Jakubowski and Kornfeld, 1999). In *C. elegans*, transgenic animals can be obtained by microinjection of engineered DNA samples into the gonad, where they generate inherited extrachromosomal arrays. This extrachromosomal array can further be integrated and stabilized in the genome through mutagenesis-induced integration, which we and others have described in detail (Rieckher et al., 2009). In conclusion *C. elegans* is an exceptionally powerful and convenient model organism for investigating diverse biological phenomena including development and ageing.

Ageing studies in *C. elegans*

C. elegans is a well-applied model to study the phenotypical changes during ageing, such as tissue-decline, rapid development of neurodegenerative diseases, decrease in learning and memory or reduction in stress-resistance, and the underlying genetic mechanisms (Collins et al., 2008). Ageing-associated pathways in *C. elegans* can be identified through measuring the lifespan of genetically modified animals, application of chemical compounds or alterations of environmental conditions (Olsen, 2006). Various molecular pathways were discovered to influence ageing, including the insulin-like/IGF-1 pathway, TOR signaling in dietary restriction, the AMP kinase driven catabolic pathways, sirtuins, the inhibition of respiration, global protein turnover and telomere shortening (Antebi, 2007; Kenyon, 2010; Tavernarakis, 2008).

The various ageing-related mechanisms studied so far intermingle and involve the activation of transcription factors, which in turn activate or suppress diverse genes that orchestrate in regulating stress response and ageing. The most common transcription factors, which are well conserved across species, are the FOXO transcription factor DAF-16, the Nrf-like xenobiotic-response factor SKN-1, which mainly regulates oxidative stress response, the heat shock response factor HSF-1 and the hypoxia-inducible factor HIF-1 (An and Blackwell, 2003; Hsu et al., 2003; Lin, 1997; Zhang et al., 2009). The genetic pathways controlled by those mechanisms coordinate and interact in an intricate network and converge on the regulation of stress response and ageing (Narasimhan et al., 2009). Interestingly, exposure to mild stress leads to a somewhat reduced activation of the stress response network, which prepares organisms to deal with stronger stress insults and age-related stress accumulation, which results in longevity. This phenomenon is called hormesis and can be triggered upon mild heat or oxidative insults (Gems and Partridge, 2008; Ristow and Schmeisser, 2011).

Neuronal ageing in *C. elegans*

Although a lot of knowledge has been gained about the role of neurodegenerative

diseases in ageing, also through studies in *C. elegans*, relatively little is known about the genetic and cellular mechanisms that maintain neuronal integrity during normal ageing (Dimitriadi and Hart, 2010; Peng et al., 2011). Although neuronal loss in all metazoans is minimal during ageing, there are altered functional activations and various cellular changes, which in humans for example manifest in cognitive decline and dementia (Bishop and Yankner, 2010).

Especially because the neuronal system of the nematode is a simple one, phenotypical changes can be monitored in longitudinal studies in single cells and regarding the whole network (Peng et al., 2011). Morphological studies on mechanosensory neurons in aged animals reveal subtle phenotypes, including bubble-like lesions, blebbing and occasional branching. Progression of normal neuronal ageing seems to be regulated by DAF-16 signaling (Pan et al., 2011). The spontaneous age-related neurite branching is also correlated with the activity of Jun kinase signaling, which also regulates *C. elegans* lifespan (Tank et al., 2011). Both, HSF-1 and DAF-16 seem to regulate neurite sprouting and synapse deterioration in the ageing neuronal network. Locomotory healthspan seems to correlate with synaptic integrity (Toth et al., 2012).

Several *C. elegans* neurons have been implicated in the control of lifespan (Jeong et al., 2012). Animals with defective sensory cilia have impaired sensory perception but are long lived, and extended studies implicate the gustatory and olfactory system in the control of ageing (Alcedo and Kenyon, 2004; Kenyon and Apfeld, 1999). A pair of sensory neurons in the head, the ASIs, senses the nutritional environment. Dietary restriction activates SKN-1 and downstream-activated genes are transcribed to signal other tissues in the animal to increase metabolic activity, involving hormonal signals in the regulation of dietary restriction mediated ageing (Bishop and Guarente, 2007). The AFD thermosensory neurons regulate nematode lifespan through sterol endocrine signaling at high temperatures, which depends on the activation of HSF-1 (Lee and Kenyon, 2009).
Altogether, there seem to be exciting parallels between the complex mammalian brain and the simple neuronal network of *C. elegans* in response to ageing, which increases the impact of findings on neuron-specific regulation of ageing.

Protein synthesis and the control of ageing

A well-studied field in ageing concerns the decline of protein synthesis and protein degradation during ageing. Intriguingly, normal ageing is accompanied by irreversible modifications on proteins, such as oxidation through oxygen free radicals and increased glycation, which also decreases protein functionality (Hipkiss, 2008). Deamidation, racemization, isomerization and various others cause other protein modifications. These age-related defaults go along with an increased decline in protein turnover, proper folding and cellular maintenance mechanisms (Rattan, 2010). General protein synthesis rates decline during ageing, although the integrity of the translational machinery seems unaffected (Tavernarakis and Driscoll, 2002).

Various studies show a possible causative relationship between mRNA translation and ageing in *C. elegans*. The ribosomal-protein S6 kinase (S6K), which is controlled by the kinase target of rapamycin (TOR) controls phosphorylation of the translation-initiation factor 4 binding proteins (eIF4E BPs). Those are inhibitors of translation, since they bind eIF4E and impair recruitment of the 40S ribosomal subunit to the 5'-cap structure (Tavernarakis, 2008). TOR-deficiency reduces the rate of translation and induces longevity in the nematode (Vellai et al., 2003). Global protein synthesis in animals depleted for translation initiation factors is also reduced. Further, several studies show that inhibition of S6K (RSKS-1) and depletion of either translation initiation factors eIF2β (IFTB-1), eIF4E (*C. elegans* isoform IFE-2) and eIF4G (IFG-1) significantly increases lifespan of *C.*

elegans. (Hansen et al., 2007; Pan et al., 2007; Syntichaki et al., 2007). Also, inhibiting 40S or 60S ribosomal subunits and interference with mitochondrial specific translation delays the ageing process (Chen et al., 2007; Hansen et al., 2007). Similar studies in yeast and Drosophila show that this effect might be conserved across species (Steffen et al., 2008; Zid et al., 2009). The lifespan regulation mediated by TOR and translation initiation pathways appear to be independent, but interface with insulin/IGF-1 signaling at different levels (Hansen et al., 2007; Tavernarakis, 2008).

A striking feature of animals lacking translation initiation factors is their robustly enhanced resistance to extrinsic and intrinsic stress, which concerns heat stress, chemicals or genetic manipulations that increase oxidative stress, starvation and UV light. Increased stress resistance points to enhanced activity of cellular maintenance and repair mechanisms, as seen in animals with lowered protein synthesis rates (Ma and Blenis, 2009). Together, these results push forward the hypothesis that lowering protein synthesis rates by translation inhibition might lower general cellular energy consumption, which results in higher energy availability for cellular maintenance and subsequently longevity (Hansen et al., 2007; Pan et al., 2007; Syntichaki and Tavernarakis, 2007; Tavernarakis, 2008).

Recently, a genome-wide RNAi screen in *C. elegans* revealed that depletion of translation initiation factors upregulates various genes involved in oxidative stress defense that are activate by the transcription factor SKN-1, but not DAF-16. Conversely, the lifespan extending effects depend on interplay of DAF-16 and SKN-1 (Wang et al., 2010). SKN-1 and its targets acting in detoxification might be activated because generally reduced levels of protein synthesis also lowers otherwise naturally acting antioxidants. The activation of DAF-16 possibly relates to its function in regulating metabolic rates: When *C. elegans* is deprived of nutrients, young larvae enter a diapause stage termed dauer, which are extremely longlived and have reduced metabolism that is tightly regulated by the insulin-signaling pathway and DAF-16. Interestingly, dauer larvae show reduced levels of eIF4G (Pan et al., 2007).

The multiple Biological Functions of mRNP Granules

The strong correlation of protein synthesis and ageing trigger the thought that pathway, which interface with translational control might regulate the ageing process. Based on this rationale, mechanisms that control transport, stability and degradation of mRNAs are possible targets of investigation. As many cellular molecules, mRNAs are subject to age-related changes and eventually cleared from the cell (Cookson, 2011). The overall levels of mRNA of an aged tissue differ compared to its young equivalent. This has been detected via RNA sequencing in examples including the mouse cerebral cortex and the human brain (Dillman et al., 2013; Kumar et al., 2013). Whether such changes in mRNA levels have a causative relationship of the ageing process has not been determined.

When studying mRNA related mechanisms, one has to be aware that mRNAs are never bare. From birth to final degradation, mRNAs are constantly coated with proteins. Nascent mRNAs are co-transcriptionally decorated with an array of RNA binding proteins (RNPs), which together form functional and dynamically changing messenger ribonucleoprotein (mRNP) complexes. The specific mRNP arrangement determines the present mechanistic step of the mRNA, which includes nuclear mRNA processing, export/transport, translation, editing, storage and final turnover. Depending on the status of the mRNP, its components are entirely exchanged.

A vast amount of literature describes research on the mRNP life cycle and a number of excellent reviews summarize the underlying intricate molecular mechanisms (Decker and Parker, 2012; Franks and Lykke-Andersen, 2008; Müller-McNicoll and Neugebauer, 2013). The best-portrayed mRNP granules are processing bodies (P-bodies) and stress granules, which form primarily in the cytoplasm. They have been studied mostly in yeast and mammalian cell culture, and their structure, components and functions are highly conserved across eukaryotes (Erickson and Lykke-Andersen, 2011). A deeper knowledge of P-bodies and SGs is relevant for the understanding of other, functionally related aggregates, such as the neuronal transport granules and the germline specific P granules (Updike and Strome, 2010; Zeitelhofer et al., 2008b). This introduction will focus on some main aspects and functions of mRNP granules, which in recent years have been described to be sites for mRNP storage, transport and turnover, processes that tightly interface with the regulation of protein synthesis, and that could very well play a role in the regulation of ageing.

P-bodies are nodes of mRNA decay mechanisms

P-bodies were first discovered as a novel cytoplasmic domain stained by the human autoantibody for the mRNA processing factor GW182 (Eystathioy et al., 2002). Since then some 400 peer-reviewed articles were published trying to decipher the function of this novel cytoplasmic structure. It soon turned out that P-bodies contain enzymes that act in various mRNP degradation pathways and could be sites mediating these processes (Ingelfinger et al., 2002; Lykke-Andersen, 2002; Sheth and Parker, 2003). When studying P-bodies it is therefore essential to familiarize with the various mechanisms that facilitate mRNA decay.

A number of mechanisms for mRNA degradation have been described, which includes deadenylation-dependent and -independent pathways, the endonuclease-mediated decay, mechanisms that are based on errors or specific signals within in the mRNA sequence, such as nonsense mediated decay (NMD), non-stop decay (NSD) and no-go decay (NGD), or AU-rich elements (ARE) mRNAs, and finally pathways that employ

small regulatory RNAs including micro RNA (miRNA), silencing RNA (siRNA), piwi-interacting RNAs (piRNAs) and repeat associated siRNAs (rasiRNAs). Most of those pathways intermingle by sharing components, especially the factors that mediate final exonucleolytic degradation of the mRNA. Further, components of all of the mentioned mRNA decay mechanisms have been addressed to act in or through P-bodies (Garneau et al., 2007). I will briefly summarize the deadenylation-dependent pathway, which is employed for bulk mRNA turnover, and its major path of decapping followed by mRNA degradation.

A newly synthesized mRNA includes two stability factors, which firstly have to be removed before degradation can occur: The 5' 7-methylguanosine cap and the 3' polyadenosine (polyA) tail. Those structures interact with the factors eIF4E and PABP, respectively, which protects mRNA from degradation and triggers translation initiation (Bernstein et al., 1989; Schwartz and Parker, 1999). Bulk mRNA degradation begins with the reversible procedure of poly-A tail shortening, a process known as deadenylation. Initially, the PABP-dependent ploy(A) nuclease Pan2/Pan3 trims the poly-A tail to a length of 60-80 nucleotides, which is observed both in yeast and mammals (Brown et al., 1996). Further deadenylation is taken over by a major deadenylase component that consist of the factors Ccr4/Pop2(Caf1)/Not, which is a nine subunit complex with two core deadenylases CCR4 and POP2 (or CAF1) (Yamashita et al., 2005). The poly(A)-specific ribonculease (PARN) has 5' cap-dependent deadenylase activity and is found in mammals, Xenopus laevis oocytes, plants and insects (Copeland and Wormington, 2001; Opyrchal et al., 2005; Wiederhold and Passmore, 2010).

The shortening of the poly-A tail irreversibly leads to degradation by either direct 3' to 5' degradation though the exosome or, more commonly, decapping and subsequent 5' to 3' degradation. In brief, the eukaryotic exosome is a remarkable complex that in its core is homologous to Escherichia coli RNPs polynucleotide phopshorylase (PNPase) and the RNAse II. The intricate structure of the exosome differentially associates with other factors that employ its mRNA degradation function for mRNA surveillance in the nucleus, or for the cytoplasmic NMD, NSD, ARE-mediated and bulk mRNA decay. For the latter, the exosome utilizes Ski2/Ski3/Ski8 complex and Ski7 proteins as cofactors (Houseley et al., 2006).

More commonly, following deadenylation, the decapping enzyme Dcp2 removes the 5'-cap of mRNAs in interaction with its coenzyme Dcp1. Dcp2 contains a functional pyrophophatase-related MutT domain, which is necessary and sufficient for decapping (Dunckley, 1999). Removal of the cap structure is followed by activation of the 5'-3' exoribonuclease Xrn1 and mRNA degradation (Beelman and Parker, 1995; Kenna et al., 1993; Larimer et al., 1992).

It appears that a large set of co-factors and modulators is required to facilitate decapping. This core set of decapping components forms a sophisticated network of direct interactions as experimentally shown by protein binding experiments and supported by co-immunoprecipitation and two hybrid analyses (Decker and Parker, 2012; Decker et al., 2007; Nissan et al., 2010). Two complexes emerge that assemble on mRNAs targeted for decapping: One consists of the Pat1 protein, the heptameric Sm-like complex Lsm1-7, and Xrn1 and assembles on the 3' end of deadenylated mRNAs (Tharun, 2009). The other component assembles in parallel or sequentially at the 5'-cap, and consists of interacting proteins Dcp1, Dcp2, Edc3 or Scd6, and Dhh1. At the 3'-end Pat1, and at the 5'-cap Edc3 appear to be important for complex assembly, as they modulate and interact with many components of the decapping machinery (Fromm et al., 2011; Pilkington and Parker, 2008; compare Figure 1). Once the two complexes assemble on the mRNA, mRNPs aggregate via the prion-like domain contained in of Lsm4, the Yjef-N domain, which is at the C-terminus of Edc3, or the amino-terminal domain of Pat1 to form microscopically visible cytoplasmic granules (Buchan et al.,

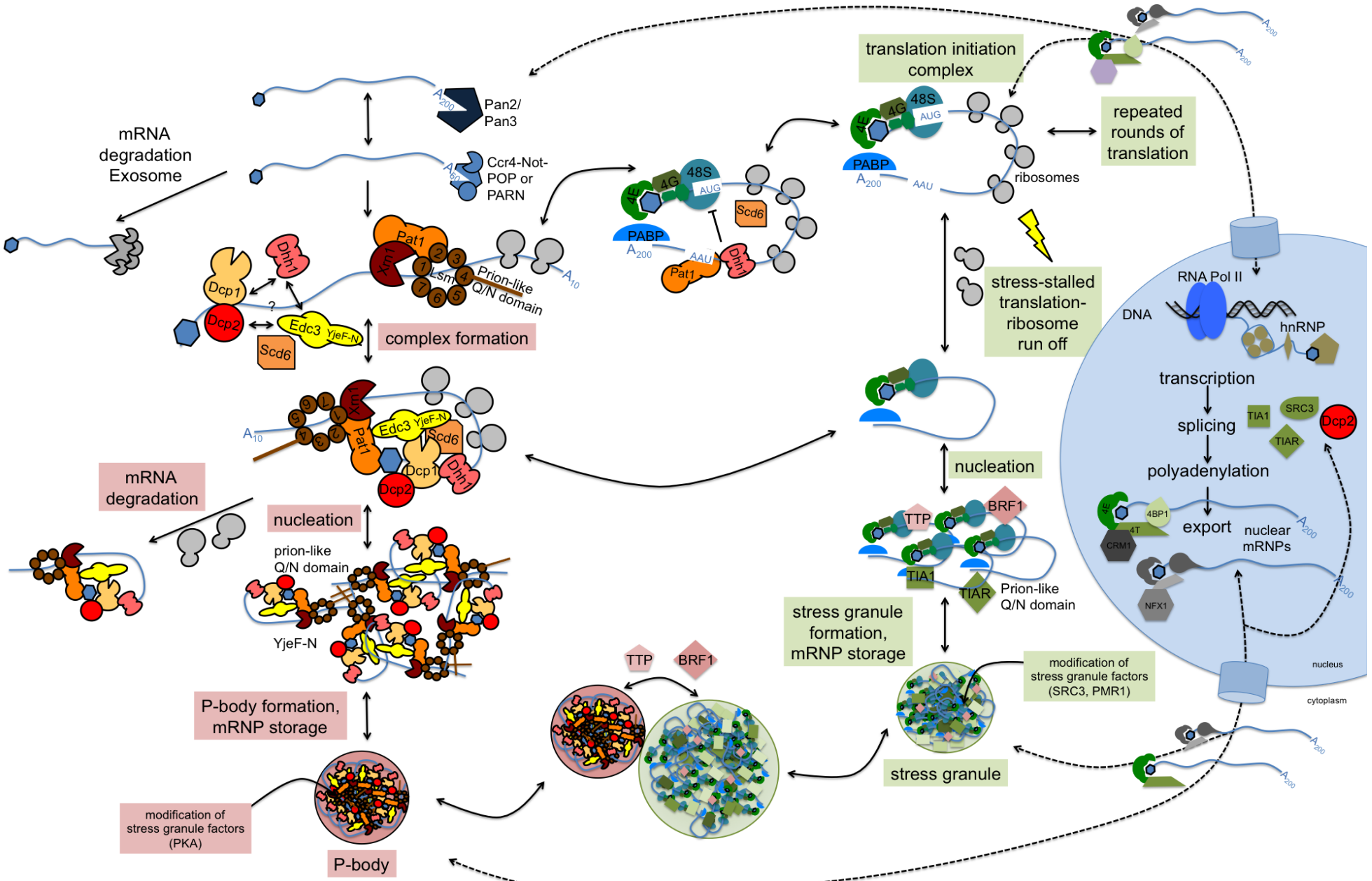
mRNA degradation Exosome
Pan2/ Pan3
Ccr4-Not- POP or PARN
Dcp1
Dcp2
Dhh1
Edc3
YjeF-N
Scd6
Xrn1
Pat1
Lsm
Prion-like Q/N domain
complex formation
translation initiation complex
48S
4G
4E
AUG
PABP
AAU
repeated rounds of translation
ribosomes
stress-stalled translation-ribosome run off
RNA Pol II
DNA
hnRNP
transcription
splicing
polyadenylation
export
nuclear mRNPs
TIA1
SRC3
TIAR
4BP1
4T
CRM1
NFX1
nucleus
cytoplasm
nucleation
BRF1
TTP
mRNA degradation
prion-like Q/N domain
YjeF-N
stress granule formation, mRNP storage
modification of stress granule factors (SRC3, PMR1)
stress granule
P-body formation, mRNP storage
modification of stress granule factors (PKA)
P-body

Figure 1: The mRNP cycle from birth of an mRNA, over translation to degradation. When mRNAs are produced they co-transcriptionally associate with hnRNPs to undergo transcription, splicing and polyadenylation. In the process they are being redecorated with factors assigning them for export into the cytoplasm. Here, mRNPs can associate with factors handing them over to mRNP degradation, translation or storage into P-bodies or stress granules. Packaging of mRNPs into granules requires run-off of polysomes of the mRNA. In both cases, nucleation is achieved via protein-protein interaction mediated by specific sequences, including prion-like domains. Finally, mRNPs are packed into P-bodies or stress granules, and various packed proteins can be modified within those structures. Both granules can dock and interact by exchanging factors, re-assigning them for storage or degradation. Some P-body or stress granule factors have been shown to re-locate to the nucleus, where they are possibly involved in processes of splicing or mRNP export. The representative model has been modified from various literature resources (Anderson and Kedersha, 2008; Decker and Parker, 2012; Franks and Lykke-Andersen, 2008; Kedersha and Anderson, 2002; Müller-McNicoll and Neugebauer, 2013).

2008; Decker et al., 2007; Ling et al., 2008, Figure 1).

Edc3 is a central module of P-bodies

Edc3 (EDC-3 in *C. elegans*) is a central activator of 5' assembling decapping complex and was firstly identified in yeast as stimulator of mRNA degradation (Kshirsagar and Parker, 2004). Its importance in decapping, intriguing structural composition and contribution to P-body formation triggered a great deal of interest. Structural identification and extensive interaction studies revealed that Edc3 belongs to the Lsm16 family of proteins and consists of at least three functional domains that are highly conserved across species including yeast, *Drosophila*, *C. elegans* and humans (Ling et al., 2008; Tritschler et al., 2010). The N-terminal Lsm domain and a directly connected linker region bind Dcp1:Dcp2 in Drosophila and yeast (Tritschler et al., 2007). More specifically, a small N-terminal domain in Dcp2, located closely to the catalytic Nudix domain, is responsible for Edc3 binding and degradation of specific mRNA targets in yeast (Harigaya et al., 2010).

The interacting region of Dcp2 in humans was assigned to be a short helical leucine-rich motif (HLM). Edc3 competes with the structurally related Scd6 to promote Dcp1:Dcp2 mediated decapping, presumably by preventing the complex to change conformation. Further, the HLMs in Edc3 and Scd6 are important for Dcp1:Dcp2 recruitment to P-bodies (Fromm et al., 2011). Two-hybrid assays revealed that an interaction between Dcp1 and Edc3 is promoted by the additional presence of Ge-1 in human cells, homologue of yeast Edc4, which is structurally related to Edc3 and mainly becomes active in ARE-mediated decay (Bloch et al., 2011; Fenger-Grøn et al., 2005). A central FDF domain in Edc3 binds RNA helicases such as Dhh1/DDX6 in yeast and humans, while the C-terminal YjeF-N domain is required for self-association and promotes P-body assembly in yeast (Decker et al., 2007; Ling et al., 2008; Tritschler et al., 2010; compare Edc3 in Figure1).

Edc3 might be a target of the insulin-signaling pathway in humans. The phosphatidylinositol 3-kinase/AKT pathway phosphorylates Edc3 at Ser-161 and subsequently recruits 14-3-3-binding protein in muscle cells. This causes changes in Edc3 interaction with PABP, decrease in P-body number and impairs the miRNA mechanism (Larance et al., 2010). Edc3 specifically mediates degradation of mRNAs RPS28B and the intron-containing YRA1 pre-mRNA in yeast. The latter encodes for the export factor Yra1p and autoregulates its own expression. Sequences within YRA1 inhibit pre-mRNA splicing and promote export into the cytoplasm, where degradation occurs in an Edc3 dependent manner (Dong et al., 2007). Other sequence modules within YRA1 pre-mRNA suppress its translation by recruiting NMD and the Dcp1:Dcp2 decapping complex (Dong et al., 2010). The well-defined and conserved structural complexity, the various intriguing functional implications including its central role in assembly of the mRNA decapping complex and P-bodies make Edc3 and its interactors Dcp1 and Dcp2 promising target of our study.

P-body assembly and their possible biological functions

P-bodies mainly consist of translationally silent mRNPs, which dynamically assemble and disassemble. This conclusion derives from several examples: (I) Trapping mRNAs in polysomes, through RNAse A or cycloheximide treatment, leads to a decrease in P-body formation (Eulalio et al., 2007; Teixeira et al., 2005). When treated with puromycin, which promotes release of mRNA from polysomes, P-body size increases (Eulalio et al., 2007). (II) The decapping machinery is in competition with the translation initiation complex for the mRNA cap (Schwartz and Parker, 1999; 2000). More specifically, binding of decapping activators Dhh1, Pat1 and Scd6 to mRNAs assigned for translation inhibits the 48S complex and subsequently arrests translation (Nissan et al., 2010; Swisher and Parker, 2010). Binding of those factors might stall translation and gives time for full recruitment of the decapping complex. Alternatively, this process might follow a program that requires ordered assembly of the decapping machinery (Decker and Parker, 2012). Consequently, no translation factors are found in P-bodies, with the exception of eIF4E and its transporter eIF4E-T (ANDREI et al., 2005).

(III) Depletion of factors that promote mRNA decay, such as Dcp1, Dcp2 and Xrn1, increase accumulation of mRNPs in P-bodies (Cougot et al., 2004; Sheth and Parker, 2003). (IV) Stress induction through, e.g. ultraviolet (UV) light, osmostic stress, glucose deprivation or arsenite treatment can significantly induce P-body formation (Kedersha et al., 2005; Teixeira et al., 2005). Further, P-bodies are known to form upon viral infection and depending on the case might promote viral life cycle and might be involved in host defense (Beckham and Parker, 2008a). (V) Genome wide RNAi screens determined that P-bodies contain a possibly large number of factors unrelated to mRNA decay, which covers translational, protein metabolism and stability, signaling and transcription (Decker and Parker, 2012; Ohn et al., 2008; Sun et al., 2011). These and other observations have led to the construction of a well-accepted model of P-body assembly, which is presented in Figure 1, based on several excellent reviews and perspectives (Balagopal and Parker, 2009; Buchan and Parker, 2009; Decker and Parker, 2012; Franks and Lykke-Andersen, 2008).

Finally, it is important to note, that several findings indicate that microscopically visible P-bodies might be the consequence rather then the cause of mRNP degradation. Their depletion in yeast or mammalian cells does not inhibit mRNA decay, translational repression, miRNA mediated mRNA decay or mRNA stability during stress insults (Buchan et al., 2008; Decker et al., 2007; Eulalio et al., 2007). These results indicate redundancy of mRNP degradation mechanisms, and also that P-bodies might not be the center of mRNA decay. P-bodies could rather serve as local area of concentration for factors that are required for mRNA decay or, in the case of stress granules, for translation initiation (Decker and Parker, 2012). Most importantly, next to their possible role in mRNA degradation, P-bodies are sites of mRNP storage. They require mRNAs for assembly and their size increases upon stress insult, which leads to accumulation of stalled mRNPs (Teixeira et al., 2005).

Intriguingly, recent research in yeast suggests that the cAMP dependent protein kinase (PKA) specifically regulates P-body assembly and size by directly phosphorylating Pat1, which like Edc3, is a scaffolding center for forming the mRNP degradation complex. Further, P-bodies are required for long-term survival of yeast in quiescent state (Ramachandran et al., 2011; Shah et al., 2012; Tudisca et al., 2010). These results indicate a direct regulation of P-body formation and underline a potential biological function of those structures, which goes beyond their proposed roles in mRNP degradation and storage.

Composition and formation of stress granules

Stress granules show several parallels to P-bodies in composition, induction and possible function. Both have been observed to appear and co-localize in various species, including yeast, humans, nematodes and the fruitfly (Anderson and Kedersha, 2008; Farny et al., 2009; Jud et al., 2008). Both structures contain translationally stalled mRNAs derived from diassembled polysomes and they share few components, including Xrn1, eIF4E, and the miRNA regulating Ago2 (Kedersha et al., 2005; Leung et al., 2006). Further, stress granules and P-bodies can be simultaneously induced through various stressors (Kedersha et al., 2005; Wilczynska et al., 2005). However, they are strikingly different in many aspects.

Stress granule formation was known before discovery of P-bodies, and shown through accumulation of PABP, TIA-1, TIAR and the upon arsenite-induced stress phosphorylation of eIF2α (Kedersha et al., 2000; 1999). While P-bodies form in unstressed condition and predominantly contain components of mRNA decay, it became apparent that stress granules consist of mRNAs with full length poly(A) tail and of translation initiation factors, which include the 40S ribosomal subunits, eIF4E, eIF4G, eIF4A, eIF4B, PABP, eIF3, eIF2α, and translational inhibitors TIA-1 and TIA-1 related protein (TIAR) (Anderson and Kedersha, 2008, compare Figure 1). This composition can vary significantly depending on species and type of stress insult responsible for formation. In yeast, heat shock recruits eIF3 to stress granules, while glucose-deprivation does not (Buchan et al., 2008; Grousl et al., 2009). Also, in *C. elegans*, stress granules form differentially, depending on the stress insult (Jud et al., 2008).

Generally, stress granules form when translation initiation is impaired, not only upon stress insult, but also due to addition of drugs that block translation initiation, such as the marine sponge product pateamine A (PatA), upon poliovirus infection or puromycin-induced dissociation of mRNA from ribosomes (Dang et al., 2006; Kedersha et al., 2000; Mazroui et al., 2006). Overexpression of suppressors of translation initiation can also induce stress granules, while drug-mediated trapping of mRNA at polysomes via cycloheximide results in their loss (Buchan et al., 2008; Kedersha et al., 2005; Wilczynska et al., 2005). As determined through various genome wide screens and depending on experimental conditions, stress granules can be influenced by and harbor a large array of protein components including RNA helicases, translation and stability regulators, and factors involved in cell signaling (Anderson and Kedersha, 2008; Ohn et al., 2008; Sun et al., 2011).

Several factors have been shown to influence stress granule aggregation: (I) posttranslational modifications of mRNPs, (II) protein-protein interactions of RNPs, (III) possibly the microtubule network and (IV) viral induction (Buchan and Parker, 2009; White and Lloyd, 2012). First, phosphorylation of eiF2α was the first evidence for an involvement of posttranslational modifications. Loss of the phosphorylation site in eIF2α resulted in decreased stress granule formation upon arsenite treatment (Anderson and Kedersha, 2006; Kedersha et al., 1999). The deacetylase HDAC6 and its ubiquitin binding domain is important for stress granule assembly, which seem generally strongly positive for ubiquitin. HDAC6 also interacts with tubulin and HSP90 and might coordinate ubiquitination and transport of stress granule components (Kwon et al., 2007). Also, O-Glc-NAc and arginine methylation significantly contribute to stress granule assembly (Goulet et al., 2008; Ohn et al., 2008). Second, protein-protein interactions in stress granules are mostly determined by Q/N-rich structures, leading to prion-like aggregation of TIA-1, which intriguingly is inhibited by molecular chaperone HSP70 (Gilks et al., 2004). Third, drugs that depolarize microtubules, such as nocodazole, or genetic interruption of dynein and kinesin prevent stress granule and also P-body formation (Fujimura et al., 2009; Loschi et al., 2009). Fourth, similar to their interaction with

P-bodies, viral infection can employ stress granules for reproduction, in this case by taking over protein production and arresting the host translational machinery (Montero et al., 2008). It is still under debate whether stress granules might act protective against viral attacks (Beckham and Parker, 2008b; White and Lloyd, 2012).

Formation of stress granules depends on the type of stress insult and has been categorized into several reversible stages (Anderson and Kedersha, 2002; 2008, compare Figure 1). In brief, stress granule formation begins with stalled translation initiation as transcripts are converted into 48S mRNPs and their ribosomes dissociate (Kedersha et al., 1999). The next stage is a primary aggregation, which can be initiated by numerous proteins, including the prion-like proteins TIA-1 and TIAR, and they always nucleate around non-polysomal 48S mRNPs (Dang et al., 2006). Other important stress granule nucleators are TTP and BRF1, which bind AU-rich sequence in the 3'UTR of mRNAs, therefore promoting ARE-mediated decay (Sanduja et al., 2010). Nucleation then triggers recruitment of eIF3, eIF4F, PABP-1 and small ribosomal subunits, which is followed by protein-protein interaction-driven aggregation into microscopically visible stress granules (Anderson and Kedersha, 2008). In the next step, specific stress induced factors might co-localize to stress granules, which lack mRNA binding ability, but modify the activity of translational suppressors. This has been shown for various examples, including the steroid receptor coactivator-3 (SRC-3), which inhibits cytokine translation during immune response, by recruiting TIA-1 and TIAR to stress granules (Yu et al., 2007). Also, the mRNA endonuclease PMR1 associates with and might modify TIA-1 to regulate mRNA localization to stress granules (Yang et al., 2006).

The final step involves an intricate sorting system for mRNPs, which can rapidly shuttle in and out of stress granules, as shown for the examples of FRAP assays on GFP tagged TIA-1 or PABP (Kedersha et al., 2000). Transcripts can be reinitiated and associated with polysomes for translation, stored or redirected to P-bodies for storage or final degradation (Anderson and Kedersha, 2006; Kedersha and Anderson, 2002; Kedersha et al., 2005, compare Figure 1). Curiously, TTP and BRF1 can be actively sorted into stress granules by phosphorylation through MAKAP kinase-2 (MK-2) and their overexpression stabilizes interaction between P-bodies and stress granules (Kedersha et al., 2005; Stoecklin et al., 2004). These and other results promote the view that some mRNPs might transit through stress granules before being localized to P-bodies and that those two structures are interlinked in cellular stress response management (Anderson and Kedersha, 2008; Kedersha et al., 2005).

Stress granules might directly regulate various stress responses

The function of stress granules is not clearly resolved. There seems no doubt that they promote translational repression, since their appearance correlates with decreased global protein synthesis. On the other hand, they are not required to suppress translation, as shown in numerous studies. In yeast, mutant strains lacking stress granules, translation is fully suppressed upon glucose deprivation, and in HeLa cells, suppression of translation initiation factors, such as eIF4E and eIF4G does not induce stress granule formation (Anderson and Kedersha, 2009; Buchan et al., 2008; Mokas et al., 2009). Also, they are not necessary to maintain stability of mRNAs upon stress insult (Buchan et al., 2008). Similar as it was suggested for P-bodies, stress granules might be sites that concentrate translation initiation factors and mRNAs locally, to trigger translation of specific proteins that form during stress response. Although direct evidence for this hypothesis is missing, some evidence exists that the appearance and disappearance of various cytoplasmic protein foci in yeast is directly controlled by the availability of specific metabolites (Narayanaswamy et al., 2009;

O'Connell et al., 2012).

An intriguing hypothesis that stress granules might repress translation during stress, is supported by findings related to heat shock response: while most mRNAs during heat stress target to stress granules, mRNAs for HSP70 and HSP90 are excluded and are kept in translational cycles (Anderson and Kedersha, 2002; Stöhr et al., 2006). Moreover, in mouse embryonic fibroblasts, the prion-like domain of TIA-1 sequesters HSP27, HSP40 and induces HSP70, which acts as a feedback regulator of prion-like structures (Gilks et al., 2004). HSP72, the majorly induced factor upon heat shock response in human cell lines, disassembles stress granules that form upon prolonged inhibition of the ubiquitin-dependent proteasome system (UPS) and promotes re-initialization of translation (Mazroui et al., 2007). The factors eIF4E and its transporter localize to P-bodies and form heat-induced stress granules in HeLa cells, which mainly assemble at the nuclear envelope (ANDREI et al., 2005; Suzuki et al., 2009). Treatment with HSP90 inhibitors geldanamycin and radicicol prevents P-body formation and lowers induction of those stress granules during heat stress (Matsumoto et al., 2011). Together, these results point to a co-function of stress granules and HSPs in maintaining translation processes during heat stress.

The fact that the translation initiation factor eIF4E (IFE-2 in *C. elegans*) localizes to both P-bodies and stress granules and that both structures interact and form upon stress accumulation make them intriguing targets of investigation for a possible involvement in regulation of stress response and ageing processes.

Neuronal Granules: Regulating local protein synthesis

The neuronal system is shaped and altered by sensory input, may it be the mammalian brain, in which trillions of synapses interconnect billions of nerve cells, or in the simple neuronal network of *C. elegans*, in which 302 neurons connect and communicate. It is the experience-dependent plasticity, which occurs at the level of dendrites and synapses that underlies the networks ability to adapt to environmental changes and store information (Hobert, 2003; Schratt, 2009). The molecular mechanisms underlying these changes are intricate gene expression programs that alter synapse structure and function, and one major contributor is the local control of mRNA translation in dendritic spines (Fortin et al., 2012).

RNA compartmentalization and local protein synthesis has been extensively studied in the past, and defects in mRNP localization have been linked to neurological disorders, such as the fragile X syndrome, or muscle atrophy (Dahm et al., 2007; Zalfa et al., 2006).

Nevertheless, media for mRNP transport in neurons are not well understood. As presented in the previous chapters, P-bodies and stress granules are localized areas of translational regulation, that employ various systems of mRNP degradation and stabilization and could therefore account for possible sites for control of local protein synthesis in neurons (Zeitelhofer et al., 2008b). A crucial control mechanism for post-transcriptional regulation of gene expression is the miRNA machinery, which has been shown to localize to P-bodies (Erickson and Lykke-Andersen, 2011). Various studies found numerous miRNAs to regulate synaptic plasticity in neurons (Edbauer et al., 2010; Impey et al., 2010; Kauppinen et al., 2009; Schratt, 2009; Schratt et al., 2006). For example, miRNA132 locally stimulates actin assembly, by inhibiting activator p250GAP and induces dendritic spine expansion, while miRNA138 inhibits a RhoA suppressor, which subsequently promotes actin depolymerization and spine collapse (Fortin et al., 2012). The miRNA134 co-localizes to granules with its target LimK1 to regulate actin filament dynamics and dendritic spine structure (Schratt et al., 2006). How could the miRNA machinery, and possibly other systems for translational repression reach their targets in neurons?

Several studies show that mRNP

transport along axons is mediated by granules (Hirokawa, 2006; Kiebler and Bassell, 2006): The first in vivo example is the human homologue of the Drosophila protein Staufen, a double-stranded RNA binding protein that shows dynamic movement when ectopically in hippocampal neurons (Köhrmann et al., 1999). Such transport granules lack translation initiation factors such as eIF4E and eIF4G and might suppress local protein synthesis in neurons (Krichevsky and Kosik, 2001). Injected tagged mRNA is transported in granules via the cytoskeleton in neurites of hippocampal neurons (Shan et al., 2003). Granule mediated transport of survival motor neuron protein 1 (SMN1), which is involved in spinal muscular atrophy, follows a similar mRNP transport system (Zhang et al., 2003). The zipcode-binding protein 1 (ZBP1) transports β-actin mRNA into developing neurites and suppresses its translation during transport, by employing mRNP transport particles (Dahm et al., 2007; Hüttelmaier et al., 2005).

More concrete evidence for the relationship between those neuronal transport granules and P-bodies comes from studies of cultured Drosophila neurons: Staufen-containing mRNP granules show co-localization with factors for the miRNA machinery (Xrn1), NMD (Upf1) and general mRNA turnover (Dcp1, Dcp2, Dhh1, Xrn1, Scd6 and Tra1). Those granules seem to interact with Drosophila FMRP, homologue of FMT1 in humans, which is involved in fragile X syndrome and negatively regulates dendritic growth. Therewith, P-bodies and neuronal granules might interact in transport of mRNPs and co-regulate dendritic development (Barbee et al., 2006). Similar findings come from studies in rat hippocampal neurons, in which P-body factors Xrn1, GW182, Dcp1 and specific mRNAs co-localize with ZBP1 and FMRP and move along axons (Cougot et al., 2008). Indeed, more detailed analysis of these processes in Drosophila neurons show that neuronal transport granules and P-bodies do not co-localize, but interact by docking, similar to processes observed between P-bodies and stress granules. When synapses are stimulated, P-bodies at dendrites disassemble, indicating that upon synapse activation, P-body aggregated mRNAs might be translated (Kedersha et al., 2005; Zeitelhofer et al., 2008a; 2008b). The neurotransmitter zinc seems to be involved in local protein synthesis in synapses: upon stimulation, zinc is released from neurotransmitters, causes disruption of polysomes and aggregation of Dcp1 protein in RNA-dependent manner (Blumenthal et al., 2009).

The docking events between neuronal transport granules and P-bodies observed in neurons and their disappearance upon neuronal stimulation raise the speculation of an active role of mRNP granules in the regulation of local protein synthesis at synapses. Little more is known about P-body functions in neurons and the effects of their abrogation on neuronal cells or networks are unknown.

P granules: Control of oogenesis and embryogenesis

The model organism *C. elegans* has been extensively employed to study germline-specific granules, termed Germ granules or P granules, which are non–membrane-bound, ribonucleoprotein (RNP) organelles. P granules are of largely unknown function and found in oocytes and early embryos in a wide variety of organisms. The term germ granule is synonymous with perinuclear structures in mouse and human germ cells. The general presence of germ granules across species and the fact that depletion of P granule specific factors is associated with germ line defects suggests that germ granules are key determinants of the identity and special properties of germ cells. P granules consist of a heterogeneous mixture of mRNAs and proteins. Most of the known germ granule proteins, and presently all of the known P granule components in *C. elegans*, are associated with mRNA metabolism, which involves germ granules in posttranscriptional regulation. Their possible functions have been extensively studied and reviewed, although many related processes remain mysterious (Rajyaguru and Parker,

2009; Updike and Strome, 2010; Voronina et al., 2011).

The localization of P granules during *C. elegans* oocyte development has been characterized in great detail (Figure 2): Oogenesis proceeds in a syncytium (cells that contain multiple nuclei in a shared cytoplasm), with a mitotic zone near the distal tip producing nuclei. In the early stages of meiosis those produce mRNA, which associate with P granules functioning as principal sites of export and sorting of mRNAs to suitable regulatory molecules. When oocytes form around nuclei, P granules that contain maternal mRNA dissociate from the nucleus and are seen uniformly throughout the cytoplasm of the forming oocyte (Sheth et al., 2010; Strome and Wood, 1982). Upon fertilization by stored sperm produced early in development, P granules relocate to the posterior pole of the embryo, and are segregated at the first cell division into the posterior daughter cell, called P1. This process repeats during the next three cell divisions, resulting in the asymmetric localization of P granules sequentially into the embryonic blastomeres called P2, P3 and P4. In following embryonic and postembryonic development, the descendants of the P4 blastomere divide symmetrically with all cells inheriting P granules; these descendants produce only germ cells (Rajyaguru and Parker, 2009; Strome and Wood, 1982). P granule segregation does not require spindle or cytoplasmic microtubules but depends on cytoskeletal functions and microfilaments (Strome and Wood, 1983).

Various factors are known to comprise P granules and structure, size and composition is changing during oocyte development and early embryogenesis. P granules contain a large number of mRNA in low level (Schisa et al., 2001). Some of those mRNAs encode for central determinants relevant in primordial germ cell development and embryonic patterning, including the *Drosophila* nanos homologous structures *nos-1* and *nos-2* (Subramaniam and Seydoux, 1999). P granules are composed of proteins essential to establish cellular asymmetries and embryonic polarity, such as the PAR proteins (Boyd et al.,

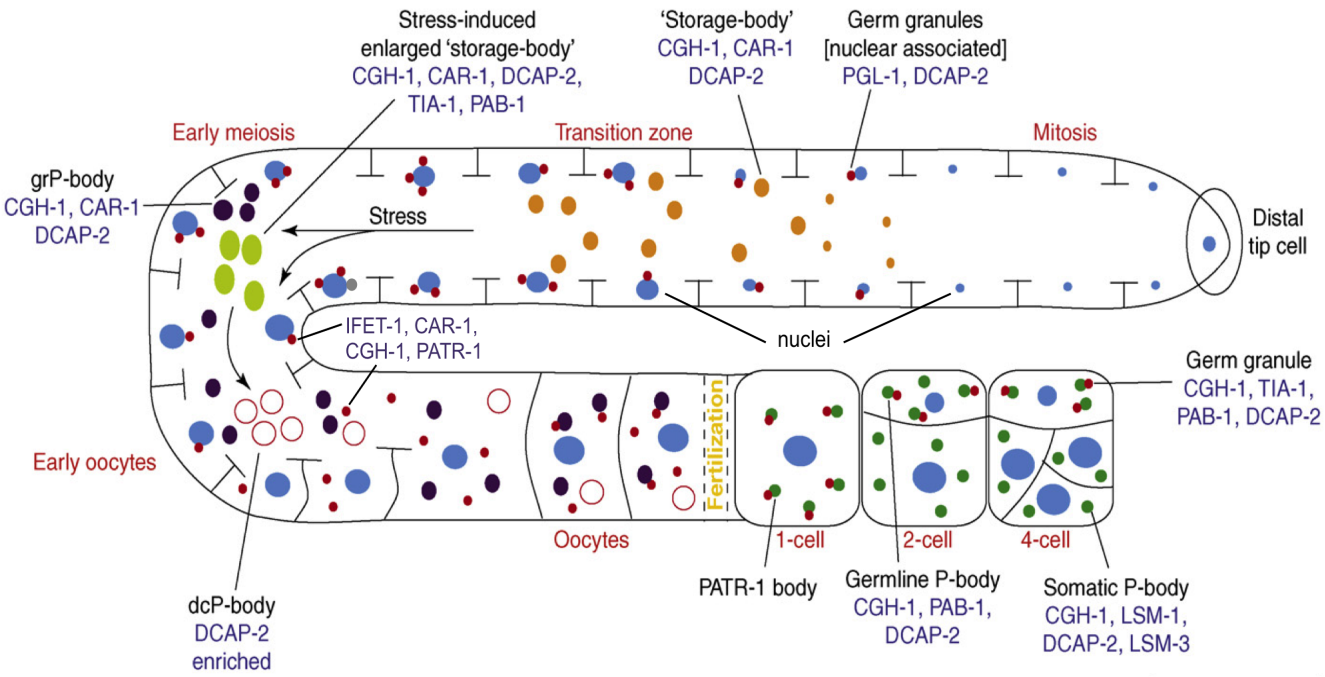

Figure 2: C. elegans oogenesis and early embryogenesis along with mRNP granules and their major components. Oogenesis in *C. elegans* occurs in a syncytium and gametes develop into mature oocytes as they pass through the different displayed stages. Oocytes are fertilized by sperm produced at earlier stage in development. Various mRNP granules are formed during oogenesis and early embryogenesis. This figure has been modified from Rajyaguru and Parker, 2009.

1996). They contain various repressors for mRNA transcription including the CCCH-finger protein PIE-1, which is produced maternally during oogenesis and acts in a concentration-dependent manner in each germline blastomere (Tenenhaus et al., 1998). PIE-1 suppresses transcription, possibly by inhibiting RNA polymerase II via presently unidentified factors (Ghosh and Seydoux, 2008). The function of PIE-1 is controlled by the P granule factor MEX-1 (two “finger” domain, similar to PIE-1), which restricts PIE-1 expression and activity to germline blastomeres during early embryogenesis (Guedes and Priess, 1997). MEX-1 also controls proper localization and activity of the maternally provided transcription factor SKN-1 and subsequently determines early cell fate (Schnabel et al., 1996). The P Granule factor MEX-3 (a presumptive RNA binding protein) apparently acts independently of the MEX-1 and SKN-1/PIE-1 regulated blastomere specification (Draper et al., 1996).

Germline proliferation and fertility is further dependent on the P granule component PGL-1 (P-granule abnormality-1), which is a RNA-binding protein and might be important for transport of maternal mRNAs from the nucleus into P granules (Kawasaki et al., 1998; Schisa et al., 2001). PGL-1 is required for RNAi functionality in the *C. elegans* germline (Robert, 2005). The Vasa family proteins GLH-1 and -4 (multiple zinc finger containing structures) mediate PGL-1 recruitment to P granules, but loss of this function does not interrupt RNAi deficiency. This indicates that proper P granule integrity is not required, but rather that specific P body factors differentially regulate germline-specific RNAi functionality (Spike et al., 2008b). Also, the PGL-1 assembly into P granules requires DEPS-1 (defective P granules and sterile-1). This factor is germ cell specific and promotes expression of RDE-4 (RNAi defective-4), essential for RNAi functionality (Spike et al., 2008a). Together these results underline an essential role for RNAi in the regulation of mRNAs localized to P granules and in the proper function of the germline.

The P granule factors OMA-1 and OMA-2 (2 CCCH fingers) are involved in the final step of meiotic cell cycle control in oocyte maturation (Shimada and Kawahara, 2002). The DEAD box RNA helicase VBH-1 (Vasa and Belle like helicase-1) and, like the closely related Drosophila Vasa and Belle, regulates embryogenesis, gamete function and prevents an early sperm/oocyte switch in the hermaphrodite gonad (Salinas et al., 2007). The abundance of mRNAs in the Ras-MAPK pathway that controls multiple steps during oogenesis is regulated by the RNA binding factor LARP-1 (La related protein-1), which localizes to P-granules, a step possibly critical for degradation of specific mRNAs during oocyte development (Nykamp et al., 2009). The central decapping enzyme DCAP-2 is also found in P granules during development, indicating that mRNA turnover happens in this type of mRNP aggregates (Lall et al., 2005). Another P granule associated function is the control of 21U-RNAs, which share structural similarities with piRNAs. Those small RNAs are involved in epigenetic control and highly regulated by the well-conserved Argonaute/Piwi family of proteins, which are known to play important roles in spermatogenesis and the germ line. The Piwi-like protein PRG-1 (Piwi related gene-1) and 21U-RNAs co-regulate proper expression of spermatogenesis specific transcripts in *C. elegans* (Wang and Reinke, 2008).

A possibly distinct type of germline specific particles is defined by CGH-1 (conserved germline helicase-1), ortholog of yeast Dhh1, which might relate those structures closer to P bodies (Navarro and Blackwell, 2005). CGH-1 appears to have differential roles, but is consistently present during oogenesis and early embryogenesis (compare Figure 2). In early germ cells some mRNAs are flowing from the nuclei through P granules into the commonly shared cytoplasm. Some mRNAs are protected though accumulation into CGH-1 specific ”storage bodies”. The CGH-1 granules contain CAR-1 (cytokinesis apoptosis RNA associated-1) and DCAP-2 (“grP body”) to form RNP com-

plexes that are critical for oogenesis by controlling germ cell apoptosis (Boag et al., 2005). The factor CAR-1 (Rap55 in humans, Trailerhitch in Drosophila) supposedly differentially regulates the diverse translation patterns in the *C. elegans* gonad. CAR-1 also controls GLP-1, the Notch receptor in *C. elegans*, and possibly other mRNAs. During oocyte formation CGH-1 granules undergo further changes, discriminating their functions in mRNA suppression, which includes more distinct recruitment of DCAP-2 ("dcP body") (Noble et al., 2008; Squirrell et al., 2005).

CGH-1 associates with GLD-1 (germ line deficient-1) which suppresses mRNAs between early and late oogenesis (Jones et al., 1996). Together they repress mRNAs in the oocyte to embryo transition and thereby act protective against precocious translation (Scheckel et al., 2012). After oocytes become cellularized and fertilized by the spermatheca, transcription ceases during diakenesis and maternal mRNAs are translated. At four cell stage embryonic transcription becomes activated and CGH-1 associates with PATR-1/PAB-1 (PABP) and other P-body and stress granule specific factors ("germline P body"), responsible for mRNA degradation (Boag et al., 2008). The two factors MEG-1 and MEG-2 (maternal effect germ-cell defective) are specific for localization to P granules only in the germline blastomeres of early embryos. Through interaction with P granule factors MES-1 (maternal effect sterile-1), PGL-1 and GLH-1 they establish proper germ cell fate in larval and adult nematodes (Leacock and Reinke, 2008).

Intriguingly, in aged *C. elegans* hermaphrodites sperm cells are depleted, hence ovulation arrests and oocytes accumulate in the gonad. Arrested oocytes form RNP granules that contain classical markers for P granules, including MEX-3 but intensely co-localize with DCAP-2, CGH-1 and DCAP-2, and remarkably with stress granule reporters PAB-1 and TIA-1 upon various environmental stress cues (Jud et al., 2008). The same is observed in animals in which sperm cells are genetically depleted, as achieved in feminized mutants (Schedl, 1988). Once those oocytes are being fertilized in delay, those stress-induced "enlarged" storage bodies disassociate, which depends on the major sperm protein (MSP) and embryos may develop normally. These results indicate that P granules can recruit P-body and stress granule factors for mRNP protection during developmental stress (Jud et al., 2008).

Nevertheless, P-bodies and germ granules seem to become entirely distinct structures during early embryogenesis since their core components and dynamics start to differ. While P granules in the progenitor germline retain CGH-1, DCAP-2 and PAB-1, activators of decapping and deadenylation become recruited in somatic cells, which includes DCAP-1, LSM-1, LSM-3 and CCF-1 (Gallo and Riddle, 2010; Lall et al., 2005). Apparently, CAR-1 and DCAP-1 containing P bodies co-regulate the late stage of early cell divisions in development by degrading mRNAs critical for exit points of cytokinesis (Squirrell et al., 2005).

Post-embryonic roles of mRNP granules in *C. elegans*

Some work on P-body specific pathways has contributed to the understanding of miRNAs pathways in *C. elegans*. This evolutionarily conserved class of approximately 21 nucleotide RNAs regulates gene expression at the posttranscriptional level. After being transcribed and processed, mature miRNAs are incorporated into the RNA-induced silencing complex (RISC) to target mRNAs based on sequence complementation in the 3' untranslated regions (UTRs). This process regulates numerous cellular processes and has been studied and reviewed extensively (Krol et al., 2010).

The developmental timing regulator AIN-1 (ALG-1 interacting protein-1) has been shown to regulate the miRNA pathway in nematodes and recruits the argonaute protein ALG-1 and ALG-2 (argonaute-like gene) to P bodies, to which most components of the miRNA silencing complex (miRISC) localize. AIN-1 and its equivalent and redundant

interacting partner AIN-2 are considered the human GW182 counterpart in *C. elegans* (Ding et al., 2005; Zhang et al., 2007). Together they employ some 100 miRNAs to regulate up to 3500 potential targets in the nematode, many of them involved in cell fate specification during post-embryonic development (Zhang et al., 2007). *C. elegans* AIN-1 employs the poly(A)-binding factor PAB-1 (human PABPC1), similarly to human miRNA mediated degradation pathways, despite very low conserved sequence similarity between AIN-1 and human GW182 (Kuzuoglu-Öztürk et al., 2012). The cofactor of miRISC in the worm NHL-2 forms a complex with CGH-1 and modulates efficacy of miRNA target interaction (Hammell et al., 2009). Degradation of miRNA targeted mRNA is mediated by the exonuclease XRN-1 and XRN-2 (Chatterjee and Grosshans, 2009). Recent discoveries revealed that DCS-1 (also known as DcpS in *C. elegans*), a decapping scavenger, recruits XRN-1 for miRNA mediated mRNA turnover (Bossé et al., 2013).

Little else is known about possible P-body specific functions in post-embryonic development of *C. elegans*. A systematic RNAi screen for P-body and stress granule formation in adult animals has been performed and 224 genes were identified to increase P-body formation. 83 of those genes are related to nonsense mediated mRNA decay (NMD), RNAi and miRNA pathways, but a large number of genes is involved in translational mechanisms, or mechanisms seemingly unrelated to mRNA decay (Sun et al., 2011).

Nuclear communication with cytoplasmic granules via eIF4E

Nuclear pre-mRNAs are packaged into heterogeneous nuclear ribonucleoprotein particles (hnRNPs), and they accompany the mRNA from transcription through splicing events, polyadenylation and final association with nuclear export mRNPs (Müller-McNicoll and Neugebauer, 2013; Oeffinger and Zenklusen, 2012). Export of long transcripts is mediated by the nuclear export factor 1 (NFX1), while short transcripts associate with the choromosomal region maintenance protein 1 (CRM1), which is also the major export receptor for nuclear proteins (Natalizio and Wente, 2013). After passing the nuclear pore complex, some nascent mRNPs are evidently directly sorted into cytoplasmic granules for further processing or storage (compare Figure 1).

Many stress granule components are predominantly nuclear shuttling proteins. Export mediated by TIA-1 and TIAR locates mRNPs into stress granules (Kedersha et al., 1999). This process seems to be independent of the bulk protein export machinery mediated by CRM1, but depends on one of the three contained RNA recognition motifs (RRMs) (Zhang et al., 2005). TIA-1 and TIAR localize to speckles in the nucleus and function in alternative mRNA splicing (Anderson and Kedersha, 2002). Through the RRMs, both factors can bind to ssDNA, drawing a possible connection between transcriptional control, shuttling and translational repression of mRNAs (Suswam et al., 2005). The RNA binding proteins HuA to HuD act in competition to TIA-1 and TIAR in their neuronal function in alternative splicing, and are also known to aggregate mRNAs in stress granules (Gallouzi et al., 2000; Zhu et al., 2006). The steroid receptor coactivator 3 (SRC3) is an oncogene and primary transcriptional coactivator for the estrogen receptor. While its phosphorylated form acts in the nucleus, its cytoplasmic localization co-aggregates with TIA-1 and TIAR in stress granules to regulate cytokine mRNA translation (Li et al., 2007; Yu et al., 2007).

Another prominent and for our study intriguing factor that shuttles between nucleus and P bodies/stress granules is eIF4E, which acts as mRNA transport protein and oncogene that localizes to stress granules and P-bodies (Buchan and Parker, 2009; Culjkovic et al., 2007). Much focus has been given on its role in global protein synthesis and its down-regulation confers longevity, a mechanism conserved across species (Syntichaki et al., 2007; Tavernarakis, 2008). An-

other field of study for the function of eIF4E is the role in mRNA transport. The import to the nucleus of eIF4E is mediated by importin and 4E-T (eIF4E-Transporter) and retained in the nucleus by activity of 4E-BP1 (eIF4E-binding protein 1) (Dostie et al., 1999; Rong et al., 2008). eIF4E binds a specific set of mRNAs in the nucleus, by recognizing a defined USER code located in the mRNA 3'UTR. This 50-nucleotide sequence has been defined as 4E-SE and contains a special and conserved folding. Exported transcripts include such important targets as Cyclin D1 and proteins involved in export are CRM-1, TAP and LRPPRC (Culjkovic et al., 2006; Topisirovic et al., 2009). The function of eIF4E in export of mRNA and translation initiation is independent of each other; hence it can be blocked by different chemicals at different levels, including Ribavirin, Leptomycin B and Rapamycin (Assouline et al., 2009; Borden, 2011; Culjkovic et al., 2006). The factor eIF4E is an oncogene and strongly elevated in acute myeloid leukemia (AML) and other cancer types and well investigated as such (Culjkovic et al., 2007; Hariri et al., 2013). It has been shown to interact with the nuclear core complex to shuttle mRNAs and its levels are strongly elevated and retained mainly nuclear in AML (Culjkovic-Kraljacic et al., 2012).

Little is known about the role of eIF4E in transport of mRNAs to storage and decay sites as P-bodies and stress granules (Buchan and Parker, 2009). Several targets of translation initiation are known to cycle in and out of P-bodies and an exchange of mRNPs including eIF4E happens between P-bodies and stress granules (Brengues and Parker, 2007; Hoyle et al., 2007). It has been shown that specific mRNAs are directly transported via eIF4E and 4E-T to P-bodies (Andrei et al., 2005). 4E-T also controls mRNA stability, since its depletion leads to increased mRNA stability and interaction with eIF4E represses translation, a process that seems to be mediated through P-bodies (Ferraiuolo, 2005).

As mentioned earlier, perinuclear P granules are principal sites of mRNP export and accumulation in adult *C. elegans* germ cells, since they associate with clusters of nuclear pore complexes and (Sheth et al., 2010). Most intriguingly, recent findings also involve the eIF4E-T homologue IFET-1, in germ cell sex determination and normal P granule formation. Although details of its proposed activity there are still unknown, IFET-1 might repress cap-dependent translation initiation (Sengupta et al., 2013).

Some examples exist for targeted localization of cytoplasmic granule components to the nucleus. The Fas-activated serine/threonine phosphoprotein (FAST) is a factor tethered to the outer mitochochondrial membrane, which moves to stress granules upon stress insult. FAST also co-localizes with TIA-1 in nuclear speckles and promotes splicing of various factors, a function seemingly independent of TIA-1 and its metabolic function in the cytoplasm (Li et al., 2004; Simarro et al., 2007). In breast cells, the stress granule factor p90 ribosomal S6 kinase (RSK2) directly interacts with TIA-1 in stress granules and is essential for stress resistance upon serum-starvation. Curiously, upon mitogen treatment, RSK2 shuttles to the nucleus and co-regulates cyclin D1 mRNA transcription, again with TIA-1 (Eisinger-Mathason et al., 2008). Also, upon deletion of P-body proteins Edc3 and Lsm4 in yeast, Dcp2 localizes to the nucleus, and upon heat shock, various stress granule factors enrich in the nuclear region.

Together these studies indicate a possible role for stress granules and P-bodies in remodeling, storage, and decay of exported mRNAs, and further point to a coupling of cytoplasmic and nuclear gene expression control mechanisms.

Materials and Methods

Strains and transgenic lines

We followed standard procedures for maintenance of *C. elegans* strains and transgenic lines (Brenner, 1974). Animals were grown at 20°C unless noted otherwise. The following strains were used for this study: N2: Wild type Bristol isolate, RB1311: *edc-3(ok1427)*I, RB1641: *dcap-2*(ok2023)IV, KX15: *ife-2(ok306)*X, CB1370: *daf-2*(e1370) III, CB4876: *clk-1(e2519)*III, DA465: *eat-2*(ad465)II, CW152: *gas-1(fc21)*X, TK22: *mev-1(kn1)*III. For OPT and SPIM imaging we used: Is[p_{mec-4}GFP], expressing GFP in the six mechanosensory neurons; N2;E[$_{myo-2}$GFP], expressing GFP in the pharynx.

To image DAF-16 transcription factor target activation we used: CF1553: muIs84[pAD7(p_{sod-3}GFP)] and CF1580: *daf-2(e1370)*III;muIs84. To image SKN-1 target activation we applied: CL2166: dvIs19[pAF15(gst-4::GFP::NLS)] and *ife-2(ok306)*;dvIs19. To image in vivo H2O2 enrichment we used JRIS1: [p_{rpl-17}HyPer; UNC-119(+)]. To study the possible interactions of ageing pathways we created the cross *edc-3(ok1427)*III;*ife-2(ok306)*X.

Overexpression lines for this study were created as extrachromosomal arrays through microinjection. To study P body or stress granule localization and co-localization we established: N2;Ex[p_{edc-3}EDC-3::dsRED;pRF4], N2;Ex[p_{ife-2}IFE-2::GFP;pRF4] (Syntichaki and Tavernarakis, 2007), N2;Ex[p_{dcap-1}DCAP-1::dsRED;pRF4], N2;Ex[p_{lsm-3}LSM-3::dsRED;pRF4], N2;Ex[p_{edc-3}EDC-3::dsRED;p_{ife-2}IFE-2::GFP;pRF4], *edc-3(ok1427)*;Ex[p_{dcap-1}DCAP-1::dsRED;p_{ife-2}IFE-2::GFP;pRF4], which was outcrossed with N2 to create N2;Ex[p_{dcap-1}DCAP-1::dsRED;p_{ife-2}IFE-2::GFP;pRF4]. To monitor neuron specific fluorescence and co-localization with P bodies we created: N2;Ex[p_{edc-3}EDC-3::dsRED;$p_{unc-119}$GFP;pRF4], *edc-3(ok1427)*;Ex[$p_{unc-119}$GFP;pRF4], which was outcrossed with N2 to create N2;Ex[$p_{unc-119}$GFP;pRF4]. To study the effects of EDC-3 overexpression in ageing we created *edc-3(ok1427)*;Ex[p_{edc-3}EDC-3+3'UTR;pRF4] and N2;Ex[p_{edc-3}EDC-3+3'UTR;pRF4]. To examine the neuron-specific role of EDC-3 in ageing we established *edc-3(ok1427)*;Ex[$p_{unc-119}$EDC-3+3'UTR;pRF4] and N2;Ex[$p_{unc-119}$EDC-3+3'UTR;pRF4].

Molecular cloning

To investigate localization of P body specific genes we firstly constructed a DsRED reporter. We excised GFP from the construct pPD95.77 by using the restriction sites AgeI/EcoRI and inserted the same cut DsRED from pcol-12DsRED (Wong et al., 2007), thereby creating pPD95.77(dsRED). The P body specific gene *lsm-3* is located in *C. elegans* operon CEOP4548. To construct p_{lsm-3}LSM-3::dsRED we designed two primer pairs to individually amplify the gene and endogenous promoter from genomic DNA: 5'-GATTCTAGAGTGCACCAAGCTCTCAAC-3' and 5'-GATACCGGTCTTTCTTCTCAATCTGCTTG-3' for the promoter region covering 880bp upstream of the first gene mdt-9 in the operon and 5'-GATACCGGTATGGCCACCGAAAAGAAAG-3' and 5'-GATACCGGTAGGGATGCACGAATCGGTG-3' for the 566bp full sequence of *lsm-3*. Both resulting fragments were subcloned into pCRII-TOPO vector (Invitrogen). The *lsm-3* promoter was excised as AgeI/XbaI fragment and inserted into pPD95.77(dsRED) after which the gene was cloned by excision with AgeI between promoter and dsRED sequence. The resulting construct was injected into gonads of wild type animals together with transformation marker pRF4 (contains *rol-6(su1006)*). The P body reporter p_{dcap-1}DCAP-1::dsRED was created from a pBluescript II KS+ containing the whole *dcap-1* gene and promoter by amplification with 5'-GTAATACGACTCACTATAGGGC-3' and 5'-GGACCGGTCCATC-

GATATTTAGACGCCGATTG-3'. The resulting 2300bp fragment was digested AgeI/XbaI and inserted into pPD95.77(dsRED). The final construct was co-injected with pRF4 into gonads of wild type animals.

To generate the construct p_{edc-3}EDC-3::DsRED we used the AgeI-flanked primer pair 5'-ATGGATGACAAACTCATTGGAAGC-3' and 5'-ACCGGTCCATTGGA-TTGTGAAAGTCTGACAAG-3' to amplify the sequence of the gene *edc-3*, which is located in operon CAOP1484 of the *C. elegans* genome, and subcloned it into TOPO-pCRII. In parallel we amplified the putative promoter region upstream of the first gene in the operon *ran-4*, using the primers 5'- TTCTTCTAAGGCCGATTTCACAAC-3' and 5'-CGACAAATTGGGAAAAA-TAATTG-3' and creating a 1429 bp fragment, which we placed into TOPO-pCRII. From here we excised the fragment with BamHI/XbaI and placed it into pPD95.77(dsRED). To add the *edc-3* gene sequence we opened TOPO-pCRII with ApaI, created a blunt end (Klenow, NEB) and cut with AgeI. The resulting 2550bp fragment was inserted into pPD95.77(dsRED) between putative promoter and dsRED. The construct was injected along with pRF4 into gonads of wild-type animals. To study the neuronspecific role of EDC-3 in ageing and expression we created the panneuronal localization construct $p_{unc-119}$GFP. We used the primer pair 5'-CTCTCAAAATTCAGTTTTTTAAACCAC-3' and 5'-ATATGCTGTTGTAGCTGAAAATTTTG-3' to amplify 1990bp upstream of unc-119 gene and subcloned the resulting fragment into TOPO-pCRII. From there we excised the *unc-119* promoter through AgeI/XbaI restriction and inserted it into pPD95.75. The resulting construct was injected together with pRF4 into gonads of *edc-3(ok1427)* mutant worms and outcrossed with wild type to study general expression levels upon loss of decapping. We further co-injected the construct with p_{edc-3}EDC-3::dsRED and pRF4 into gonads of wild type animals to study co-localization of EDC-3 with the neuronal system. For stress granule and P-body co-localization studies we used the contruct p_{ife-2}IFE-2::GFP and co-injected it with either p_{dcap-1}DCAP-1::dsRED or p_{edc-3}EDC-3::dsRED and the transformation marker pRF4 into *edc-3(ok1427)* mutant worms or wild type, respectively. To study EDC-3 global and neuronal overexpression in ageing we constructed p_{edc-3}EDC-3+3'UTR and $p_{unc-119}$EDC-3+3'UTR. For expression under its endogenous promoter we used TOPO-pCRII containing *edc-3* promoter and EDC-3::dsRED and excised EDC-3::dsRED through flanking NotI restriction sites. The *edc-3* gene including its 3'UTR were amplified from genomic DNA with the primer pair 5'-AGAGCGGCCGCCGGTGCTAAAAGTAGACGTGGTTG-3' and 5'-AGAGCGGCCGCATGGATGACAAACTCATTGGAAGC-3' containing NotI restriction sites. The resulting fragment was NotI digested and inserted downstream of either *edc-3* promoter or *unc-119* promoter in TOPO-pCRII. The final plasmids were injected into gonads of wild type and *edc-3(ok1427)* mutant worms.

We generated several RNAi constructs for P body specific genes including *edc-3*, *ccr-4*, *dcap-1*, *dcap-2*, lsm-1, ain-1 and *ife-2* using genomic DNA as base of amplification in each case. The goal vector was pL4440 and all constructs were transformed into the RNAse E deficient *E. coli* strain HT115(DE3). For *edc-3* RNAi we amplified 1440bp with the primer pair 5'-CAGGAGAATGATGACCAGTACTATG-3' and 5'-GGAAAGTTGTAGAGAATGCGGTAG-3', subcloned into TOPO-pCRII and excised with EcoRI to put the fragment into pL4440. For *ccr-4* RNAi we used the primer pair 5'-GATTCTAGAGTGGGATTGAACACAGTAAAGC-3' and 5'-GATACCGGTCACCTCAGGAATGGTTGG-3' and the resulting 2375bp fragment was digested AgeI/XbaI to be cloned into the goal vector. For *lsm-1* RNAi we generated 5'-CATGGACTTGCCCGATCC-3' and 5'-CAGAATACAGATTCATGCATCGTG-3' primers and placed the resulting 439bp fragment into pL4440 after AgeI/XbaI digest. For the *dcap-1* RNAi construct a 1000bp fragment was excised from pBluescript II Ks+ containing *dcap-1* ORF with EcoRI/XhoI and cloned

it into pL4440. For *dcap-2* RNAi the primer pair 5'-CACGAATTCCGAATACCCC-3' and 5'-CCGCTCGAGTAACGAGACCAAGTAC-CG-3' were used to generate a 800bp fragment which was placed into pL4440 upon digest with XbaI/BamHI. For *ain-1* RNAi the construct p_{ain-1}AIN-1::GFP was digested EcoRI/XhoI and the resulting 866bp fragment was cloned into pL4440 (Ding et al., 2005). Preparation of the plasmid containing *ife-2* RNAi was described previously (Syntichaki and Tavernarakis, 2007). To study epistasis of *hsf-1*, *skn-1* and *daf-16* and longevity in decapping deficient mutants we created RNAi constructs for each of the transcription factors. For *skn-1* RNAi we used the primer pair 5'-TCAGTTCACCATCGTCCAACACCTC-3' and 5'-TGTCGTGACGATCCGTGCGTC-3', subcloned the resulting 4079bp fragment into TOPO-pCRII and excised it with EcoRI digestion to place it into pL4440. For *daf-16* RNAi a 1.2kb fragment resulted from amplification with 5'-CACTGATCTTTCAAGCCG-3' and 5'-CTTGTGCAAGAGTTAACCG-3', which was subcloned into TOPO-pCRII and excised with HindIII/XhoI and placed into the goal vector. The *hsf-1* RNAi construct was generated by amplifying a 1000bp fragment through the primers 5'-ACACTGCAGATG-CAGCCAACAGG-3' and 5'-TGTCTCGAG-GATCGTGGTCCTTC-3', which was digested PstI/XhoI and cloned into pL4440. To study the involvement of mitochondrial stability in P-body formation we used a previously described *eat-3* RNAi construct (Artal-Sanz and Tavernarakis, 2009).

Lifespan assays

Lifespan analysis was performed at 20°C unless noted otherwise. Synchronous animal populations were generated by egg-laying experiments with 10 to 15 gravid adults per plate, which were removed after 5 hours. For RNAi lifespan experiments worms were placed on NGM plates containing 1mM IPTG and seeded with HT115(DE3) bacteria transformed with either the pL4440 vector or the test RNAi construct. For assays evaluating the effect of hormesis in ageing, N-acetyl-cysteine (NAC, Invitrogen) was added into NGM media from a high concentration stock solution (500 mM). Progeny were grown through the L4 larval stage and then transferred to fresh plates in groups of 15-17 worms per plate for a total of 150–170 individuals per experiment. The day after egg laying and initiation of RNAi was used as t=0 (days from hatching). Animals were transferred to fresh plates every 2–3 days and examined every second day until death for movement, touch response and pharyngeal pumping. Worms that died due to internally hatched eggs, an extruded gonad or desiccation due to crawling on the edge of the plates, were incorporated into the data set as censored. Each survival assay was repeated at least twice and figures represent typical assays. We used the Prism software package (GraphPad Software) to carry out statistical analysis of lifespan assays, which includes the product-limit method of Kaplan and Meier and the log-rank (Mantel–Cox) test to evaluate differences between survivals and p values.

FRAP assays

To determine the role of mRNA degradation in protein synthesis rates we developed a novel FRAP assay that combines immobilization of animals on agar pads for photobleaching without anesthetics and monitoring of fluorescent recovery OP50 seeded plates. Transgenic animals carrying the appropriate fluorescent reporters were grown into the desired age. For each bleaching procedure 4-5 worms were transferred into a drop of M9 on freshly prepared 2% agarose pads. Immobilization of animals occurred within 1-2min due to absorbance of M9 into the agar. Once immobilization was complete, final positioning of worms was corrected by the use of a hair-pin. The pad was placed under a 40x lens of a Zeiss epifluorescence microscope Axio Imager Z2 without coverslide. After focusing and recording of a reference image, photobleaching of the area of interest was performed for 90 seconds at 30% luminescent power of the fluorescent illumination source (Fl illumination System X-Cite 120 XL FL PC, 120W

metal halogenide lamp) and fully opened iris. A reference image after photobleaching was recorded and worms were allowed to recover for 5min in a drop of M9 buffer. Worms were then transferred to individual NGM plates seeded with a drop of OP50 in the center and an image was taken under a 10x lens of the epifluorescent microscope, which counted as t=0 for the recovery after photobleaching. Images on plate were recorded every hour to 3 hours thereafter for at least 6 hours. To assure that only healthy animals were scored for the assay, individual animals were carefully observed for indications of damage such as locomotion or egg-laying defects, and survival over the next 2-3 days. The recorded images were then processed by the imaging software package ImageJ and mean pixel intensity of the area of interest was determined for each time point and the reference images. Evaluation of the data was performed in the Prism software package (GraphPad Software).

Time lapse recording

To monitor EDC-3 during time we mounted day 2 adult N2;Ex[p_{edc-3}EDC-3::dsRED;$p_{unc-119}$GFP;pRF4] transgenics on freshly made 2% agarose pads and sealed them with a cover slip. Live imaging was performed with a Zeiss epifluorescence microscope Axio Imager Z2 under a 25x lens. We focused on the neurons of interest and programmed a multi-fluorescent time-lapse. Movies consisted of 25-30 images over a time span of about 2min and were processed through the Zeiss software package (ZEN2011).

P-body and stress granule monitoring and quantification

Transgenic lines designed to measure P-body or stress granule formation in *C. elegans* were grown on OP50 or RNAi of interest into the desired age following the method of a lifespan assay. Individual animals were transferred into a drop of M9 buffer containing 10mM levamisol on a microscope slide and sealed with a cover slide. Imaging occurred either at a Zeiss epifluorescence microscope Axio Imager Z2 under a 10x lens (EC Plan-Neofluar, numerical aperture 0.3) with focus on the anteroposterior center of each animal, recording at least 25 whole worms. Alternatively, animals were imaged under a 25x lens (LCI Plan-Neofluar, numerical aperture 0.8, Immersion Corrected DIC) of a LSM710 Zeiss confocal microscope, Axio-observer Z1 controlled by ZEN2011. Here, we focused on the head region and 10-15 single plane images in 5µm steps of 10 worms were recorded and quantified individually or as the resulting maximum intensity projection image. To quantify P-body formation we used the software package ImageJ and measured either P-body intensity (mean pixel intensity) or P-body number (particle analysis with appropriate threshold assignment). We evaluated the data through the use of Prism software package (GraphPad Software). To qualitatively monitor P-body and stress granules formation and co-localization we imaged in 4 to 5 sections under the 25x lens at the Zeiss confocal microscope covering the full body length, recording 10-15 single planes in 3µm steps. Single planes or maximum intensity projections were thereafter assembled into a whole worm image using the software package Adobe Photoshop (CS5). For quantification of co-localization we used ZEN2011.

Stress assays

We applied several stress assays to evaluate stress response of P-body and stress granule formation in transgenic lines. To evaluate the influence of heat stress we placed day 2 adult animals on prewarmed OP50 seeded plates and incubated them for 3 and 6 hours at 35°C followed by immediate monitoring. To examine the involvement of starvation we grew animals under optimal conditions to day 2 adult stage, transferred them to empty NGM plates followed by monitoring 24 hours thereafter. To examine effects of hypoxia condition on P-body and stress granule formation we used a hypoxic chamber and applied low oxygen concentration following previously described methodology (Troulinaki and Tavernarakis, 2011). Day 2 adults were exposed to low oxygen conditions (<0.5%) at 25°C for 6h.

Animals were immediately imaged thereafter. Immediate response to strong oxidative insults was tested by incubation of worms for 30min in 20mM sodium azide (NaN_3, Sigma) or 100mM paraquat (PQ, Sigma) set up in M9 solution, followed by monitoring. To monitor slow response effects of oxidative stress we grew worms into day 2 or day 7 adults. We then transferred worms to plates with freshly applied drugs NaN_3 (150µM) or PQ (5mM). These concentrations assured a several day lasting response before death would occur and animals were imaged at day 2 after exposure. Following the same protocol for oxidative stress, we compared wild type worms grown on control or *edc-3* RNAi and *edc-3* mutants.

Statistical analysis and Text/ Figure editing

Statistical analyses were carried out using the Prism software package (GraphPad Prism 6). Mean values were compared using unpaired t-tests. To asssemble text and figures for this thesis the Microsoft Software Package Office:Mac2011, Adobe Photoshop CS5 and Adobe InDesign CS6 were used. To sort the Bibliography Papers2 was applied.

Sample preparation for OPT imaging

Glass capillaries (5 µl) were modified using a capillary puller (PN-30, Narishige, Tokyo, Japan). The tip was tapered to reduce the inner diameter for enhanced sample stability and positioning. Young adult worms can be immobilized in a 5-10 mM levamisole (Sigma-Aldrich, St. Louis, USA), or in a 10 mM NaN3) solution for 15 min at 20°C and then transferred in a drop of halocarbon oil (refractive index n=1.42). While levamisole temporarily suppresses muscular activity, NaN_3 inhibits both cytochrome c oxidase and adenosine triphosphate (ATP) synthase. Residual anaesthetic was removed by moving the worm in the oil with a hairpin. Animals were sucked into the tip of the capillary by a pipette. The capillary was carefully cleaned with 70% ethanol and then sealed at both ends by slightly dipping into liquid glue (Glue-All, Multi-Purpose Glue, Elmer's Products, OH, USA).

The Tomographic setup

The light source comprises superbright LEDs (Luxeon V Star 5 W, Philips Lumileds Lighting, San Jose, CA, USA) in numerous colors, allowing excitation of most commercially available fluorescent dyes. White LEDs are used for transmission (absorption) imaging. Although, for this study blue LEDs were employed for excitation due to the use of GFP, the system is not restricted, allowing any chromophore or fluorescent protein can be visualized by using appropriate light sources. The sample holder is based on a rotation system, containing a high resolution rotation stage (8MR180, Standa, Vilnius, Lithuania) with 36000 steps per revolution. Attached is a custom made capillary holder, holding standard single use micro-capillaries (Blaubrand® - intraMARK, BRAND GmbH, Wertheim, Germany). Capillaries are immersed in a cus-

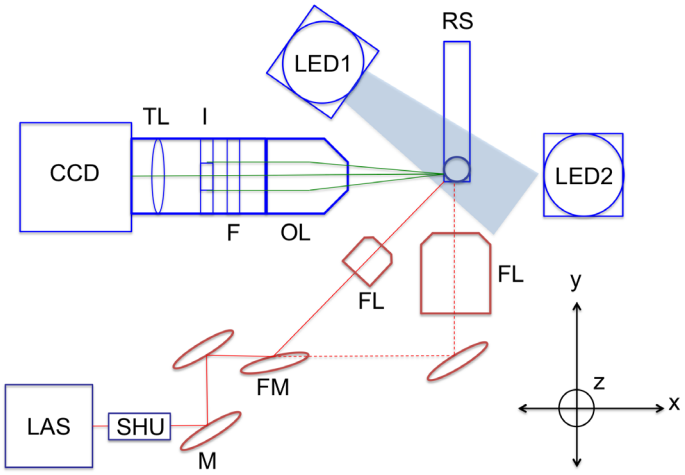

Figure 3: Scheme of the combined OPT and SPIM setup. Compartments of the firstly developed and published OPT setup are shown in blue, parts of the added SPIM system are represented in red. All compartments displayed are: LED1: blue light source, LED2: white light source, LAS: Laser, CCD: CCD camera, TL: tube lens, I: Iris, F: fluorescence filter, OL: optical lens, FL: focal lens, RS: rotating specimen, FM: flexible mirror, SHU: Shutter.

tom-made refractive index matching vessel, assembled of 50x24x0.15 mm borosilicate cover slips (nw = 1.474), containing 87% glycerol solution (Sigma-Aldrich, St. Louis, MO, USA) as a refractive index matching fluid (nf = 1.474) to minimize internal reflections and refraction of the excitation and emission light. The imaging unit consists of a lens tube system (InfiniTube™, Infinity, Boulder CO, USA) attached to a custom-made filter slide, which can hold up to three 25 mm diameter fluorescence filters (in this particular study, we used a 525 ± 17.5nm band-pass filter for GFP, 593 ± 20nm for DsRed, both Semrock®, Rochester NY., USA). In this study, we used a 10x infinity corrected microscope objective lens (Mitutoyo, Kawasaki, Japan). The objective lens has a numerical aperture NA of 0.28, which is reduced to typically around 0.22 by the iris diaphragm. The NA for trans-illumination is < 0.035, for fluorescence illumination it is ca. 0.1. Except for the collimation lens L, all lenses are corrected for chromatic aberrations. The detection filter F2 and the iris are placed next to the back focal plane of the objective. Depending on the specimen size, infinity corrected lenses with a range of other magnifications are available and can also be used. The objective lens is attached to a thermoelectrically cooled, electron multiplying CCD with 1002 x 1004 pixels (Ixon DV885, ANDOR™ Technology, Belfast, Northern Ireland). To increase the focal depth of the system, a variable iris is placed behind the objective, as described previously (Ripoll and Ntziachristos, 2004). The tilt of the sample is corrected mechanically prior to the experiment, while drifts and sample movements are corrected by applying algorithms during post-processing. A scheme of the system is shown in Figure 3 and a representative drawing in Figure 4a.

Data acquisition and 3D reconstruction

Data was acquired using custom software based on LabView™ to control specimen positioning, the camera and the rotation

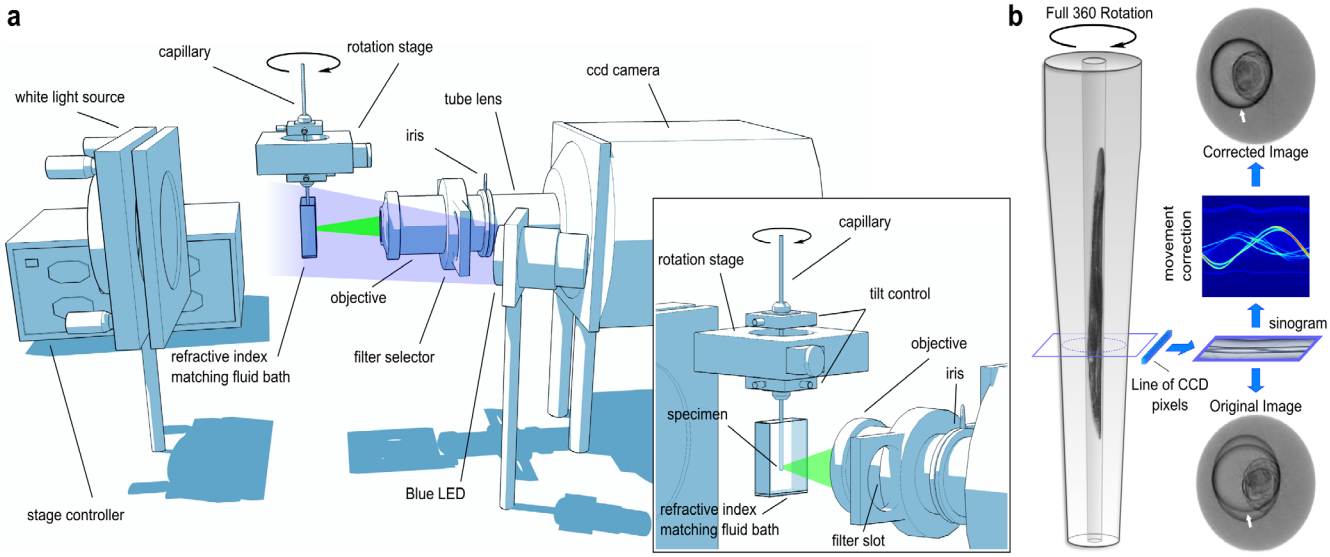

Figure 4: Overview of the experimental optical projection tomography system for in vivo imaging. (a) All basic compartments to operate the OPT system are displayed. A detailed close-up of the rotation stage and capillary is shown in the inset. The tilt screws on the rotation stage allow fine adjustment of the orientation and focusing of the sample. In this study, a white (LED2) or a blue (LED1) light source is used for sample illumination. Depending on the fluorophores used, appropriate light sources (and filters) can be easily interchanged. The detection system has a numerical aperture of NA=0.22. A detailed description of the system is provided in the text of Materials and Methods and in the scheme in Figure 4. **(b)** Delineation of image processing steps. A sinogram is obtained for each line of CCD pixels and all 3600 measurements. After processing this sinogram to correct for movements of the specimen or drifts introduced by the experimental setup, the final adjusted image of a specimen slice is generated. The volumetric representation of the sample is obtained by stacking sequential slices. White arrows indicate the position of the inner wall of the capillary.

stage. The software made use of specific functions developed in C++ for speed improvement. The experiment graphical user interface (GUI) is capable of changing all experimental parameters (camera, stage movement, and filters). 500 images of the rotating specimen were taken from equidistant angles (in 0.72° steps) and stored as one collected file with a size of approximately one gigabyte. The software is developed in MATLAB (http://www.mathworks.com/) and includes a user-friendly interface and a detailed how-to-do-manual. The full software package is available under the GNU General Public License (GPL; http://www.gnu.org/licenses/gpl.html) and can be downloaded at the following address: http://elegans.imbb.forth.gr/opt/. Bright light image data was obtained by back-illumination with a white light LED. A separate set of fluorescence data was recorded under epi-illumination with a blue light LED, which was selected in accordance to the fluorophore used in this study (GFP). An in-house developed toolbox of custom MatLab evaluation scripts was used to analyze the 3D data stacks containing the projection views on a PC (2.8GHz, 4GB RAM). To account for movement and motility of the live specimen and also for minor non-circular motion of the rotation stage, we developed software which considers changes in the predicted trajectories of the sinograms (images consisting of data from a single line of CCD pixels for all angular measurements) and corrects for these prior to data reconstruction (Birk et al., 2010, Zhu et al., 2012, for principal see Figure 5b). Correction along the rotation axis for the data shown here took only a couple of seconds, while the iterative correction took about 1h. Resolution is significantly degraded if this approach is not used, indicating its importance when imaging in vivo biological material with OPT. Once raw data were processed to correct for movement and drifts, in both fluorescence and white light mode, 3D reconstructions were calculated by sequentially stacking 2D slices reconstructed using a filtered back-projection algorithm with a Hann-Filter implemented together with an inverse Radon-transform (Kak and Slaney, 1988).

For reconstructions of data received by SPIM imaging in chips we used the Freeware Fiji with the add-on Volume Viewer.

The updated SPIM-OPT setup

Various attachments to the already designed OPT setup made SPIM imaging possible: Lasers with wavelengths 532nm, 488nm (Roitner Lasertechnik, Germany), 405, 594 and 635 (Thorlabs GmbH, Germany) were supplemented. A complex custom-made mirror system commonly directed the beams through a shutter (VCM-D1,Uniblitz Electonics, NY), a prism (Zeiss) and finally a focal lens (Zeiss, PLAN APO, 10x optical lens, 0.28, WD=33.5) to create a thin laser-light sheet, which is focused on the sample. A flexible mirror in the laser-light path could be applied to redirect the beam around the prism though a focal lens (Thorlabs) to the sample for laser-source based OPT-imaging (see scheme in Figure 3). We updated the custom-made operating software described for the OPT setup to accommodate the needs for X, Y or Z-sectioning of the sample for SPIM imaging capacity.

Preparation and loading of the microfluidcs device

The microfluidic chip applicable for OPT and SPIM recording was created in collaboration with M. Ghanad-Rezaie and N. Chronis, following procedures described previously (Chronis et al., 2007). Briefly, chips including a front and a backside were designed in the software AutoCAD (Figure 6a) and silicon masks were produced by the Microfabrication facility at the University of California, Berkeley. We cast a polydimethylsiloxane (PDMS) prepolymer mixture (Sylgard 184, Dow Corning) over the molds and cured over night in a 65°C oven. PDMS prints were peeled off from the mold and treated with air plasma to activate the surface for binding. Front and backside of the PDMS were aligned, glued to each other and cut along the edges to exactly fit a 2ml plastic tube (Ep-

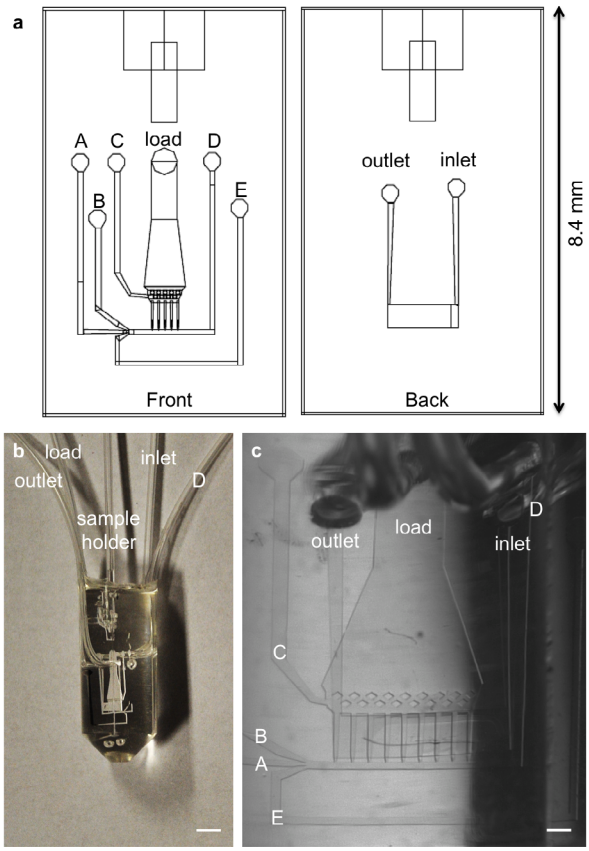

Figure 5: The OPT and SPIM compatible microfluidics device. (a) Schematic drawing of front and backside of the chip as designed in AutoCAD and printed on the silicon mask. **(b)** Photograph of a ready-to-use chip with connected tubings for loading, inlet and outlet and sample holder. The chip has a cylindrical design, which permits imaging of the loaded specimen from equidistant angels, as required for OPT. Also, SPIM imaging is possible from any angle of the chip position. **(c)** Microscopic image of the chambers and channels within the chip. Worms enter the chip via the load valve and can be placed into the conic chambers through pressure and suction application via inlet and outlet, which can be reversed for unloading. Up to 9 worms can be accomodated in the chip for rapid high-throughput imaging. A to E are optional channels that could be connected for chemical treatment of worms within the chip.

pendorf). We created fluidic inlets and outlets in the PDMS using fine bending die (0.5mm diameter; Harris Uni-Core). We attached hollow steel pins (0.3mm inner diameter, 0.5mm outer diameter; Kahnetics) to the inlet and outlet of the chips and connected them to fine polyethylene tubing (0.4mm inner diameter, 0.6mm inch outer diameter; BD Intramedic) to facilitate chip-to-tube interface. Finally, a glass capillary was attached as sample holder for the final chip. Chip, attached tubing and sample holder were placed into the plastic tube, which was then filled with PDMS prepolymer mixture and again cured, this time for 2 hours in a 90°C oven. After curing, the ready cylindrical shaped microfluidic chip was removed from the plastic tube. Worms were anaesthetized in 5mM levamisol or NaN_3 in M9 buffer and first loaded into 3ml plastic syringes with attached tubing. Finally, worms were pumped into the chip opening “load” by applying pressure to the syringe and suction through another syringe attached to the outlet (Figure 5b and 5c). Unloading occurs through applying pressure via the inlet and outlet and suction via the load valve.The tubing was disconnected; loaded chips were placed into the sample holder of the OPT-SPIM setup and subsequently imaged.

Results

The Role of mRNP Turnover in Ageing

Formation of P-bodies increases during ageing and upon stress insult in *C. elegans*

Our goal was to determine phenotypical changes of mRNPs during ageing. We chose to investigate key enzymes acting in decapping, the major step in control of cytoplasmic bulk mRNA degradation and a mechanism well conserved across species (Decker and Parker, 2012). We created DsRed tagged DCAP-1, which has previously been shown to co-localize with other P-body components and perform conserved roles in *C. elegans* (Ding et al., 2005; Sun et al., 2011). Additionally, we created transgenics carrying DsRed tagged decapping enzymes LSM-3 and EDC-3. In yeast, Lsm3 was identified as part of a deadenylation complex (Lsm1-7) that interacts with the decapping machinery and promotes mRNA decay (Tharun et al., 2000). The enzyme Edc3 plays a central role in modulation of decapping and P-body integrity, as shown previously in various studies in yeast and human cells (Ling et al., 2008). We monitored the expression pattern of all three reporters at different time points during ageing in *C. elegans* and, as expected, all factors accumulated in P-bodies. Signals of all three reporters significantly increased in during ageing as measured in the pharyngeal region (Figure 6A to 6C). While LSM-3 localizes into granules but also shows ubiquitous expression throughout cells (Figure 6, A2 to A7), EDC-3 and DCAP-1 aggregate into clearly distinct foci (Figure 6, B2 to B4, and C2 to C4), which increase in size and number, as animals are getting older.

Ageing is accompanied by decreased ability of cells to cope with intrinsic or extrinsic stress. We wanted to see whether mRNP accumulation changes upon various stress insults. We treated day 2 animals carrying the DCAP-1 reporter for P-bodies with stressors such as heat shock for several hours at 35°C, 24 hour starvation, 6 hours exposure to hypoxia and incubation for 30 min in 20 mM of oxidative stressor NaN3. Except treatment with NaN_3, all stress factors resulted in increased P-body formation (Figure 6D). We also observed significant increase of EDC-3 specific P-body formation in day 2 animals upon exposure to heat (Figure 8G).

A central factor for cellular stress regulation are mitochondria, which control formation of free radicals (Lenaz, 2001). We aimed to investigate the involvement of disrupted mitochondrial integrity on P-body formation. To achieve this, we down-regulated EAT-3, a homologue of human Opa1, which has been shown to maintain the inner membrane of mitochondria and regulate susceptibility to oxidative stress in *C. elegans* (Kanazawa et al., 2008). Down-regulation of eat-3 gene dramatically increased DCAP-1 P-body formation in whole animals during ageing (Figure 8E). Together these results show that during ageing and stress response P-bodies increase in size and number.

IFE-2 might regulate P-body and stress granule accumulation in aged animals and upon stress insult

We were interested to see whether genetic factors of ageing influence P-body formation. The *C. elegans daf-2* pathway controls longevity and is orthologous to the mammalian insulin-like signaling cascade (Kenyon, 2010). We down-regulated the *daf-2* gene by RNA intereference (RNAi) in animals carrying the DCAP-1 reporter. Throughout lifespan P-body formation was significantly lower compared to control animals (Figure

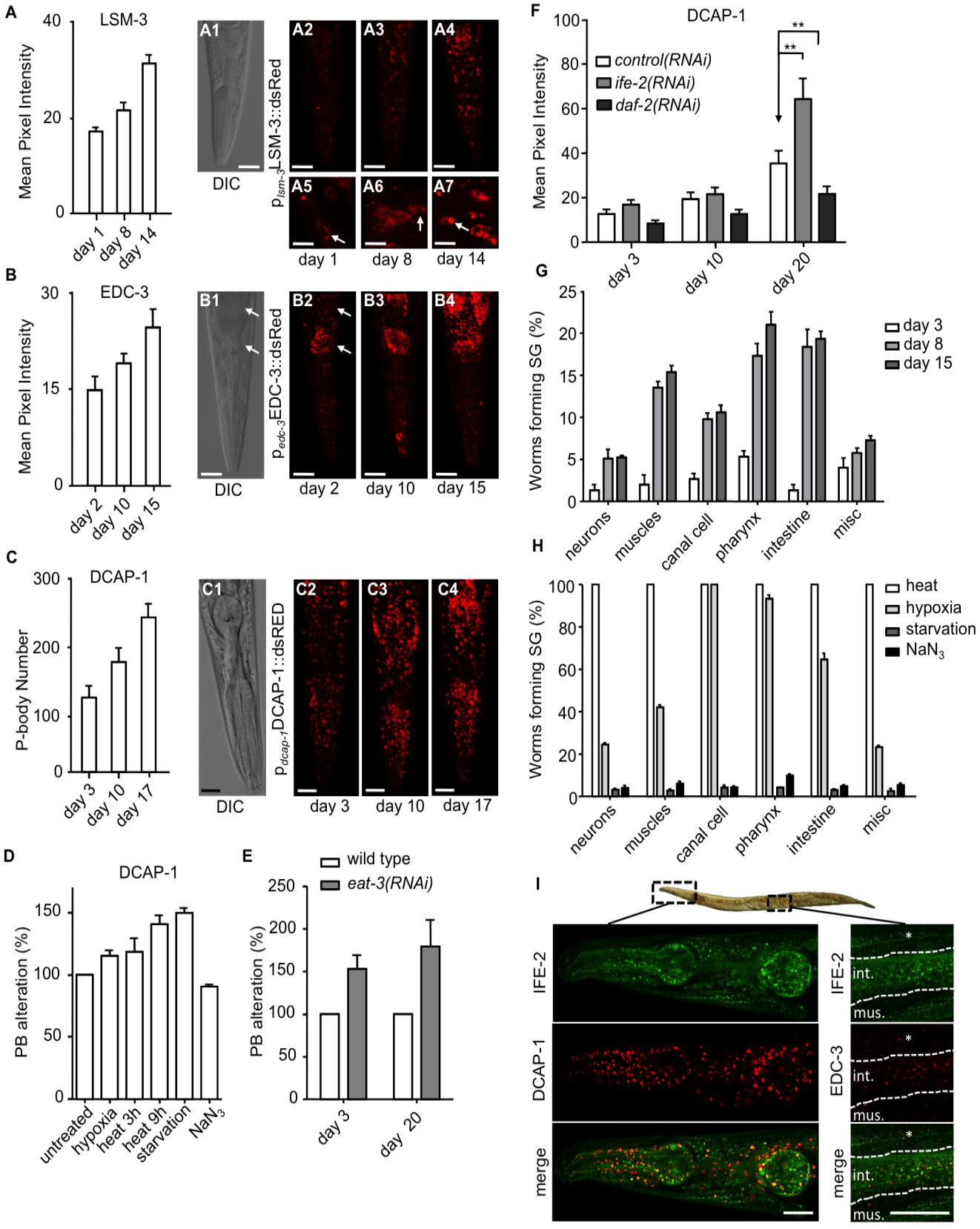

Figure 7: P-bodies and stress granules are biomarkers of ageing and stress response in C. elegans. (A) Mean pixel intensities of animals expressing p_{lsm-3}LSM-3::dsRED specific signal is measured during ageing (error bars show SEM, n=10, experiment was performed three times). (A1) shows a representative DIC image of a day 3 old animals for the pharyngeal region, in which (A2-A4) are representative maximum intensity projection confocal microscopy recordings of LSM-3 specific fluorescent expression. (A2) depicts expression levels at day 1, (A3) at day 8 and (A4) at day 14. Size bars correspond to 50µm. (A5-7) Representative single plane confocal images for LSM-3 specific P-bodies. White arrows depict areas of substantial size increase of P-bodies at different time

points: (A5) day 2, (A6) day 10, and (A7) day 14. **(B)** Mean pixel intensities are quantified for p_{edc-3}EDC-3::dsRED fluorescent expression during three time points in age (error bars show SEM, n=10, experiment was repeated three times). (B1) shows a representative DIC image of the head region while white arrows indicate the areas of interest for measurement as the intestine and the nerve ring located close to the anterior bulb of the pharynx. (B2-B4) show representative maximum intensity projection confocal images for EDC-3 specific fluorescent expression in the head region, while (B2) depicts day 2, (B3) day 10 and (B4) day 15 animal. Size bars correspond to 50µm. **(C)** P-body number counted for p_{dcap-1}DCAP-1::dsRED expression in the pharyngeal region in day 3, day 10 and day 17 old animals (error bars show SEM, n=10). (C1) depicts a representative DIC image for the region of interest and (C2-C4) are representative maximum intensity projections of confocal images for which (C2) shows DCAP-1 expression at day 3, (C3) at day 10 and (C4) at day 17. Size bars correspond to 50µm. **(D)** Alterations in P-Body intensities upon various stress insults are normalized to average expression levels in p_{dcap-1}DCAP-1::dsRED specific expression of day 2 adults. Stress response of P-bodies were measured in worms after 6h treatment in hypoxia chamber, 3h or 6h exposure to 35°C heat, 24h deprivation of food and 30 min incubation in 20µM sodium azide (error bars show SEM, n=40, three independent experiments each). **(E)** P-body intensity alterations are plotted against age stages day 5 and day 20 of control compared to eat-3 RNAi treated animals (error bars show SEM, n=40, three independent experiments). **(F)** Mean pixel intensities of p_{dcap-1}DCAP-1::dsRED measured during ageing in the pharyngeal region upon treatment with RNAi for *ife-2* and *daf-2* genes compared to control in day 3, day 10 and day 17 old animals (error bars show SEM, n=10, p**<0.001, p***<0.0001 experiment was repeated three times). **(G)** Percentage of animals forming stress granules upon the stress insults heat, hypoxia, starvation or sodium azide. Stress granules are counted in neurons, muscles, canal cells, pharynx, intestine and other tissues (misc), (error bars indicate SEM, n=50). **(H)** Percent animals forming stress granules during ageing in various tissues observed at the time points day 3, day 8 and day 15 (error bars indicate SEM, n=50). **(I)** Single plane confocal images showing co-expression of p_{dcap-1}DCAP-1::dsRED or p_{edc-3}EDC-3::dsRED with p_{ife-2}IFE-2::GFP upon heat stress insult. (I1 to I3) Representative images show DCAP-1 and IFE-2 co-localization in the head region. (I4 to I6) EDC-3 and IFE-2 are shown to co-localize in neurons (asterisk), intestine (int) and muscle cells (mus).

6F). We further focused our attention on *ife-2*, which has been shown to regulate ageing via control of global protein synthesis in *C. elegans* (Syntichaki et al., 2007). Its homolog eIF4E is also known to localize to both P-bodies and stress granules upon arrest of mRNA translation (Buchan et al., 2008). Further, loss of translation initiation leads to increased P-body formation in yeast (Nissan et al., 2010). Down-regulation of *ife-2* significantly enhances P-body formation in aged animals (Figure 6F).

We tempted to show whether eIF4E localizes to mRNP aggregates in *C. elegans* and used animals expressing IFE-2 specific translational reporter to visualize granule formation. Generally, IFE-2 is ubiquitously expressed across all cells and tissues in *C. elegans* (Figure 7 and 8). We observed appearance of granulation in specific tissues during ageing and upon various stress insults. The number of animals aggregating IFE-2 in granules significantly increased between days 3 and 8 across tissues including

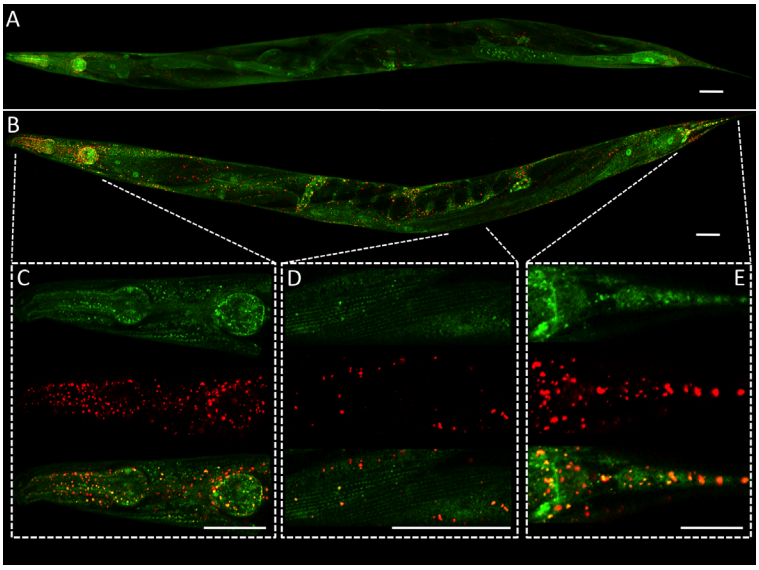

Figure 7: DCAP-1 P-bodies and IFE-2 stress granules co-localize upon heat stress throughout all tissues in C. elegans. All size bars correspond to 50µm. **(A and B)** Merged maximum intensity projections of confocal images of day 3 adult animals co-expressing p_{dcap-1}DCAP-1::dsRED and p_{ife-2}IFE-2::GFP. **(A)** Animal prior to heat shock. **(B)** Animal after 1.5 hours heat shock. **(C-E)** Single plane confocal images showing IFE-2, DCAP-1 and merged expression patterns. **(C)** Close up on pharyngeal region. **(D)** Muscle cells around the midsection of the animal. **(E)** Tail region of the animal.

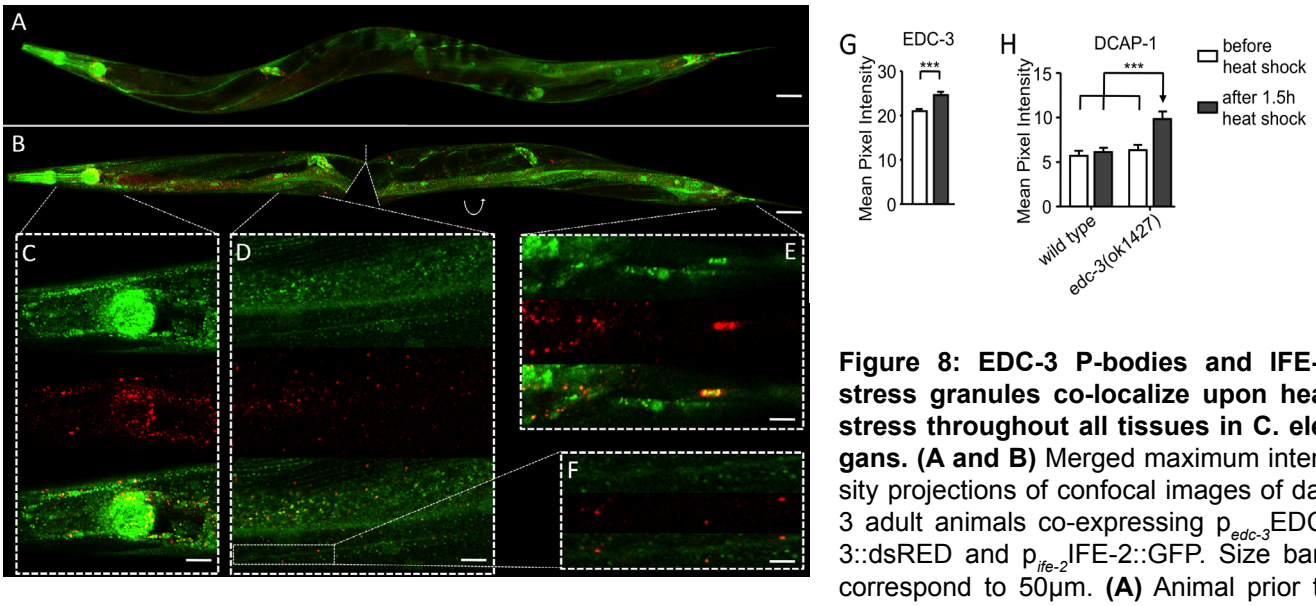

Figure 8: EDC-3 P-bodies and IFE-2 stress granules co-localize upon heat stress throughout all tissues in C. elegans. (A and B) Merged maximum intensity projections of confocal images of day 3 adult animals co-expressing p_{edc-3}EDC-3::dsRED and p_{ife-2}IFE-2::GFP. Size bars correspond to 50µm. **(A)** Animal prior to heat shock. **(B)** Animal after 1.5 hours heat shock. **(C to F)** Single plane confocal images showing IFE-2::GFP, EDC-3::DsRED and merged channels of selected regions. **(C)** Head region around posterior bulb. Size bar corresponds to 20µm. **(D)** Muscle cells and part of axon of the ventral nerve cord (VNC) around the midsection of the animal. Size bar corresponds to 10µm. **(E)** Tail region of the animal. Size bar corresponds to 5µm. **(F)** Co-localization of EDC-3 and IFE-2 reporters along the axon of the VNC of the zoom in on the inlay of D. Size bar corresponds to 5µm. **(G)** Mean pixel intensity of p_{edc-3}EDC-3::dsRED for whole animals measured before and after 1.5 hours exposure to heat in day 1 adults (error bars indicate SEM, n=40, p***<0.0001). **(H)** Measurements of p_{dcap-1}DCAP-1::dsRED after 1.5 hours heat shock in wild type or *edc-3* mutant animals at day 1 of adulthood (error bars indicate SEM, n=40, p***<0.0001).

neurons, muscles, pharynx, canal cell and intestine (Figure 1G). We tested the stress insults hypoxia (6h in hypoxia chamber), heat (1.5h at 35°C), NaN3 (30min incubation in 20mM), starvation (24h food deprivation) and prolonged incubation in liquid medium (1h in saline solution) and noted that stress granule formation was total upon heat stress in all tissues and animals. Hypoxic condition induced stress granules in some tissues to a lower extend, while NaN3 and starvation did not show such effects (Figure 6H).

We were interested to see whether IFE-2 specific stress granules co-aggregate with P-bodies, as it has been shown in yeast and mammalian cells (Balagopal and Parker, 2009). We created co-expressing transgenics and observed that upon heat stress IFE-2 granules co-localize with DCAP-1 and EDC-3 P-bodies throughout tissues (Figure 6I, Figure 7 and Figure 8). We also observed localization of P-bodies and IFE-2 stress granules in bordering proximity, which has previously been described as docking of granules (Balagopal and Parker, 2009). These results show that the eIF4E homologue IFE-2 localizes to stress-induced granules that co-localize with P-bodies in *C. elegans*.

The decapping activator EDC-3 modulates lifespan in *C. elegans*

Since decapping specific reporters increase in intensity during ageing, we asked whether interference with specific components of the pathway could result in lifespan alterations. To answer this question, we down-regulated key target genes of the general mRNA degradation pathway by RNAi, including the well conserved *lsm-1*, *ccr-4*, *dcap-1*, *dcap-2* and *edc-3* in wild type nematodes. While knockdown of *edc-3* resulted in a significant elongation of lifespan, the other genes did not show any effect on ageing (data not shown). To extend our study on the role of EDC-3 in ageing we performed life span experiments with animals carrying the *edc-3(ok1427)* allele, which showed an even more robust longevity effect compared to *edc-3* RNAi (Figure 9A). Conversely, over-

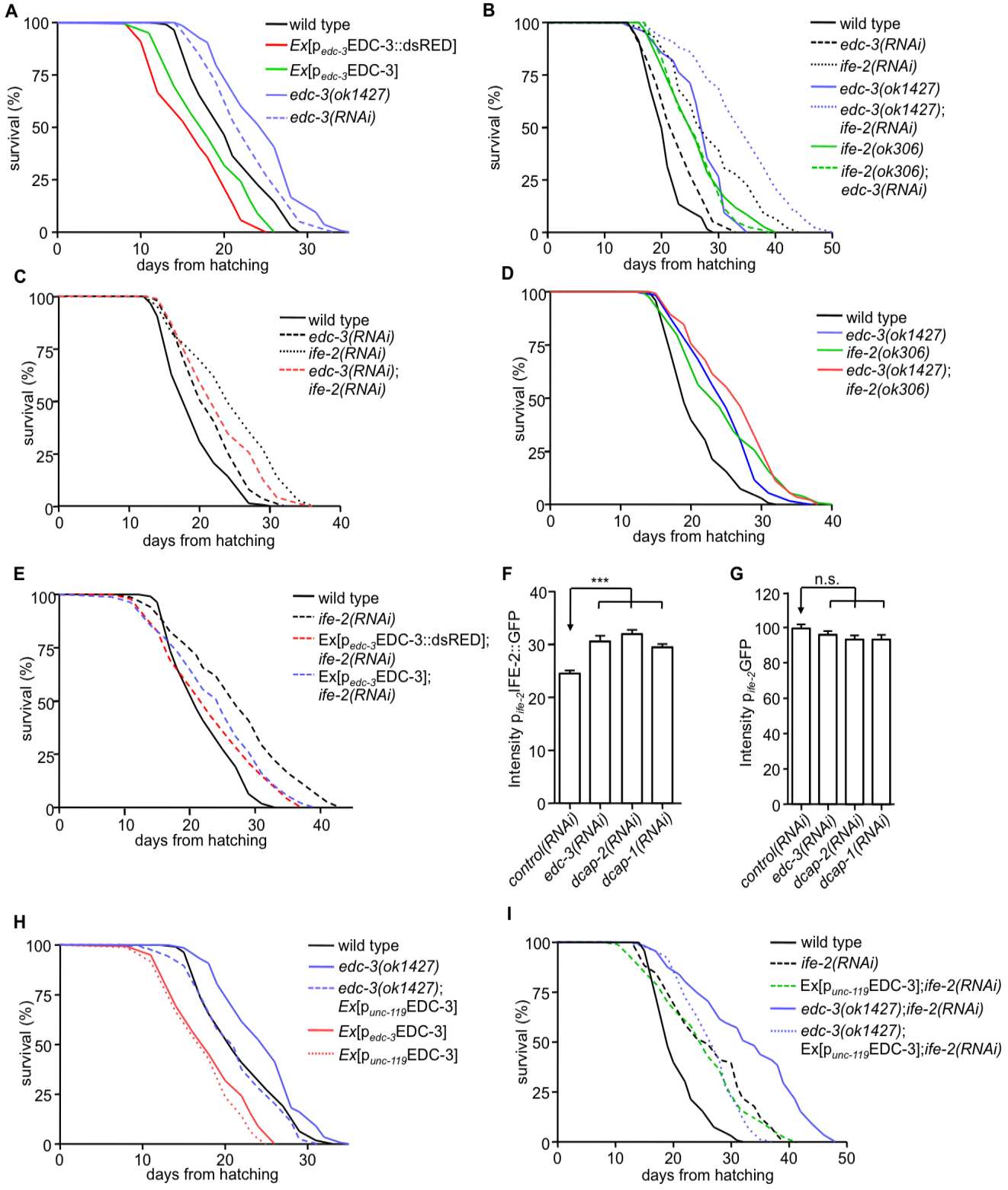

Figure 9: EDC-3 stabilizes IFE-2 and regulates ageing in a neuron-specific manner. All lifespan assays were performed at 20°C and percentage of survival is plotted against age. **(A)** Animals carrying extrachromosomal array for overexpression of EDC-3 under its endogenous promoter are short-lived compared to wild type. Down-regulation of *edc-3* gene by RNAi results in longevity, which is more substantial in animals harboring the *edc-3(ok1427)* allele. **(B)** Animals carrying the mutant allele *ife-2(ok306)* or *edc-3(ok1427)* show extended lifespan compared to wild type, while RNAi for *ife-2* causes more substantial longevity than RNAi for *edc-3* gene. Upon down-regulation of *edc-3*, *ife-2* mutant lifespan is not further enhanced. Knockdown of *ife-2* gene in *edc-3* mutants causes substantial lifespan increase. **(C)** Lifespan comparison of animals upon down-regulation of *edc-3* and *ife-2* genes individually or double RNAi treatment. **(D)** Animals harboring either the mutant allele *ife-2(ok306)* or *edc-3(ok1427)* are long-lived compared to wild type, while the double-mutant does not show any further increase in lifespan. **(E)** Animals carrying extrachromosomal arrays for overexpression of EDC-3 under its endogenous promoter grown on

control or *ife-2* RNAi. **(F)** Down-regulation of *dcap-1*, *dcap-2* and *edc-3* in animals carrying the IFE-2 translational reporter (Error bars show SEM, n=40, p<***0.0001, three independent experiments). **(G)** The three genes *dcap-1*, *dcap-2* and *edc-3* are downregulated in animals carrying the transcriptional reporter for IFE-2 (Error bars show SEM, n=40, p>0.05, three independent experiments). **(H)** Lifespan comparison between wild type and animals carrying *edc-3(ok1427)* allele overexpressing EDC-3 under the control of its endogenous or the panneuronal promoter of the gene *unc-119*. **(I)** Wild type or animals harboring *edc-3(ok1427)* allele and overexpressing EDC-3 in neurons are treated with control or *ife-2* RNAi.

expression of EDC-3 under the control of its endogenous promoter showed a significant reduction in lifespan (Figure 9A). These results indicate that EDC-3 modulates ageing in *C. elegans*.

We investigated whether loss of EDC-3 changes animal morphology or causes other obvious changes in behavior that might contribute to the longevity phenotype. Neither *edc-3* mutant nor *edc-3* RNAi treated animals showed significant differences in pharyngeal pumping of bacterial food, sinusoidal locomotion, dauer formation, developmental timing and tissue morphology. We observed a slight but significant reduction in egg laying and body size in *edc-3* mutant worms compared to wild type (Figure 10C)0

We investigated whether the effects of loss of *edc-3* converse with previously described mechanisms that influence ageing in nematodes. Long-lived clk-1 mutants show reduced respiration promoted by an age-dependent decrease in mitochondrial function (Felkai, 1999). Additional loss of *edc-3* increases lifespan extension observed in clk-1 deficient animals (Figure 10A). Loss of the *C. elegans* insulin/IGF receptor homologue DAF-2 leads to a dramatic increase in lifespan (Kenyon et al., 2002). Down-regulation of *edc-3* further enhances longevity of animals carrying *daf-2*(e1370) allele (Figure 10B). We also studied a possible crosstalk of *edc-3* mediated effects on ageing with dietary restriction. Loss of *eat-2* causes a decrease

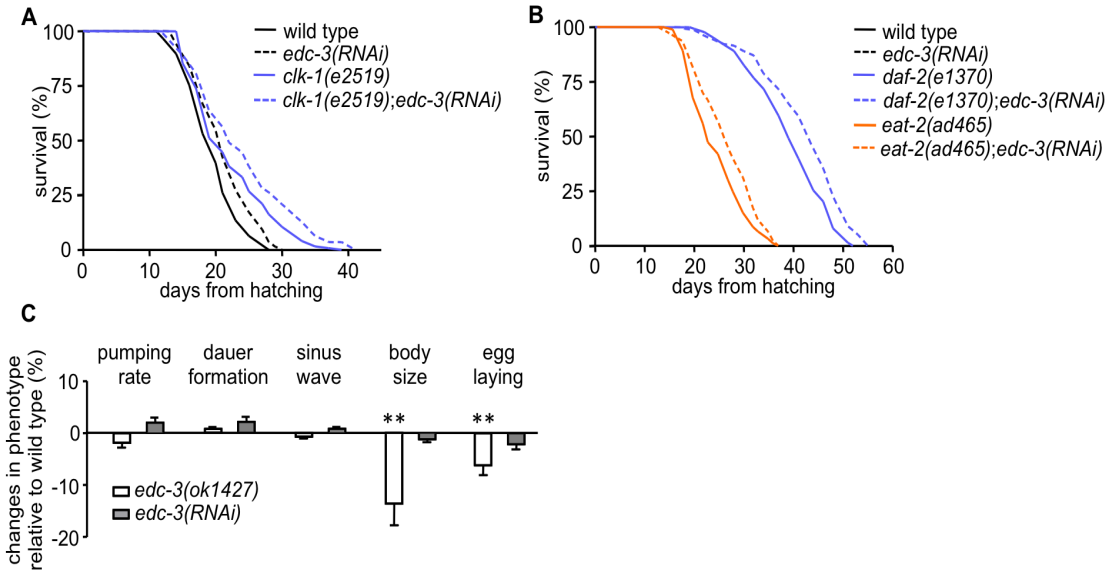

Figure 10: Extended lifespan and phenotypical analysis upon depletion of EDC-3. All life span assays were carried out at 20°C, percent of animals alive is plotted against age. **(A)** Comparison of lifespan assays was carried out for wild type or animals carrying *clk-1(e2519)* allele upon down-regulation of *edc-3* gene. **(B)** Lifespan assays upon down-regulation in animals harboring *daf-2*(e1370) or *eat-2*(ad465) allele. **(C)** Percent changes in phenotypes in relation to wild type levels measured for pharyngeal pumps (per minute), percent dauer formation upon starvation, variance in locomotion of sinusoidal wave, body length (in mm) in gravid adults, rate of egg laying within 4 hours at day one of adulthood (all measurements were repeated twice, p**<0.001).

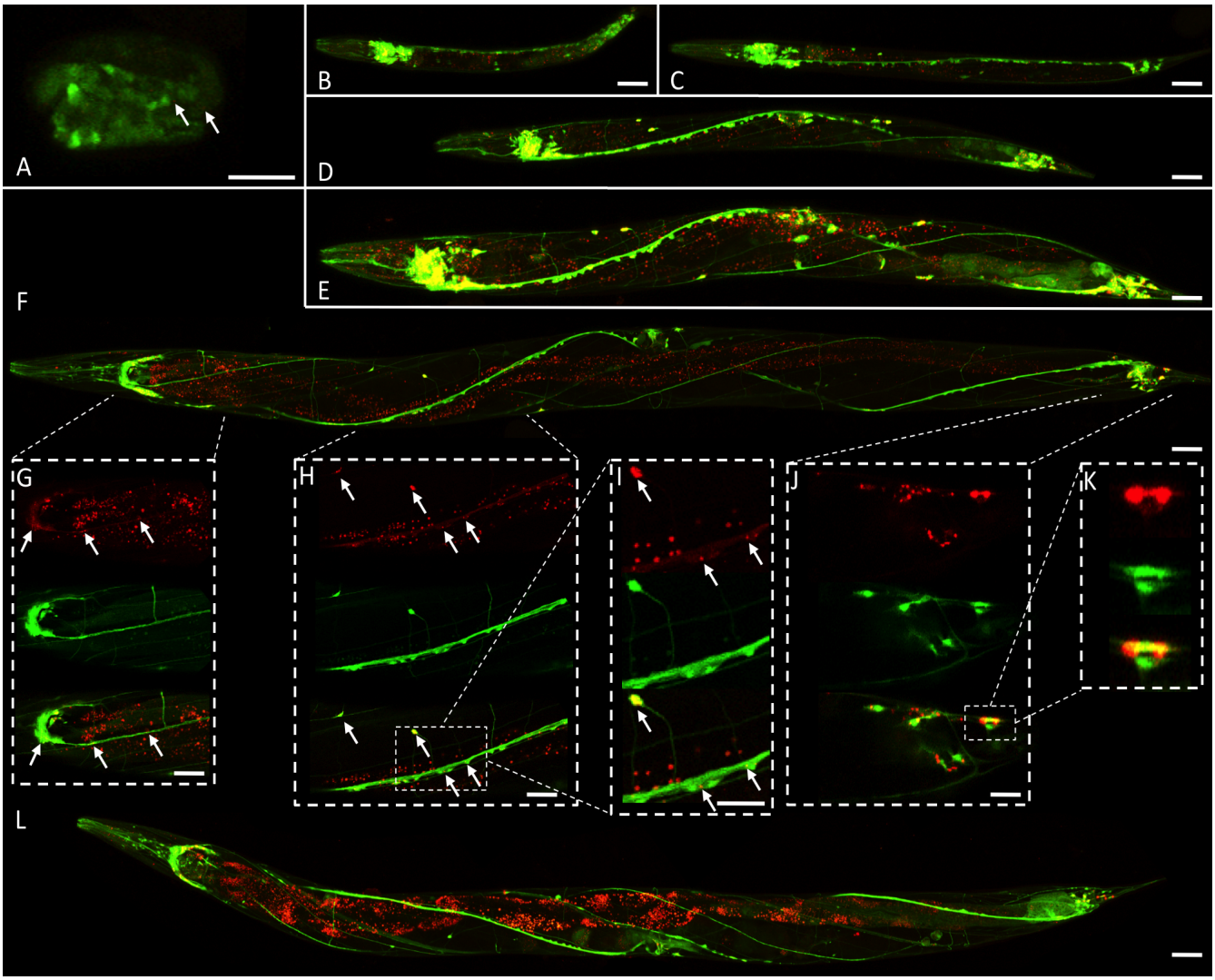

Figure 11: EDC-3 PBs localize to the intestine and the neuronal system during ageing. Animals co-expressing p_{edc-3}EDC-3::dsRED and $p_{unc-119}$GFP pan-neuronal promoter driven fluorescence. (A-F and L) Maximum intensity projections of confocal images for different developmental and ageing stages of *C. elegans*: **(A)** early embryos, **(B)** L1, **(C)** L2, **(D)** L3, **(E)** L4 larval stage, **(F)** day 3 adults and **(L)** day 8 adults. Scale bars correspond to 50µm. (G-K) Representative images show single plane confocal recordings for closer analysis of co-localization in day 3 adult animal. Size bars correspond to 25µm. **(G)** Expression of EDC-3 P-bodies in the neuronal system (white arrows point to expression in VNC) and the intestine is shown in an area close to the nerve ring. Further, ubiquitous expression of EDC-3 is observed all along axons. **(H)** Area close to the mid-body shows EDC-3 P-body expression in synapses of the VNC, some commissural neuron (white arrows), in surrounding cells of the intestine and ubiquitously along axons. **(I)** Digital zoom on the area indicated in (H) enhancing neuronal (white arrows) and intestinal expression of EDC-3. **(J)** Ubiquitous and P-body specific expression of EDC-3 in tail neurons with **(K)** close up on strong expression of EDC-3 P-bodies at hillocks of cell bodies.

in pharyngeal pumping, which in turn lowers food intake and therefore triggers dietary restriction dependent longevity in *C. elegans* (Lakowski and Hekimi, 1998). Knockdown of *edc-3* further increases lifespan of dietary restricted *eat-2* mutants (Figure 10B). These results indicate that lifespan extension upon loss of *edc-3* is independent of clk-1, *eat-2* and *daf-2* pathways.

EDC-3 and IFE-2 interact in neurons to control lifespan

We down-regulated *edc-3* in animals carrying *ife-2(ok306)* allele, which are reported to be long-lived (Syntichaki et al., 2007). Contrary to the results from other long-lived mutants, we did not observe any further increase in lifespan (Figure 9B). Conversely, *ife-2* knockdown in *edc-3* mutant worms led to a substantial increase in lifespan, which

was twofold compared to wild type animals (Figure 9B). This result prompted us to ask whether EDC-3 and IFE-2 control ageing in parallel or in a co-dependent fashion. Simultaneous down-regulation by RNAi of *edc-3* and *ife-2* did not produce any additive effect on ageing compared to single knockdown (Figure 9C). Also, lifespan assays performed with a genetic cross of strains carrying *edc-3(ok1427)*;*ife-2(ok306)* alleles compared to their controls did not show any significant further extension of lifespan (Figure 9D). Animals overexpressing EDC-3 under its endogenous promoter treated with RNAi for *ife-2* gene were short-lived compared to their respective control (Figure 9E). Further, we observed that upon down-regulation of *edc-3* or its interacting partners in the decapping process, *dcap-1* and *dcap-2*, the IFE-2 reporter signal increased significantly, while intensity levels of the transcriptional reporter for the *ife-2* gene were not affected (Figure 9F and 9G).

The decapping enzyme Dcp2 is directly bound and activated by Edc3 as it has been shown in yeast and mammalian cells (Harigaya et al., 2010). Down-regulation of DCAP-2 homologue in *C. elegans* by RNAi did not result in longevity and animals carrying *dcap-2*(ok2023) allele did not show an increase in lifespan. Double knockdown for *edc-3* and *dcap-2* genes resulted in a slight but significant reduction of lifespan (-10%), indicating an interdependent role in the regulation of ageing in *C. elegans*. Down-regulation of *dcap-2* causes significant reduction of the longevity phenotype observed in animals carrying *ife-2(ok306)* allele, while down-regulation of *ife-2* increases *dcap-2* mutant lifespan (data not shown). Together, these results suggest that the process of mRNA decapping might interact with the mechanism of translation initiation towards positively controlling the process of ageing.

The fact that *ife-2* down-regulation in animals harboring *edc-3(ok1427)* allele led to a robust lifespan extension, while *edc-3* knockdown did not result in increased longevity in *ife-2* mutants (Figure 9B), pushed forward the hypothesis that the observed interaction in ageing might be neuron-specific. Feeding RNAi is robust in virtually all cells in *C. elegans* except in neurons (Kamath et al., 2003). To verify this experimentally, we created transgenic lines expressing EDC-3 specifically in neurons under the control of panneuronal promoter for the *unc-119* gene in wild type and *edc-3* mutant animals. In both cases overexpression resulted in reduction of lifespan down to control levels (Figure 9H). Further, we down-regulated *ife-2* in animals harboring *edc-3(ok1427)* allele that overexpress EDC-3 in neurons. The result was a reduction of lifespan to levels observed in animals treated with *ife-2* RNAi . Down-regulation of *ife-2* in transgenics expressing neuron-specific EDC-3 resulted in the same lifespan extension, as seen upon *ife-2* depletion in wild type (Figure 9I). These results further indicate a neuron-specific role for EDC-3, possibly DCAP-2, and IFE-2 mediated control of lifespan.

Analysis of neuron-specific functions of EDC-3

We decided to verify the neuronal localization of EDC-3::DsRED reporter by co-localization studies with panneuronal promoter *unc-119* driven GFP. EDC-3 P-bodies are ubiquitously expressed in all tissues the four larval stages (L1 to L4); the signal reduces in adults in most tissues except intestine and neuronal network where fluorescence increases. EDC-3 specific P-bodies concentrate in cell bodies of neurons at the hillocks, but the protein is also ubiquitously expressed and forms smaller granules within axons (Figure 11 and 12A). Time lapse recording of the EDC-3 specific signal revealed that the bigger aggregates are static but smaller granules seem to dynamically flow through cells and axons (data not shown). We set out to understand the specific mechanisms EDC-3 could promote in neurons.

We expressed panneuronal GFP in wild type and animals harboring *edc-3(ok1427)* allele and studied the morphology of the neuronal system during ageing. Firstly,

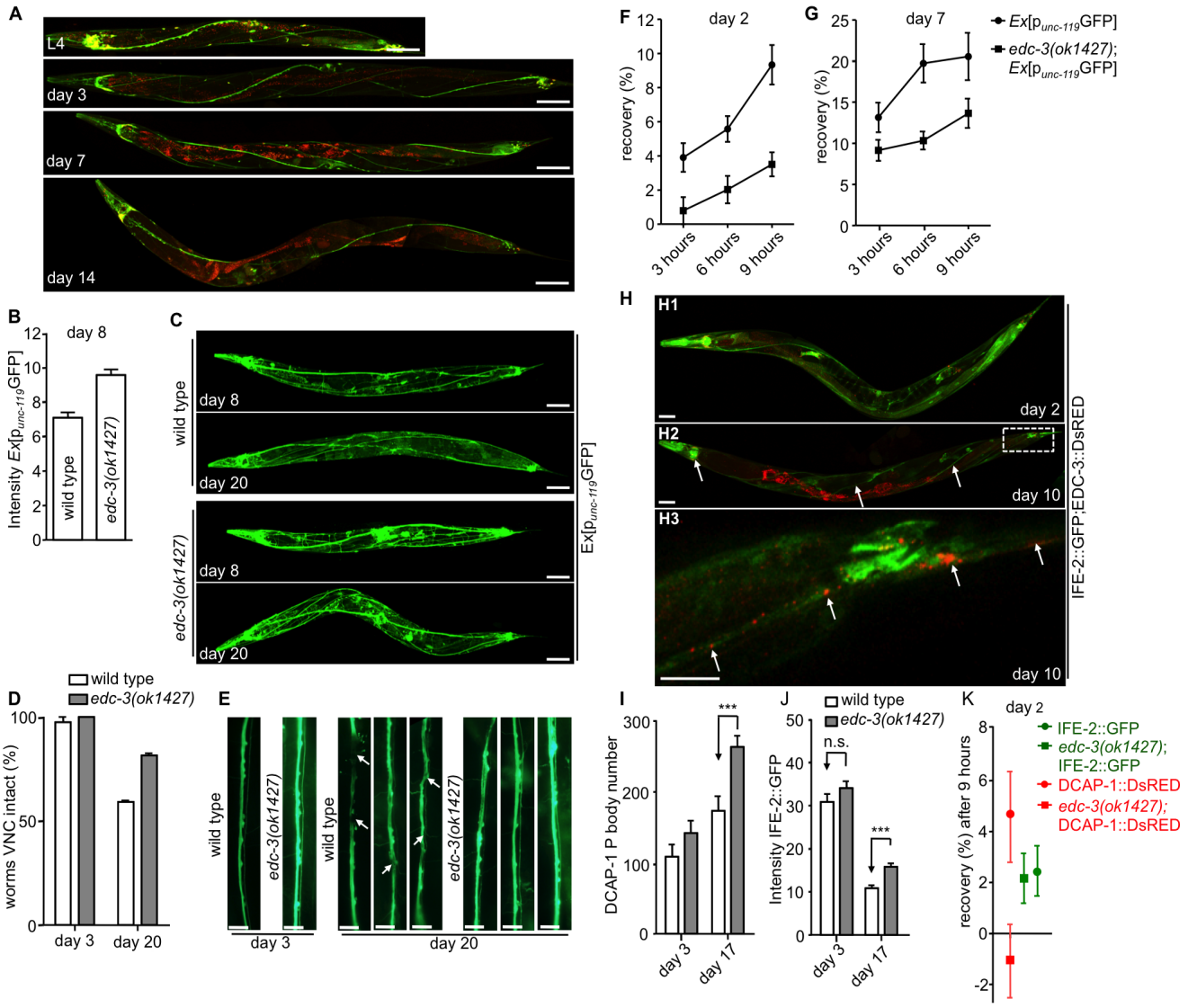

Figure 12: Studies on neuron-specific functions of EDC-3. **(A)** Animals co-expressing p_{edc-3}EDC-3::dsRED and pan-neuronal $p_{unc-119}$GFP. Maximum intensity projections of confocal images are depicted for L4, day 3, day 7 and day 14 adults. Size bars correspond to 100µm. **(B)** GFP levels in animals expressing the panneuronal reporter $p_{unc-119}$GFP compared between wild type and *edc-3* mutant animals at day 8 (error bars show SEM, n=40, three independent experiments). **(C)** Representative maximum intensity confocal images of day 8 and day 20 old animals expressing panneuronal GFP in wild type or *edc-3* mutants. Size bars correspond to 100µm. **(D)** Worms expressing the panneuronal $p_{unc-119}$GFP reporter are scored for defects and disturbance in morphology of the VNC. Wild type worms show a significantly higher irregularity in VNC appearance then *edc-3* mutants (error bars show SEM, n=25, experiment repeated three times). **(E)** Representative images of the VNC in animals at day 3 and day 20. Disturbances in neuronal morphology, such as breakage, dissolving or deformation are compared between wild type and *edc-3* mutant. Size bars correspond to 10µm. **(F and G)** FRAP in the neuronal system of animals carrying *edc-3(ok1427)* allele compared to wild type. Percentage of fluorescent recovery during time is observed in the area of the nerve ring of (F) day 2 or (G) day 7 adult animals (Error bars show SEM, n=24). **(H)** Merged maximum intensity projections of representative confocal images for animals co-expressing p_{edc-3}EDC-3::dsRED and p_{ife-2}IFE-2::GFP at (H1) day 2 and (H2) day 10 adults. (H3) Single plane confocal images show merged expression patterns of the tail area indicated in H2. Co-localization along axons and in neuronal cell bodies is depicted with white arrows. Scale bar corresponds to 50µm. **(I)** P-body count in animals expressing DCAP-1::DsRED reporter in wild type or *edc-3* mutant during ageing (error bars show SEM, n=25, p***<0.0001, three independent experiments). **(J)** Mean pixel intensity of IFE-2::GFP reporter in wild type or animals carrying *edc-3(ok1427)* allele during ageing (error bars show SEM, n=25, p***<0.0001, three independent experiments). (K) FRAP analysis of DCAP-1::DsRED and IFE-2::GFP reporters in wild type compared to *edc-3* mutants (Error bars show SEM, n=24).

we noted that GFP intensity in *edc-3* mutants was significantly increased compared to wild type in aged animals (Figure 12B). A general view on the whole neuronal system in *edc-3* mutants revealed a more stringent integrity of axonal complexity in aged animals (Figure 12C). For detailed analysis, we focused on abnormalities of the ventral nerve cord (VNC). The VNC consists of two parallel axon bundles that stretch the whole body length of the adult animal, a large bundle of approximately 40 axons that is separated by an epithelial layer from a second smaller bundle of 3 to 5 axons (White et al., 1976). We focused on quantifying obvious phenotypes in VNC bundles previously described in *C. elegans* for touch neurons, including apparent breaks, waving and acute bends of axons (Toth et al., 2012). The analysis revealed an age dependent decrease of VNC integrity in day 20 old animals, which was significantly lower in *edc-3* mutants (Figure 12D and 12E).

The indications collected for a possible interaction of EDC-3 and IFE-2 pathways during ageing in the neuronal system prompted us to measure fluorescent recovery after photobleaching (FRAP). Down-regulation of *ife-2* gene results in decreased de novo protein synthesis (Syntichaki et al., 2007). We developed a novel protocol, which does not require any anesthetic treatment, allows photobleaching of specific areas, such as the nerve ring, and recovery measurements on plate (see Materials and Methods). We showed that the neuron-specific fluorescent signal expressed in day 2 or day 7 adult wild type worms recovers in a significantly higher rate than in animals carrying *edc-3(ok1427)* allele. Interestingly, general recovery rates were higher in day 7 compared to day 2 adults (Figures 12D and 12E). We went on to study co-localization of IFE-2 and EDC-3 enzymes during age. We noted that levels of IFE-2::GFP substantially decrease during age, but appear to be stabile in specific tissues including canal cells, neurons and in the pharyngeal and tail region, while simultaneously levels of EDC-3::DsRED increased in intestinal cells and neurons (Figure 12H1 to 12H3).

We further counted DCAP-1 P-body number in animals harboring *edc-3(ok1427)* allele and observed significantly increased levels in aged worms compared to wild type (Figure 12I). Mutations in *edc-3(ok1427)* allele also significantly increased IFE-2::GFP levels in aged animals in comparison to wild type (Figure 12J). We performed FRAP analysis in animals co-expressing DCAP-1::DsRED and IFE-2::GFP. De novo synthesis of IFE-2 protein did not exceed 3% of the initial fluorescent level even after about 9 hours of recovery. In parallel, we noted that DCAP-1 signal recovered in a higher rate in wild type compared to *edc-3* mutants (Figure 12K).

Loss of EDC-3 induces stress resistance pathways and ROS formation

In order to further define the mechanism of EDC-3 in the regulation of ageing, we performed a series of experiments to determine a possible role in stress resistance. To that purpose, we studied the effect of *edc-3* down-regulation in mutants that are hypersensitive to oxidative stress. *C. elegans* carrying mutation in the mitochondrial integral membrane protein cytochrome b MEV-1, which is part of the respiratory chain complex II (ubiquinol-cytochrome c reductase) are short-lived and sensitive to stress (Ishii et al., 2011). Similarly, the subunit of mitochondrial complex I GAS-1 is required for oxidative phosphorylation, stress response and ageing (Kayser et al., 2001). Knockdown of *edc-3* gene rescued the short-lived phenotype of mev-1 and gas-1 mutants, respectively (Figure 13A and 13B). Further, we applied the chemicals paraquat (PQ) and sodium azide (NaN_3) to trigger oxidative stress response. Day 7 old animals carrying *edc-3(ok1427)* allele or treated with *edc-3* RNAi showed increased resistance to either drug (Figure 13C and 13D).

To further validate an involvement of EDC-3 gene in stress management, we studied the activation of a transcriptional reporter for the iron/manganese superoxide dismutase

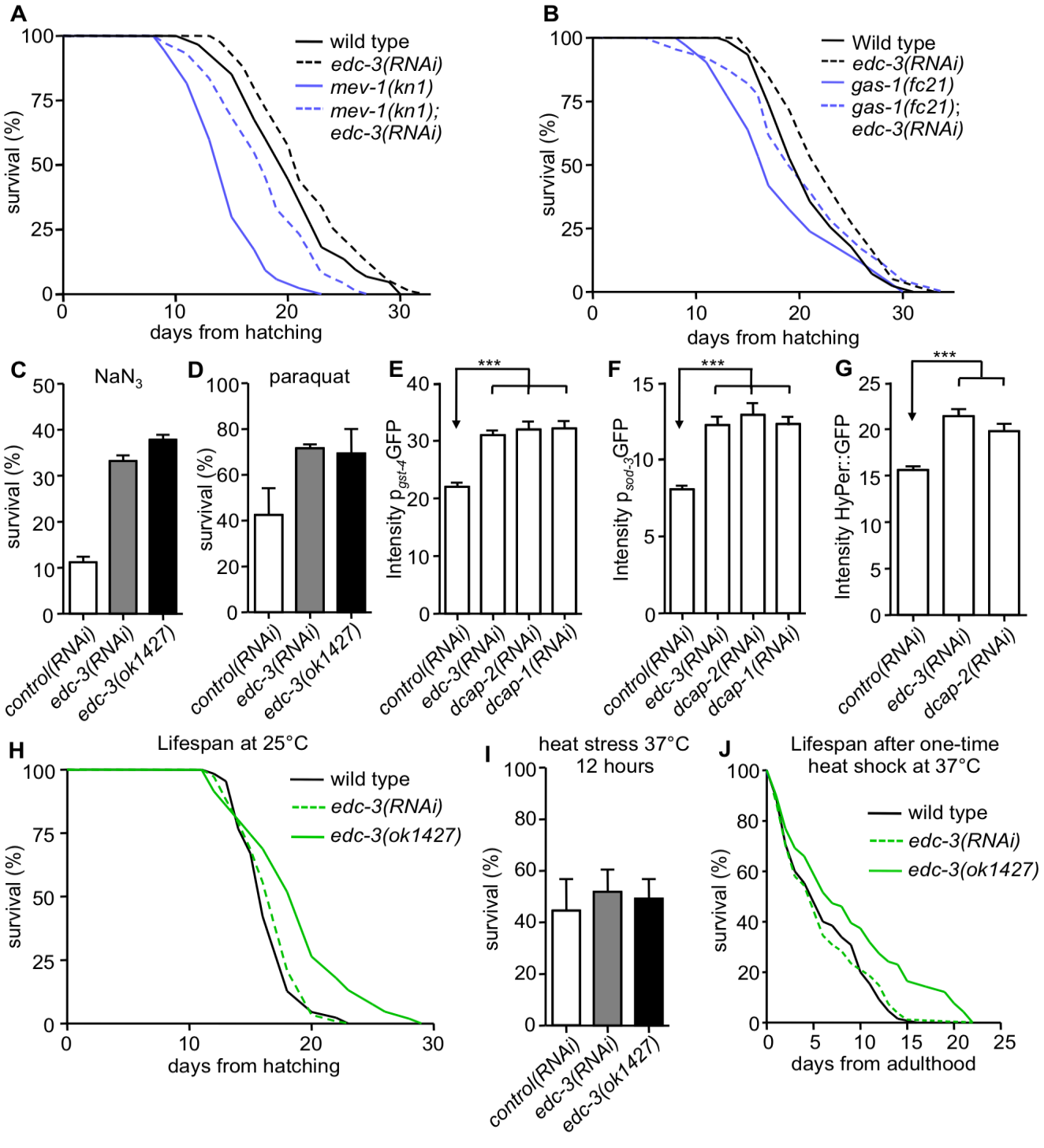

Figure 13: Loss of decapping enzymes induces oxidative stress resistance. (A and B) Lifespan assays were carried out at 20°C and animal survival is plotted against age. (A and B) Down-regulation of *edc-3* gene in wild type nematodes compared to short-lived (A) *mev-1* or (B) *gas-1* mutants. **(C)** Percentage survival of day 7 old population under oxidative stress induced by treatment with NaN_3 (three independent experiments, n=80, error bars are SEM). **(D)** Survival of day 7 old nematodes upon oxidative stress induced by the herbicide paraquat (three independent experiments, n=80, error bars denote SEM). **(E)** Fluorescent expression level of p_{gst-4}GFP reporter is significantly increased upon down-regulation of *dcap-1*, *dcap-2* and *edc-3* genes (three independent experiments, n=40, error bars denote SEM, p***<0.0001). **(F)** Fluorescent expression level of p_{sod-3}GFP is significantly increased upon down-regulation of *dcap-1*, *dcap-2* and *edc-3* genes (three independent experiments, n=40, error bars are SEM, p***<0.0001). **(G)** Mean pixel intensity of HyPer::GFP strain sensing cellular H_2O_2 level are shown upon down-regulation of *edc-3* and *dcap-2* (three independent experiments, n=80, error bars are SEM, p***<0.0001). **(H)** Lifespan assay at 25°C of animals upon loss of *edc-3*. Survival is plotted against age. **(I)** Percent of survival after 12 hours of continuous heat shock at 37°C (three independent experiments, n=100, error bars are SEM). **(J)** Animals were exposed to 4 hours heat shock at 37°C at day 2 of adulthood and thereafter scored for survival. Survival of animals upon down-regulation of *edc-3* and *edc-3* mutants is plotted against age.

SOD-3, which is involved in oxidative stress response and directly transcribed by DAF-16 (Honda and Honda, 1999). Down-regulation of either decapping activator *edc-3* or its interacting partners *dcap-1* or *dcap-2* led to a significant increase in the reporter signal p_{sod-3}GFP (Figure 13E). In animals carrying *daf-2* mutation, DAF-16 is fully activated and sod-3::GFP levels are strongly enhanced (Libina et al., 2003). Loss of decapping enzymes *edc-3*, *dcap-1* and *dcap-2* further increases the signal (data not shown). We also investigated involvement of the SKN-1 transcription factor target gst-4m which encodes a putative glutathione-requiring prostaglandin D synthase (Kahn et al., 2008). Knockdown of *edc-3*, and also *dcap-1* or *dcap-2* in worms carrying the transcriptional reporter for pgst-4GFP significantly increased the fluorescent signal (Figure 13F). To visualize possible alterations in ROS levels in EDC-3 depleted *C. elegans* we utilized a strain expressing the tagged H_2O_2 sensing protein HyPer (Back et al., 2012). Upon treatment with *edc-3* or *dcap-2* RNAi the fluorescent signal of HyPer was activated (Figure 13G).

We further decided to study the involvement of EDC-3 in resistance to increased temperature and heat shock. We performed ageing studies at 25°C and observed that lifespan extension upon down-regulation of *edc-3* was lost, while *edc-3* mutants still showed robust longevity compared to control animals (Figure 13H). A constant exposure to 37°C at day 2 of adulthood, performed over a time span of 12 hours did not result in any difference compared to wild type (Figure 13I). Conversely, when day 2 adults were heat shocked at 37°C for four hours and thereafter scored until death, lifespan of *edc-3* mutants

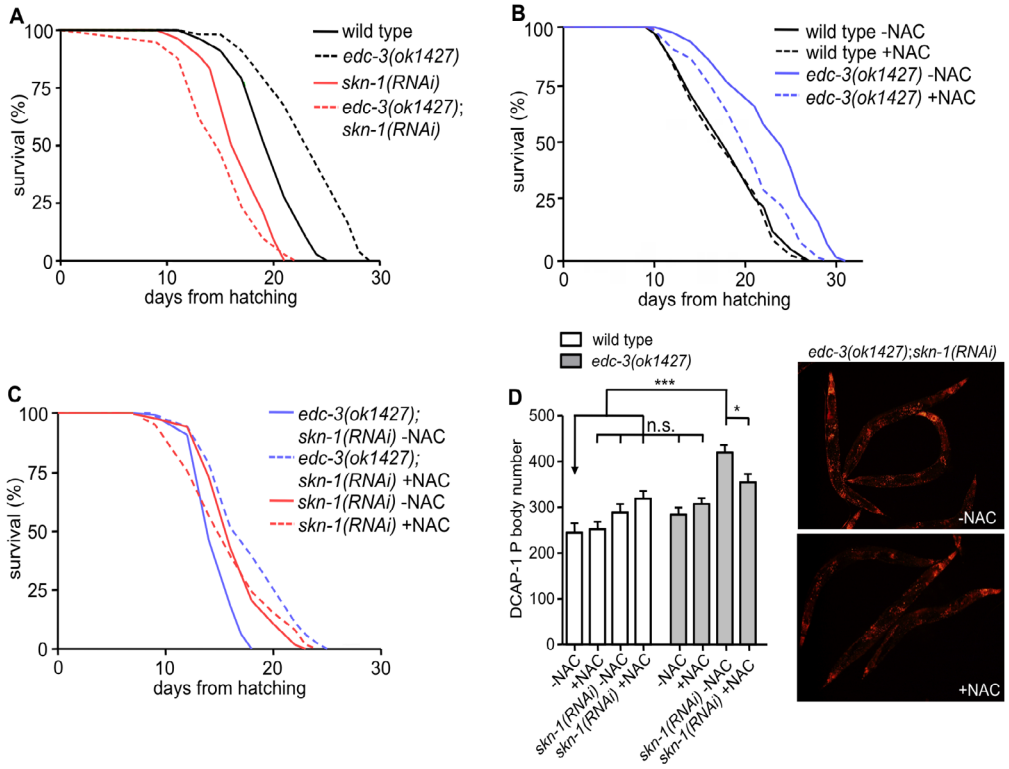

Figure 14: SKN-1 controls lifespan extension and P-body formation in *edc-3* mutants via hormesis. All lifespan assays were carried out at 20°C and animal survival is plotted against age. All P-body quantification were performed at day 8 of adulthood expressing p_{dcap-1}DCAP-1::dsRED in wild type or *edc-3* mutant animals **(A)** Lifespan measurements of wild type or animals harboring *edc-3(ok1427)* upon knockdown of *skn-1*. **(B)** Lifespan assays comparing wild type and *edc-3* mutant worms upon continuous treatment with NAC. **(C)** Lifespan comparison of animals lagging *skn-1* alone or additional loss of *edc-3*, with or without treatment with NAC. **(D)** P-body quantification upon down-regulation *skn-1* gene with or without NAC treatment (error bars show SEM, n=25, experiment was performed three times, *p<0.01, ***p<0.0001).

was increased compared to control, while *edc-3* RNAi did not result in longevity (Figure 13J). These results collectively imply a role for EDC-3 in stress regulation.

Lifespan extension upon loss of EDC-3 is mediated by HSF-1, SKN-1 and hormesis

We investigated transcriptional regulation of EDC-3 mediated control of lifespan. The forkhead box, subgroup O (FOXO) transcription factor DAF-16, which is suppressed by the activity of insulin/insulin-like growth factor (IGF) receptor DAF-2 (abnormal dauer formation-2), and the in parallel acting bZip transcription factor SKN-1 are well studied regulators of stress resistance and ageing in *C. elegans* (Kenyon, 2010; Tullet et al., 2008). Further, the heat shock transcription factor HSF-1 activates the expression of specific genes including small heat shock proteins, that promote longevity (Hsu et al., 2003). We observed equivalent rates of reduction in lifespan upon down-regulation of *daf-16* in wild type and *edc-3* mutant animals (Figure 15A). We found that down-regulation of *hsf-1* gene in animals carrying *edc-3(ok1427)* results in an epistasis effect and reduces lifespan extension to levels of wild type treated with *hsf-1* RNAi (Figure 15C). Strikingly, *skn-1* down-regulation showed substantial lifespan reduction of *edc-3* depleted animals to levels even below *skn-1* single knockdowns (Figure 14C).

Based on the epistasis study with SKN-1 and the fact that loss of EDC-3 activates oxidative stress response and ROS production (Figure 13G), we hypothesized the involvement of a hormesis-dependent response. Hormesis is defined as low-dose induction of stress, that conditions cells and organisms to higher stress resistance, which results in increased lifespan (Cypser et al., 2001). It has previously been shown that lifespan of several *C. elegans* long-lived mutants is reduced upon treatment with ROS scavengers such as N-acetyl-cysteine (NAC) or vitamin C (Yang and Hekimi, 2010). We decided to treat *edc-3* mutants with NAC and observed a significant reduction in lifespan (Figure 14B). We attempted to see whether the dramatic decrease in lifespan of *edc-3* mutants upon loss of *skn-1* might be dependent on hormesis. Indeed, treatment with NAC resulted in rescue of the epistatic effect of *skn-1* down-regulation in animals carrying *edc-3(ok1427)* allele. Life span shortage of animals upon loss of *skn-1* alone was not altered upon NAC treatment (Figure 14C).

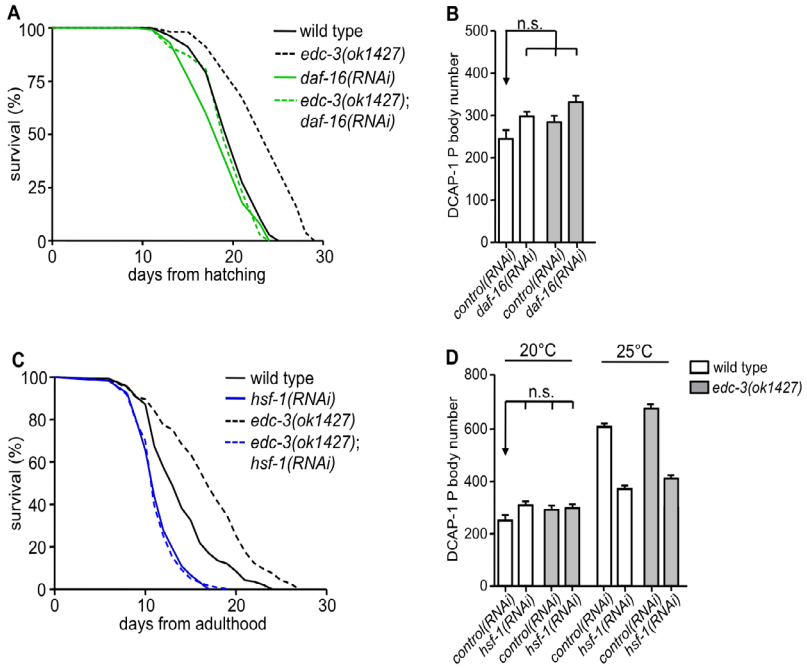

Figure 15: HSF-1 controls *edc-3* mutant lifespan and P body formation upon heat stress. All lifespan assays were carried out at 20°C and animal survival is plotted against age. All P-body quantification were performed at day 8 of adulthood expressing p_{dcap-1}DCAP-1::dsRED in wild type or *edc-3* mutant animals. **(A)** Lifespan comparison of wild type and *edc-3* mutant animals upon down-regulation of *daf-16*. **(B)** Life span assay upon down-regulation of *hsf-1* in wild type and animals harboring *edc-3(ok1427)* allele. **(C)** P-body quantification upon down-regulation of *daf-16*, **(D)** P-body quantification upon down-regulation of *hsf-1*, at 20°C (day 8) or 25°C (day 6).

Figure 16: HSF-1 controls IFE-2 stability and stress granule formation.
All measurements were performed three times, n=25, all error bars indicate SEM, p**<0.001, p***<0.0001. **(A)** Percent animals forming stress granules upon down-regulation of *daf-16*, *skn-1* or *hsf-1* genes observed in various tissues at day 8 of adulthood. **(B)** Quantification of mean pixel intensities for p_{ife-2}IFE-2::GFP of whole animals during ageing. **(C)** Mean pixel intensities of transcriptional reporter p_{ife-2}GFP during ageing. **(D)** Measurements of p_{ife-2}IFE-2::GFP expression levels upon loss of *daf-16*, *skn-1* or *hsf-1* gene in wild type animals at day 8 of adulthood. **(E)** Intensity measurements of transcriptional reporter p_{ife-2}GFP upon loss of *hsf-1* at day 8 of adulthood. **(F)** Maximum intensity projections of confocal images of day 8 adult animals co-expressing p_{ife-2}IFE-2::GFP and p_{dcap-1}DCAP-1::dsRED upon down-regulation of *hsf-1* in wild type or *edc-3* mutants. Size bars indicate 50µm. Red arrows shows nuclei with visible or enhanced IFE-2 expression, white arrows show areas of IFE-2 granulation.

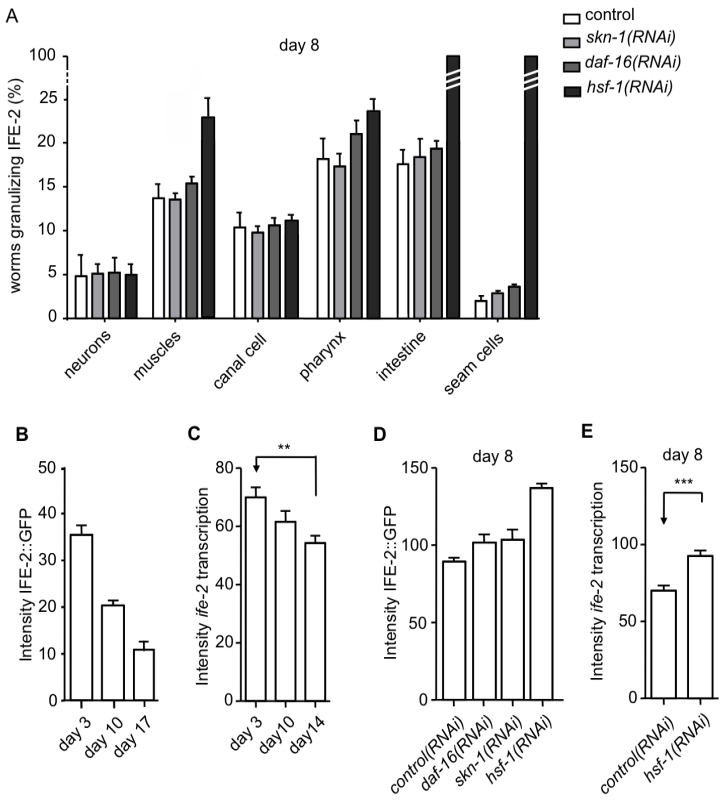

SKN-1 and EDC-3 co-regulate P-body formation

Since we showed that decapping enzymes increasingly accumulate during ageing in *C. elegans*, we decided to study a possible involvement of transcriptional regulators of ageing and stress response in the formation of P-bodies. We down-regulated *daf-16*, *skn-1* or *hsf-1* in animals carrying DCAP-1 P-body reporter. Loss of neither transcription factors during ageing and measured in day 4 (data not shown) and day 8 (Figure 14D and Figure 15B and D) wild type animals resulted in significant changes of P-body number. The fact that SKN-1 and HSF-1 act epistatic on EDC-3 prompted us to investigate whether P-body levels are altered in *edc-3* mutants upon down-regulation of *hsf-1*, *daf-16* or *skn-1*. Surprisingly, only upon knockdown of *skn-1* DCAP-1 aggregation in day 8 adults was significantly enhanced compared to control, while loss of neither *hsf-1* or *daf-16* produced such effects (Figure 14D). Since we had shown the involvement of hormesis in the lifespan extending process, we decided to treat wild type and *edc-3* mutant reporter lines with the ROS scavenger NAC. In wild type and upon *skn-1* knockdown, we detected no alterations in P-body levels. NAC also did not affect P-bodies in *edc-3* mutants, while it markedly reduced the elevated levels upon additional loss of *skn-1* (Figure 14D).

HSF-1 regulates IFE-2 and P-body formation during stress and ageing

Upon down-regulation of *hsf-1* we did not observe any changes in P body formation when animals were grown under favorable conditions at 20°C, neither in young nor in old stages (Figure 15D). However, when we maintained animals under stress conditions at increased temperature at 25°C, we recognized that P-body formation was significantly induced in day 8 old animals and that this phenotype was suppressed upon loss of *hsf-1*. The same results we obtained in animals carrying *edc-3(ok1427)* allele (Figure 15D).

We had shown that IFE-2 localizes to stress granules during ageing and we set out to investigate whether loss of transcriptional

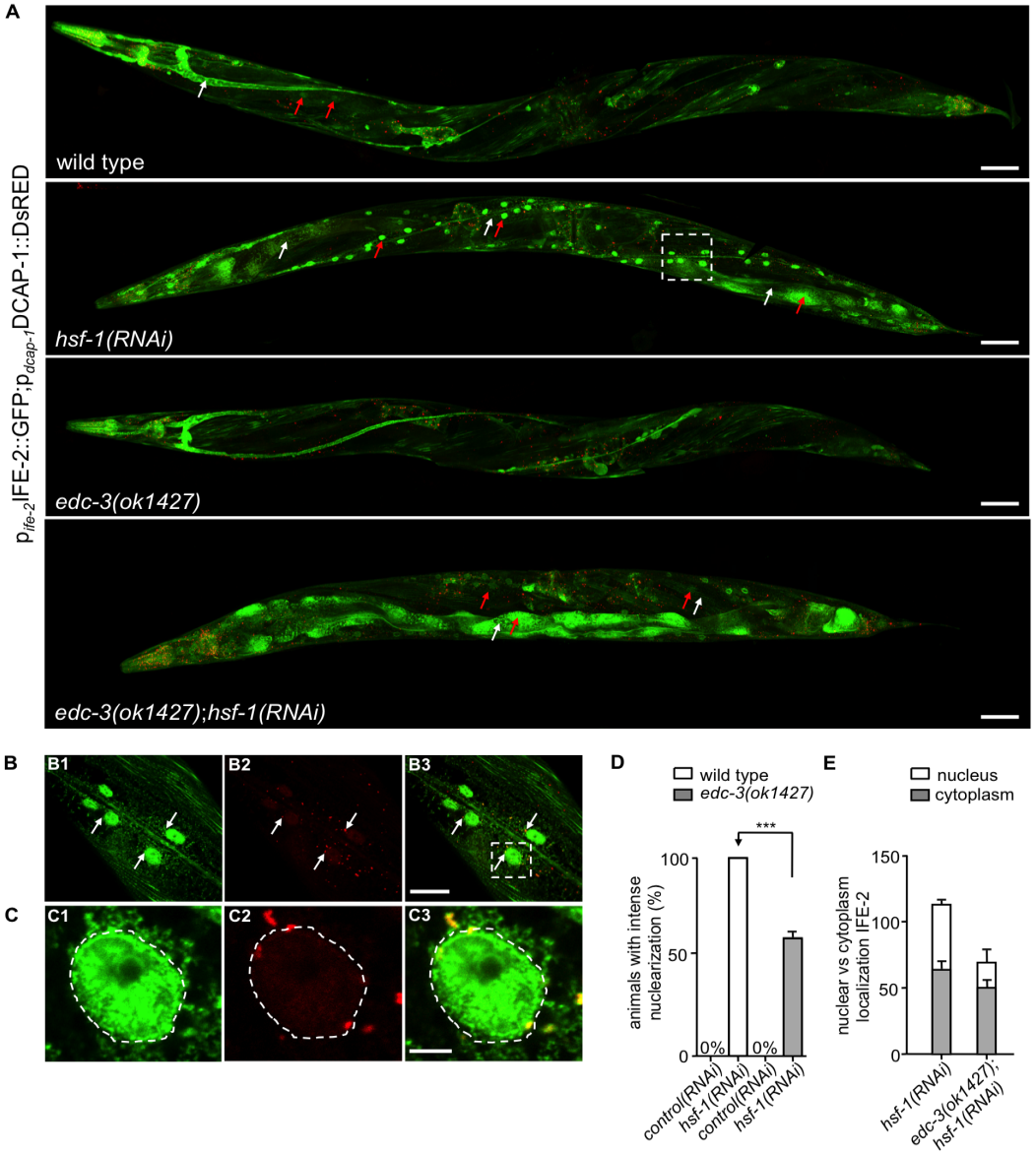

Figure 17. Heat shock response and EDC-3 co-regulate compartmentalization of IFE-2.
(A) Representative confocal images of seam cells showing extensive nuclear localization and granulation of IFE-2 and co-localization with DCAP-1 in close proximity to nuclei upon loss of *hsf-1* gene (area highlighted in F). Size bar corresponds to 10µm. Arrows indicate P-body and IFE-2 granule co-localization at nuclear periphery. (A1) Expression of p_{ife-2}IFE-2::GFP, (A2) expression of p_{dcap-1}DCAP-1::dsRED and (A3) merged fluorescent signals. Size bar corresponds to 10 µm. **(B)** Single plane confocal images show IFE-2 aggregation within the nucleus highlighted in G3 and co-localization with DCAP-1 reporter along the periphery. Dashed line indicates nuclear envelope. (B1) Expression of p_{ife-2}IFE-2::GFP, (B2) expression of p_{dcap-1}DCAP-1::dsRED and (B3) merge of signals. **(D)** Quantification of percentage of animals displaying enhanced nuclearization phenotype as observed and represented in panels G to I. **(E)** Ratios of mean pixel intensities measured in the nuclear area and compared to standardized size in the cytoplasm compared between wild type and *edc-3* mutant animals.

regulators of stress and ageing might regulate this phenomenon. We monitored animals carrying IFE-2::GFP reporter upon down-regulation of *daf-16*, *skn-1* or *hsf-1* at day 4 and day 8 of adulthood. In aged animals, loss of *skn-1* and *daf-16* did not alter IFE-2 granulation compared to control animals, while loss of *hsf-1* resulted in a severe increase of IFE-2 granules in several tissues including muscle, intestine and seam cells (Figure 16A and Figure 17A). We quantified general expression levels of IFE-2::GFP during ageing and observed that the reporter signal gradually decreased as animals aged (Figure 16B). Also, the transcriptional reporter driven by the *ife-2* promoter decreased, although not as significantly (Figure 16C). We measured IFE-2::GFP reporter signal in aged animals and ob-

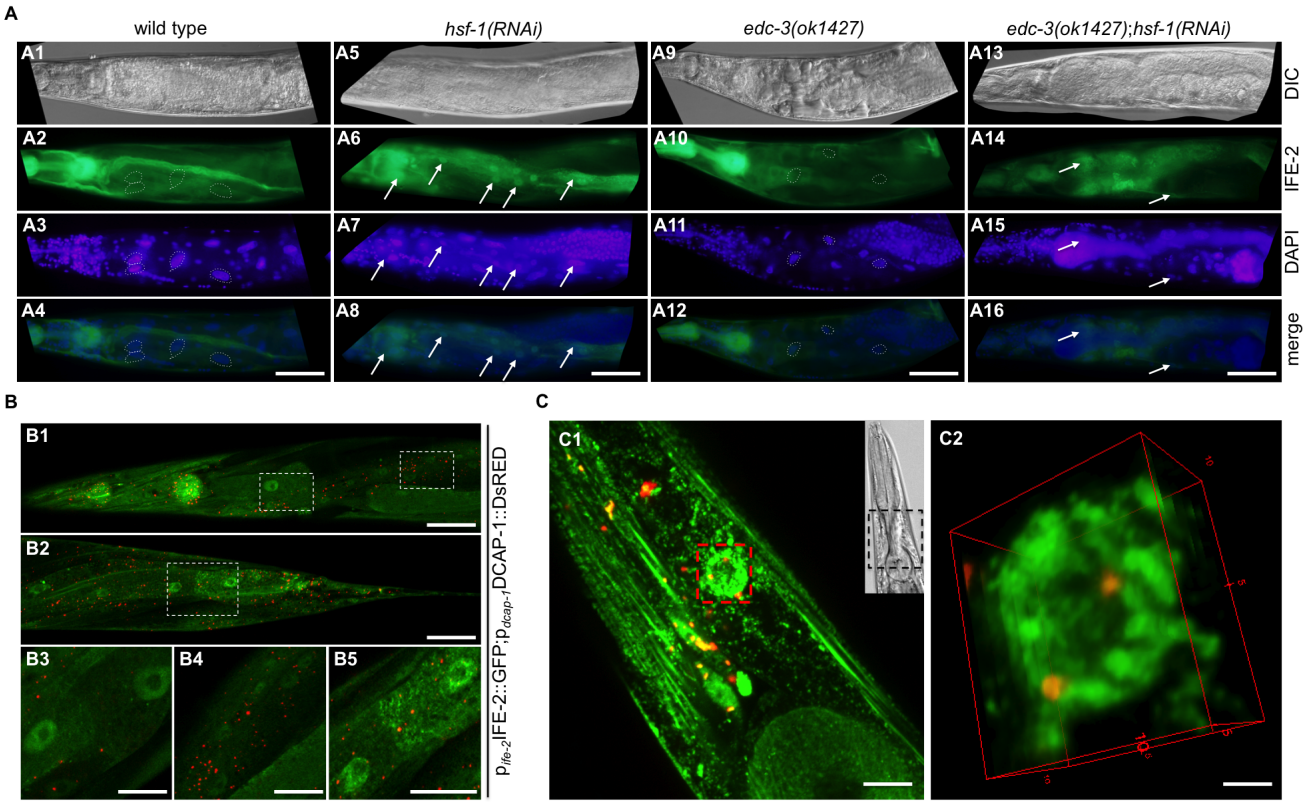

Figure 18: Extended analysis of nuclearization of IFE-2 upon loss of *hsf-1* gene in wild type and *edc-3* mutant animals. (A) Epifluorescent images of ventral part of day 8 old animals expressing p_{ife-2}IFE-2::GFP co-stained with DAPI, and DIC reference image. (A1 to A4) Otherwise wild type animals show co-localization of homogeneously expressed IFE-2 with DAPI throughout all tissues and cell types. (A5 to BA) Upon down-regulation of *hsf-1*, IFE-2 signal co-nuclearizes with DAPI across tissues including intestinal, muscle and seam cells. (A9 to A12) Animals carrying *edc-3(ok1427)* allele appear similar in co-localization pattern compared to wild type. (A13 to A16) Knockdown of *hsf-1* in *edc-3* mutant animals causes less significant nuclearization of IFE-2 signal compared to wild type treated with *hsf-1* RNAi. Size bars in all merged images indicate 50µm. **(B)** Confocal images of wild type animals co-expressing p_{ife-2}IFE-2::GFP and p_{dcap-1}DCAP-1::dsRED with focus on areas of the animals showing nuclearization of IFE-2 in what we identify as hypodermal and muscle cells: (B1) Anterior region and (B2) posterior region of the animal. Size bars indicate 50µm. (B3 to B5) Close view on nuclei of areas indicated in B1 and B2. Size bars correspond to 5 µm. **(C)** Confocal imaging based 3D analysis of nuclear IFE-2 granulation and co-localization with DCAP-1. (C1) Single plane confocal image of pharyngeal region of a day 8 adult animal co-expressing p_{ife-2}IFE-2::GFP and p_{dcap-1}DCAP-1::dsRED upon down-regulation of *hsf-1* in wild type. The DIC image inlay indicates the recorded region close to the second bulb of the pharynx. Size bar corresponds to 10µm. (C2) 3D reconstructed nucleus based on multiple confocal planes displaying co-localization of DCAP-1 and IFE-2 granules in the nuclear envelope. Size bar corresponds to 1µm.

served that upon loss of *skn-1* and *daf-16* levels were comparable to wild type, while suppression of *hsf-1* resulted in a substantial increase (Figure 16D). Stress granule formation and a general increase of IFE-2::GFP levels were also obtained in *edc-3* mutant animals (data not shown). Measurements at the same age of animals carrying the *ife-2* transcriptional reporter also showed significantly increased fluorescence (Figure 16E).

HSF-1 and EDC-3 co-regulate compartmentalization of IFE-2 between cytoplasm and nucleus

Additional to the increase and granulation of IFE-2 signal we detected a third drastic phenotypic change upon down-regulation of *hsf-1* in aged animals: IFE-2 signal was dramatically enriched in nuclei of various tissues including muscle, intestine, as well as epidermal and seam cells (Figure 17A and Figure 18A). The IFE-2 homologue eIF4E has been reported to be involved in transport of specif-

ic mRNAs from the nucleus to the cytoplasm (Culjkovic et al., 2006; 2007). Curiously, we observed that IFE-2 was present in nuclei of wild type animals and the intensity compared to the cytoplasm was somewhat higher in some cell types, including intestinal and hypodermal tissues (Figure 18B). Also, we recognized that DCAP-1 P-bodies localized in close to direct proximity to nuclei (Figure 17B and C, Figure 18C).

To verify nuclearization, we performed DAPI staining in wild type and *edc-3* mutants with or without *hsf-1* RNAi treatment at day 8 of adulthood. We confirmed that IFE-2 is expressed within the cytoplasm and nuclei of wild type and *edc-3* mutant (Figure 18A). Down-regulation of *hsf-1* strongly enriched the IFE-2 signal in nuclei (Figure 18A and 18C). We recorded IFE-2 nuclearization in seam cells of animals treated with *hsf-1* RNAi by confocal microscopy scans and confirmed increased nuclear signal and granulation. Further, we detected that IFE-2 granules also form within the cell core and co-localized with DCAP-1 P-bodies in the cytoplasm and at the periphery of nuclei (Figure 17B and C, Figure 18C). We did not observe any similar phenotypes upon down-regulation of *skn-1* or *daf-16* (data not shown).

Since we had observed an epistasis effect of HSF-1 on EDC-3, we were interested to investigate IFE-2 related phenotypes upon *hsf-1* down-regulation in animals carrying *edc-3(ok1427)* allele. We detected three notable phenotypes compared to control treated with *hsf-1* RNAi: (I) IFE-2 signal was also significantly upregulated in *edc-3* mutants, (II) granulation of IFE-2 was similar to control but (III) nuclearization of IFE-2::GFP was significantly lower compared to control. We set out to quantify the difference in nuclear enrichment of IFE-2 and noted that just about 50% of *edc-3* mutants upon *hsf-1* down-regulation resembled this phenotype (Figure 17D). Further, we measured the intensity ratio of IFE-2 specific signal in the nucleus compared to the cytoplasm. Nuclei with enriched IFE-2 signal in animals carrying *edc-3* mutation were showing relatively reduced levels compared to the control (Figure 17E). Together these results point to a significant role of HSF-1 and EDC-3 in the co-regulation of IFE-2.

Discussion

The role of mRNA turnover in ageing

The involvement of mRNP turnover in regulation of various cellular mechanisms has been studied in detail (see Introduction). Whether this process might be involved in the regulation of ageing remains unknown. The work presented here provides an array of evidence for a possible mechanism underlying the control of ageing in *C. elegans* by the highly conserved modulator of decapping EDC-3. We collected compelling proof that EDC-3 controls lifespan through various modes: (I) EDC-3 interfaces with protein synthesis, possibly through interaction with IFE-2 specifically in neurons, and thereby also regulates neuronal integrity. We also find that EDC-3 mediated control of ageing possibly acts cell-non-autonomously; (II) EDC-3 is involved in the induction of mitohormesis and the subsequent activation of stress response factor SKN-1; (III) EDC-3 might stimulate eIF4E mediated export of mRNPs from the nucleus to the cytoplasm and thereby promote translation in various tissues in *C. elegans*.
Further, we identify that P-bodies and stress granules function as biomarkers of ageing. The assembly of those cellular aggregates might be controlled by the transcriptional activity of the well-known regulators of stress response and ageing HSF-1 and SKN-1. These findings indicate that P-bodies and stress granules might have a causative correlation with stress and ageing processes (compare Figure 20, 21 and 22).

Neuronal specific regulation of ageing by EDC-3

Our results provide phenotypical support for the idea that EDC-3 influences ageing largely through its neuron-specific activity. First, we observed a significantly milder effect of *edc-3* RNAi (15%) versus the *edc-3* specific mutation on health and longevity of *C. elegans* (30%; compare Figure 10A). This difference could be explained by the fact that functionality of RNAi is impaired in neuronal tissue of nematodes (Kamath et al., 2003). Also, neuron-specific expression of EDC-3 driven by a well-studied pan-neuronal promoter for the gene unc-119 is sufficient to rescue EDC-3 mediated lifespan regulation (Figure 9H and 9I; Maduro, 1995). Further, expression analysis of EDC-3 revealed its increased accumulation during ageing in two cell types: the intestine and neurons (Figure 11 and 12A). Both tissues are known to significantly contribute to control of ageing: The intestine is a major site for lipid storage that responds to daf-2/*daf-16* pathway, while specific sensory systems such as the ASI neurons, have been shown to regulate ageing in *C. elegans* (Ashrafi et al., 2003; Bishop and Guarente, 2007).

Additionally, we performed time lapse recording of EDC-3 in neurons and recorded that EDC-3 P-bodies localized to specific sites within neurons, including hillocks, along axons and in cell bodies (compare Figure 11). Those P-bodies were static but we detected smaller fractions of EDC-3 aggregates dynamically drifting within neurons (data not shown). This indicates that EDC-3 could be part of neuronal transport granules, as previously suggested for other P-body components (Zeitelhofer, 2008; Barbee et al., 2008). More evidence for neuronal specific functions of EDC-3 comes from experiments with animals carrying *edc-3(ok1427)* allele, which display various neuron-specific phenotypes, including increased cellular maintenance during ageing, increased levels of GFP, but lowered de novo protein synthesis (Figure 12D, 12E and 12F). Which neural specific mechanisms does EDC-3 employ to control ageing?

Direct suppression of IFE-2 mediated protein synthesis by EDC-3

Together, our study contains multiple evidence that EDC-3 and IFE-2 might interact in neurons to control ageing. One central observation was that suppression of *edc-3* activity by RNAi in *ife-2* mutants did not alter lifespan, while RNAi mediated down-regulation of *ife-2* in *edc-3* mutant animals led to a dramatic longevity effect (Figure 9B). It was shown in the past that IFE-2, one isoform of its homolog eIF4E, promotes longevity by regulation of global protein synthesis in *C. elegans*. This study also showed that *ife-2* RNAi and animals carrying *ife-2(ok306)* allele show similar lifespan extensions, from which the authors originally concluded that the effect of loss of protein synthesis in neurons on ageing are negligible (Syntichaki et al., 2007). Our repetitions of these experiments revealed that in fact *ife-2* RNAi shows a significantly increased longevity compared to *ife-2* mutants (Figure 9B). Further, simultaneous down-regulation of *edc-3* and *ife-2* by double RNAi or double-knockouts did not result in any additional lifespan extension (Figure 9C and 9D). These results show that a simultaneous IFE-2 presence and EDC-3 absence specifically in neurons is required for the dramatic lifespan increase observed in Figure 10B, hence particularly beneficial for longevity (see Figure 19).

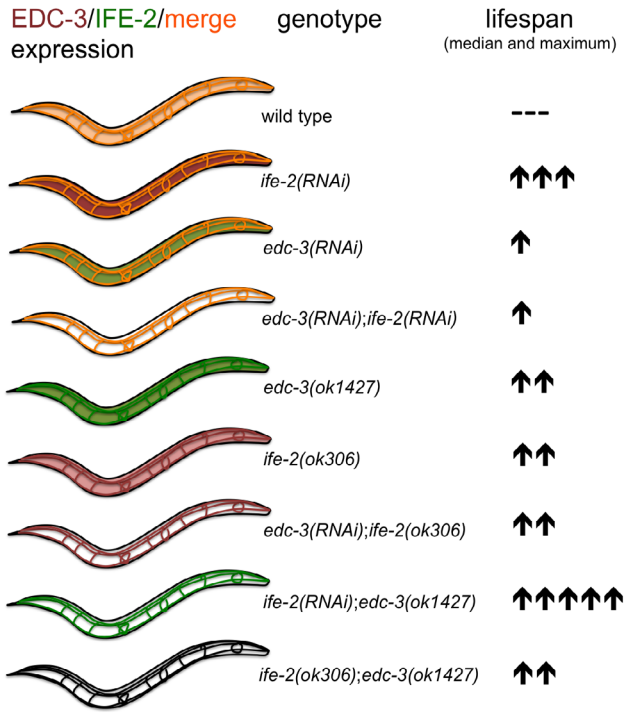

Figure 19: EDC-3 and IFE-2 pathways interact in the regulation neuronal ageing in *C. elegans*. The left column represents theoretical localization expression of EDC-3 and IFE-2, the middle column shows the corresponding genotype, the right column shows semi-quantitative changes in lifespan (compare also Figure 10). The strongest lifespan extension occurs when EDC-3 is depleted in all tissues and IFE-2 is down-regulated in non-neuronal tissues, as achieved through RNAi (compare Figure 10B).

We found indications that absence of EDC-3 might directly influence IFE-2 protein during ageing in neurons: Down-regulation of *edc-3*, and its interacting partners in the decapping process *dcap-1* and *dcap-2*, resulted in stabilization of IFE-2 protein, but did not alter transcriptional regulation (Figure 9E and 9F). Intriguingly, IFE-2 signal strongly decreased during ageing, with the exception of few tissues, which we identified as the canal cells, some axons and cell bodies of the ventral nerve cord, and the areas of the pharynx and tail that include muscles and a highly condensed network of neurons (Figure 12H; pharyngeal neurons; tail neurons). Further, the IFE-2 translational reporter shows an increased signal in aged *edc-3* mutants compared to control animals (Figure 12J). Indeed, several studies in yeast show that formation of the mRNP degradation complex competes for the mRNA cap with translation initiation mediated by eIF4E (Schwartz and Parker, 1999; 2000). The enzymes Scd6, Pat1 and Dhh1 involved in initiation of degradation directly suppress translation factors (Nissan et al., 2010). The same study states that in yeast Edc3 promotes assembly of the degradation complex downstream of translational repression. Our results do not contradict these findings but indicate that *C. elegans* decapping enzymes are more directly involved in suppression of translation. This is further supported by the effect that general neuronal GFP levels driven by *unc-119* promoter are upregulated in aged *edc-3* mutants (Figure 12B). This result indicates that stability of GFP in neurons could be enhanced

upon loss of EDC-3, which might be due to impaired mRNP degradation.

Paradoxically, we showed through FRAP assays that loss of EDC-3 robustly suppresses de novo protein synthesis in neurons (Figure 12F and 12G). The explanation of this contradictory result might derive when considering the nature of mRNP granules: P-bodies are known to be storage site for mRNPs. Such arrested mRNPs can exit P-bodies or stress granules, and reenter translational cycles (Brengues et al., 2008; Teixeira et al., 2005). Blocking mRNA degradation, especially at the stage of decapping, which is mediated by Edc3, results in an increase of P-body formation (Sheth and Parker, 2003). We observed a strongly increased P-body signal in aged *edc-3* mutants as compared to their control (Figure 12I). We hypothesize that loss of EDC-3 stabilizes mRNPs by storing them into P-bodies and detaining them from translation. Transcripts that are crucial for cell maintenance and stress resistance might be staying available for a longer time and might reenter translation cycles in a slower rate during ageing (see Figure 20). The increased stability of IFE-2 specifically in neurons of animals of the genotype *ife-2(RNAi);edc-3*(ok1427) (compare figure 12H and 12J, and Figure 19) might mediate a more robust translation in stress resistance and cell maintenance in the long term, and therefore explains the dramatic lifespan increase in those animals. Generally, lowered protein synthesis rates are hypothesized to result in higher availability of energy for cellular maintenance mechanisms and stress response pathways (Tavernarakis, 2008). The direct observation of increased neuronal network stability in ageing upon loss of EDC-3 supports this postulation (Figure 12C to 12E). Together, these results indicate that a carefully adjusted balance between mRNP storage, protein synthesis and cellular maintenance are essential for the regulation of normal neuronal ageing.

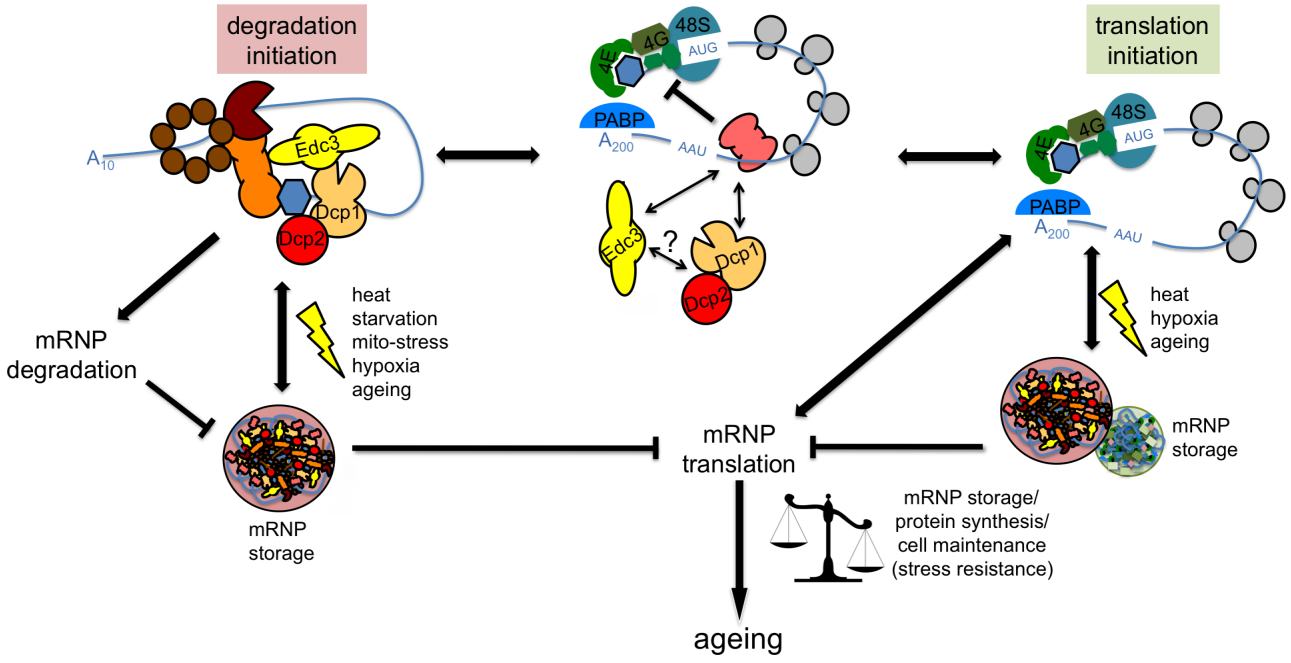

Figure 20: mRNP turnover and translation initiation interface in the regulation of translation and control of ageing in *C. elegans*. We hypothesize that Edc3 activity contributes to competition between translation and degradation initiation, possibly by binding mRNA degradation factors and recruiting the decapping complex. Presence of Edc3 dynamically promotes mRNP degradation and storage in P-bodies upon various stress insults and during ageing. Increased mRNP storage decreases mRNA availability for translation and a tightly regulated balance of mRNP storage, protein synthesis and cell maintenance controls ageing.

EDC-3 lifespan regulation and oxidative stress response

It is becoming increasingly apparent that cellular stress response mechanisms interact with factors that influence ageing, suggesting that longevity is closely related to the ability of organisms to respond to both intrinsic and extrinsic stress (Kourtis and Tavernarakis, 2011). We showed through various experiments that loss of EDC-3 prolongs lifespan (Figure 9A; Figure 10A and 10B) and increases resistance to various stress insults: Mutations in the genes gas-1 or mev-1 lead to increased oxidative stress by perturbing the electron transport chain in mitochondria, which results in an increased rate of ageing (Ishii et al., 1998; Kayser et al., 1999). Down-regulation of *edc-3* rescued decreased lifespan of both mitochondrial mutants (Figure 13A and 13B). We also measured an increased resistance to oxidative stressors paraquat and sodium azide (Figure 13C and 13D). A leading hypothesis for ageing of cells and organisms is the accumulation of reactive oxygen species (ROS), such as superoxide (O2•-) and hydrogen peroxide (H2O2), which in turn causes protein, lipid and DNA damage and results in age-related decline of cells and tissues (Harman, 1992). Cells respond with the activation of genetic mechanisms to counteract stress insult. Consequently, upon loss of EDC-3, we measured activation of two genes involved in oxidative stress response, gst-4 and sod-3. Those genes were also activated upon down-regulation of DCAP-1 and DCAP-2 (Figure 13E and 13F).

Various transcription factors are known to control ageing and stress response, including the factors DAF-16, SKN-1 and HSF-1 (Kenyon, 2010). Upon down-regulation of *hsf-1* and *skn-1*, but not *daf-16* genes, we measured a complete rescue of longevity in animals carrying *edc-3(ok1427)* allele (Figures 14A, 15A and 15C). Curiously, in the case of epistasis of SKN-1, lifespan was even reduced below that of the control population (Figure 14C). SKN-1 is the major regulator of hundreds of genes involved in oxidative stress response and ageing in *C. elegans* (Park et al., 2009). Also, we measured significantly induced formation of ROS upon *edc-3* or *dcap-2* down-regulation (Figure 13G). Accumulating evidence from studies in *C. elegans* point to a regulation of ageing by induction of mitohormesis, which can be counteracted by ROS scavenging (Ristow and Schmeisser, 2011; Yang and Hekimi, 2010). We observed a robustly decreased longevity phenotype of *edc-3* mutants and animals treated with *edc-3* RNAi upon NAC treatment (Figure 14B and data not shown). Further, the epistasis effect of SKN-1 on EDC-3 was largely rescued when animals were treated with NAC (Figure 14C). The experimental series leads us to conclude, that loss of EDC-3, and maybe DCAP-1 and DCAP-2, triggers mitohormesis in *C. elegans*, which perturbs ROS balance and employs SKN-1 activation to increase longevity (Figure 21).

The exact processes that trigger mitochondrial ROS production upon loss of *edc-3* are unknown. However, it is accepted that P-bodies, including all components for RNAi, actively and dynamically associate with mitochondria and that loss of mitochondrial function suppresses effectiveness of miRNA and siRNA mediated RNAi in mammalian systems (Huang et al., 2011). Also, an array of miRNAs is enriched within mitochondria, some of which might be regulating mitochondrial translation (Bandiera et al., 2011; Bian et al., 2010). We found that upon loss of the mitochondrial protein EAT-3, homologue of OPA1 in humans, DCAP-1 P-body intensity is generally increased (Figure 6E). EDC-3 modulates decapping, interacts with the Ago2 mediated miRNA silencing complex (Franks and Lykke-Andersen, 2008). We speculate that EDC-3 through its central role in P-bodies might be involved in the regulation of mitochondrial functions including mitochondrial translation and integrity and could therefore induce ROS production in a more direct manner (Figure 21).

Another, explanation might correlate with findings that show a general SKN-1 activation upon loss of translation initiation. The factors that activate SKN-1 in that case are

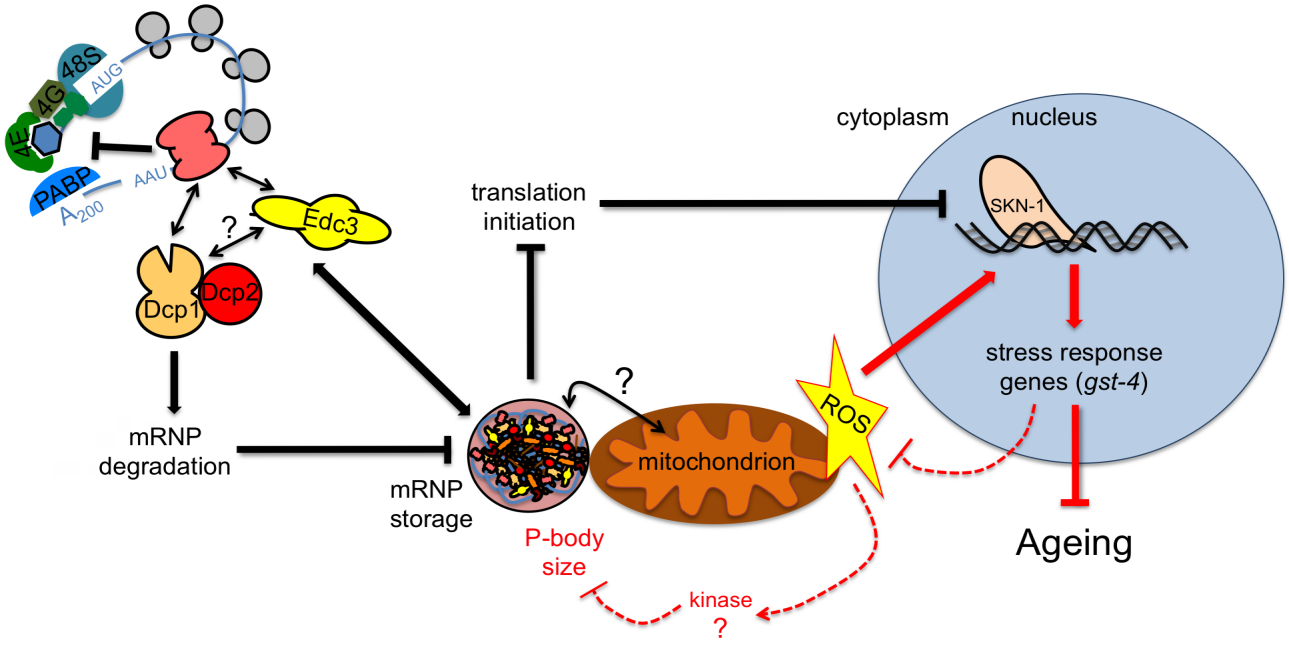

Figure 21: EDC-3 might control ageing via activation of SKN-1 through mitohormesis and translation initiation. By differentially regulating mRNP degradation and storage in P-bodies, EDC-3 controls translation initiation, which is known to interface with control of SKN-1. Also, the function of degradation factors accumulated in P-bodies might control mitochondrial integrity and ROS levels, which regulates SKN-1 and stress response genes. ROS possibly directly regulates P-body size, mRNP storage and degradation activity to maintain stress response (compare Figure 15).

unknown (Wang et al., 2010). Our findings show that loss of EDC-3 suppresses de novo protein synthesis, possibly by accumulating mRNPs in P-bodies, and subsequently activate SKN-1. Curiously, we tested whether ROS scavenging might also affect lifespan extension in animals with impaired translation initiation. We found that upon down-regulation of *ife-2* gene, NAC treatment did not result in decreased lifespan (data not shown), which indicates that SKN-1 activation upon loss of EDC-3 via ROS or suppression of translation act in parallel (Figure 21).

HSF-1 co-regulates EDC-3 lifespan and nuclear and cytoplasmic functions of IFE-2

Our data provide evidence that heat shock response interacts with mRNP turnover and translation. Intriguingly, we detected IFE-2::GFP protein in nuclei across several tissues in *C. elegans* (Figure 17A and 18B). Upon loss of HSF-1, we noticed three distinct phenotypes connected to IFE-2 protein: (I) we found extensive IFE-2::GFP granulation in tissues including seam cells, intestine and in the area of the pharynx (Figure 16A and 17A); (II) we observed a substantial general increase in IFE-2::GFP protein levels and transcriptional upregulation (Figure 16B and 16C); (III) we revealed dramatic nuclear accumulation and granulation of IFE-2 (Figure 17A to 17C).

Multiple functions have been described for eIF4E, the human homologue of IFE-2: Next to its function as central translation initiation factor, it is a known oncogene, localizes to the nucleus and has been directly implicated in nuclear export of specific mRNAs (Culjkovic et al., 2006; Mamane et al., 2004). Our findings indicate that eIF4E major functions could be conserved in *C. elegans* and might be directly suppressed by HSF-1 activity. Loss of HSF-1 boosted transcription of *ife-2* gene and accumulation of IFE-2 protein (Figure 16B and 16C), which we observed in young and aged animals. Peculiarly, nuclear and cytoplasmic aggregation upon loss of HSF-1 only occurred in older nematodes (day 8), indicating an age-dependent

effect. IFE-2 stress granules co-aggregate with DCAP-1 in the cytoplasm (Figure 17B). Detailed dissection of IFE-2 nuclear localization revealed granulation within the nucleus and the perinuclear space.

Intriguingly, in *edc-3* mutants, we detected a decreased nuclearization phenotype of IFE-2 upon down-regulation of *hsf-1* gene. Only half the amount of *edc-3* mutants expressed enhanced nuclear localization and the ratio between nuclear and cytoplasmic IFE-2 was lower compared to wild type (Figure 17D and 17E). These results indicate that EDC-3 is involved in the regulation of IFE-2 mediated nuclear function. We were not able to conclusively detect P-bodies within nuclei of *C. elegans* but our confocal images suggest that DCAP-1 co-accumulates with IFE-2 at the nuclear envelope (Figure 17C and 18C). Suppression of eIF4E mediated mRNA export, specifically by knockdown of a known co-factor LRPPRC, accumulates eIF4E in P-bodies (Topisirovic et al., 2009). Co-localization of eIF4E and P-bodies at the nuclear envelope is also observed upon heat stress induction in HeLa cells (Suzuki et al., 2009).

We consider that IFE-2 in *C. elegans* next to its role in translation initiation, serves a conserved nuclear function as export factor for mRNPs. Upon stress insult, or as animals' age, this function might decline and IFE-2, and its cargo, might co-accumulate in nuclear granules, as well as in stress granules and P-bodies in the cytoplasm. We also assign a novel role for HSF-1 in controlling these processes: heat shock response appears to control *ife-2* transcription and stability, as well as IFE-2 aggregation. These findings also link HSF-1 function to the control of global protein synthesis, which is a critical determinant of ageing (compare proposed model in Figure 22).

HSF1 is the major regulator of heat-shock response in vertebrates by inducing expression of heat-shock proteins (HSPs) and other cytoprotective proteins. In unstressed cells, HSF1 in an inactive monomeric form and becomes activated upon heat and other stress stimuli, forms trimmers and expedites a site-specific DNA-binding activity (Kourtis and Tavernarakis, 2011). Only one study, which investigates its oncogenic roles, links HSF-1 to translational control: Loss of Hsf1 in mouse embryonic fibroblasts, which were grown under serum starvation showed reduced levels of S6K and three ribosomal subunits, as compared to control cells. However, the authors find that eIF4E protein levels stay unaffected (Dai et al., 2013). Therefore our findings appear to be a pioneer study in HSF-1 mediated control of translation.
Loss of EDC-3 results in a general increase of P-bodies and IFE-2 during high age, but suppresses the nuclear enrichment of IFE-2 (Figure 6I and 6J, Figure 17D and 17E). Import of eIF4E is regulated by the eIF4E-Transporter (4E-T), which also co-localizes to P-bodies (Dostie et al., 1999). The *C. elegans* homologue of 4E-T, IFET-1, is important for P-Granule formation and co-localizes with P-bodies (Sengupta et al., 2013). We speculate that loss of EDC-3 might sequester IFE-2 and its nuclear transporter in P-bodies, thereby suppressing nuclearization and consequently mRNP export. Recent studies indicate that mRNA decay factors such as Dcp1a, Edc3 and the exonuclease Xrn2 function in nuclei and suppress expression of specific genes by (Reines, 2012). Although by imaging we did not detect DCAP-1 or EDC-3 in the nucleus, we cannot exclude that nuclear degradation processes are conserved in *C. elegans* and might contribute to IFE-2 nuclear transport functions through presently unknown mechanisms.

We had also observed robust resistance to heat stress of *edc-3* mutants (Figure 13H and 13J), which indicates activation of heat shock response pathways in those animals. Down-regulation of *edc-3* by RNAi did not result in a similar phenotype, possibly because RNAi does not affect specific neurons involved in heat stress resistance, including the AFD neurons (Lee and Kenyon, 2009). We speculate that loss of EDC-3 in neurons activates HSF-1, which mediates increased heat stress resistance during ageing and longevity.

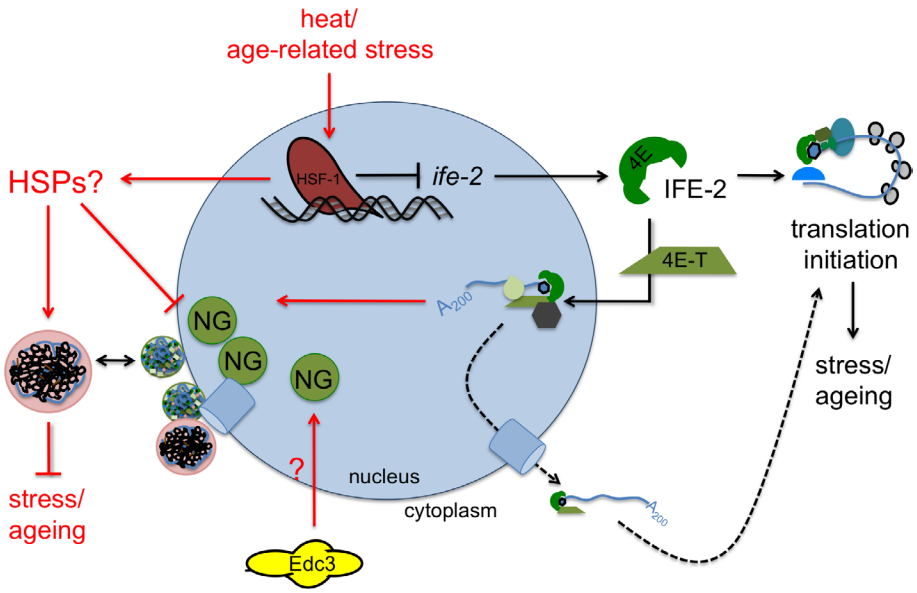

Figure 22: Heat shock response regulates IFE-2 compartmentalization and granule formation in *C. elegans*. HSF-1 regulates *ife-2* gene transcription and protein stability. IFE-2 (eIF4E) appears to follow a conserved nuclear function as mRNP transport protein in the nematode. Heat and age-related stress activate HSPs, which differentially regulate accumulation of mRNPs in stress and nuclear granules, as well as P-bodies, possibly to maintain proper cellular stress response. EDC-3 plays a so far unidentified role in nuclear granulation of IFE-2.

Since loss of HSF-1 also acts epistatic on lifespan extension observed upon loss of EDC-3 (Figure 15C) and controls expression of IFE-2, which is a well-known determinant of ageing, we speculate that the observed phenomena interface to regulate *C. elegans* lifespan. Additional experiments need to be performed to address this intriguing issue. However, our results raise the speculation that the multiple functions of IFE-2 in translation initiation, mRNP accumulation and transport between nucleus and cytoplasm are linked and might co-regulate the process of ageing in communication with mRNP degradation and transcriptional regulation in heat stress response.

Decapping factor EDC-3 as determinant of ageing

Our results demonstrate that loss of EDC-3 results in longevity in a largely neuron-dependent manner. We tested the implication of other mRNP degradation factors in ageing, including LSM-1, DCAP-1, DCAP-2 and CCR-4 (compare Figure 1). Down-regulation of either factor by RNAi did not result in any significant lifespan alterations in wild type animals (data not shown). Animals carrying *dcap-1* or *dcap-2* mutant alleles showed increased obvious developmental defects including reduced egg laying, altered locomotion and embryos tend to hatch within the mother (bagging), as well as altered morphology (data not shown). These phenotypes point to the possibility that the decapping proteins are essential for correct embryonic development of *C. elegans*. Indeed, DCAP-1 and DCAP-2 are both shown to regulate mRNP stability in P granules during *C. elegans* oogenesis and embryogenesis (see Introduction). When performing lifespan experiments, we exposed *C. elegans* to RNAi post-embryonically to avoid interference with development. Why does specifically loss of *edc-3* gene, but none of its known interactors, especially *dcap-1* or *dcap-2*, extend lifespan in the nematode?

EDC-3 did not display developmental defects compared to wild type, egg laying was slightly, and body size significantly reduced (Figure 10C). Reduced body size points to a changed metabolic rate as observed in various long-lived mitochondrial mutants in *C. elegans*. However, this feature cannot be directly correlated with ageing or specific changes in metabolism (Braeckman, 2009). The fact that EDC-3 is not essential for embryonic development might be significant for the explanation of its role in control of lifespan. From studies in yeast it is known that Edc3 is dispensable for efficient decapping and maintenance of steady state-lev-

el of most transcripts, while its recruitment of Dcp1:Dcp2 is crucial mRNA degradation (Kshirsagar and Parker, 2004).

Edc3 also interacts with various other degradation enzymes, promotes decay of specific mRNAs and is considered a central scaffolding factor for the mRNA decapping complex and P-bodies (see Introduction). We observed that deletion of EDC-3 abandons recovery of the DCAP-1 specific P-body signal in FRAP experiments (Figure 12K), which could be due to the generally lowered protein synthesis rate in *edc-3* mutants and/or its predicted role in P-body assembly. Further, loss of EDC-3 increases accumulation of P-bodies during ageing (Figure 12I). This corresponds to results obtained in Edc3 depleted yeast, which show increased P-body formation (Sheth and Parker, 2003). We conclude that EDC-3 activity in *C. elegans* might be redundant and non-essential for development, but significantly influences P-body assembly through its scaffolding role in forming the decapping complex, as it has been shown for other, structurally related enzymes, including Scd6 and Pat1 (Fromm et al., 2011; Nissan et al., 2010). This scaffolding role might be central to its function in ageing, since it suppresses degradation but does not abandon it. Further, its role in suppressing specific mRNPs, as shown for some cases in yeast, could contribute to determine longevity (Dong et al., 2010). Direct mRNA targets of degradation by EDC-3 and its exact roles in *C. elegans* decapping need to be determined in future experiments.

Cell-autonomous versus -non-autonomous regulation of ageing by EDC-3

The evidence for a largely neuron-specific function of EDC-3 is persuasive. However, several experiments made us inquisitive about the possibility that pathways controlled by EDC-3 might be acting cell-nonautonomously in the regulation of ageing: (I) Full epistasis effects of the transcriptional regulators SKN-1 and HSF-1 on EDC-3 is observed upon down-regulation of RNAi, which as stated before is not as effective in all neurons (Figure 14A and 15C). (II) P-body formation in *edc-3* mutants was altered compared to control animals across tissues in age-dependent fashion (Figure 12I). (III) Further, aged *edc-3* mutants showed dramatic P-body accumulation across all tissues upon loss of *skn-1*, which was rescued in part by NAC treatment (Figure 15C). (IV) Loss of HSF-1 resulted in an IFE-2 nuclearization phenotype, predominantly observed in muscle and hypodermal tissues, which was suppressed in *edc-3* mutants in the same tissues in aged animals (Figure 17D to 17E).

The more direct explanation for the full epistasis effect of SKN-1 and HSF-1 on EDC-3 during ageing is that RNAi might still affect down-regulation in a subset of neurons critical to mediate regulation in ageing cell-autonomously, but it does not account for the age-dependent effect observed in other tissues in *edc-3* mutants. Endocrine signaling pathways control ageing in *C. elegans* through functions in different tissues (Kleemann and Murphy, 2009). For DAF-2/DAF-16 insulin-like signaling tissue-specific functions in ageing have been assigned largely to neurons and the intestine, while recent studies point to cell-nonautonomous regulation in ageing (Libina et al., 2003; Zhang et al., 2013). Our study largely excludes employment of DAF-16 in control of EDC-3 mediated lifespan. However, SKN-1 appears to control the production of an unknown endocrine signal specifically in the ASI neurons to influence metabolism in the intestine upon dietary restriction (Bishop and Guarente, 2007). Further, mitochondrial perturbation in neurons can be received and reacted upon in distant tissues, such as the intestine, which is mediated by so-called, still largely hypothetical mocleucles named “mitokines” (Durieux et al., 2011). In our study, EDC-3 mediates longevity in neurons through discussed mechanisms, which includes induction of a hormesis effect, possibly mitohormesis. Mitochondria might produce signals for distant communication, which are received and copied in target cells and down-regulation of *skn-*

1 or *hsf-1* produce the observed phenotypes across tissues. Biomarkers for this process in *edc-3* mutants are P-bodies, which are expressed in differential levels but become ubiquitously induced upon loss of *skn-1*, or IFE-2 compartmentalization upon loss of *hsf-1*.

Sites of mRNP turnover and their roles in ageing

A central observation of our study describes the formation of mRNP aggregates during ageing and stress response. Our experiments for the first time show that the P-body specific reporters for DCAP-1, EDC-3, LSM-3, as well as IFE-2 stress granules, increasingly accumulate during stress response and ageing within a whole organism (Figure 6A to 6E). It has been proposed that P body formation is a consequence, not a cause of the function of their components in mRNA silencing and decay (Eulalio et al., 2007). It is therefore convenient to speculate that P bodies, and possibly also stress granules, form as a consequence of stress and ageing and do not play a causative role. However, our study contributes several intriguing observations that point to a more direct involvement of mRNP aggregates in the control of ageing and stress management.

Firstly, we observed that response to various stressors results in different levels of P body and IFE-2 stress granule formation and also varies across tissues (Figure 6D, 6E and 6H). Hypoxia and heat stress induced both P-body and stress granule formation and cause co-accumulation of both (Figure 6I, Figure 7, Figure 8). Starvation caused P-bodies to accumulate, but not stress granules. Under the conditions we use, sodium azide treatment does not significantly induce mRNP accumulation in *C. elegans*. These results might indicate that storage of mRNPs as a response to stress is selectively regulated. In yeast, the cAMP-dependent protein kinase (PKA) specifically regulates P-body formation upon glucose-deprivation, while stress granules occur independently regulated (Shah et al., 2012; Ramachandran et al., 2011).

Arrest of translation, as it occurs upon stress insult, or down regulation of translation initiation factors leads to increased P-body formation in yeast and is de facto required for the assembly of mRNPs into P-bodies (Coller and Parker, 2004; Schwartz and Parker, 1999). We observed that upon down-regulation of *ife-2* gene, P-body number dramatically increased in aged animals (Figure 7F). It is well established, that protein synthesis decreases during senescent decline (Tavernarakis, 2008). Intriguingly, we measured a substantial decrease of IFE-2 translational and transcriptional reporter signals (Figure 16B and 16C), while P-body formation increases in an inverse manner during ageing (Figure 6A to 6C). Together, these results confirm previous findings, which state that mRNPs are stored into P-bodies upon decreased translation or during stress insult, which appears to be a steady state during high age. We also found, that down-regulation of *daf-2* results in significantly lower mRNP accumulation during ageing when measured at the same points in chronological age compared to control and *ife-2* depleted animals (Figure 6F). Loss of *daf-2* or *ife-2* result in longevity by apparently distinct pathways, and it is not clear whether daf-2 mutants display reduced translation initiation (Fuchs et al., 2010). Apparently, P-body assembly in either genetic background is differentially controlled, although both mutants exhibit robust resistance to various stress factors (Syntichaki et al., 2007, Honda and Honda, 1999). Curiously, in mammalian cells, the P-body factor EDC3 is phosphorylated in response to insulin signaling via the AKT kinase. Depletion of insulin severely decreases EDC3 phosphorylation, efficiency of miRNA mechanism and P-body formation in this system, thereby possibly controlling mRNP turnover, mRNA stability and translation (Larance et al., 2010).

The findings about P-body and stress granule formation due to various stress insults, translational inhibition and ageing led

us to test the possible causative involvement of transcriptional control. Grown under optimal conditions, down-regulation of stress and ageing regulators HSF-1, DAF-16 or SKN-1 did not result in any significant P-body or stress granule accumulation in day 4 old animals (data not shown). Down-regulation of HSF-1, but not SKN-1 or DAF-16, in aged (day 8 of adulthood) worms resulted in severely increased cytoplasmic and nuclear IFE-2 stress granule accumulation across tissues including intestine, seam cells, muscles and the head region (Figure 16A and 17A). These granules partly co-localize with DCAP-1 P-bodies (Figure 17B and 17C, Figure 18C). The age-related phenotypes observed upon loss of HSF-1 showed similarities to the appearance of stress granule formation upon heat stress (Figure 6I, Figure 7 and Figure 8). HSF-1 regulates ageing in *C. elegans* by activation of shps, which act as molecular chaperons to prevent aggregation-induced cytotoxicity during ageing (Hsu et al., 2003). In neurodegeneration, aggregates are thought to act protective for the cell by accumulating and storing damaged proteins (Ross and Poirier, 2005). Stress granules accumulate mRNPs that are stalled in translation but that can reenter translation initiation (Anderson and Kedersha, 2002). In mammalian systems, various examples show co-regulation of HSPs, such as HSP70 and HSP90, and stress granules maintains translation during heat stress (see Introduction). Therefore, HSF-1 and subsequently HSP activity might be required to prevent aggregation of proteins essential for stress response in *C. elegans* stress granules.

In parallel studied mRNP aggregation upon heat stress in HSF-1 depleted animals. Aged wild type animals grown at 25°C showed some induction of stress granule formation but dramatically increased formation of P-bodies compared to aged animals grown at optimal temperature. Upon loss of HSF-1, P-bodies failed to form (Figure 15D). Loss of HSF-1 is known to strongly decrease lifespan and heat stress resistance (Figure 15C; Chiang et al., 2012). We conclude that P-body formation upon heat stress is actively promoted by HSF-1 controlled factors, possibly HSPs. To our knowledge we show for the first time that a transcription factor actively promotes granule formation. However, it is reported that HSF-1 activation/trimerization itself is promoted by mRNP complexes containing translation elongation factor eEF1A and the mRNA HSR1, which points to a possibly direct interaction between HSF-1 and mRNP granules (Shamovsky et al., 2006).
What mechanisms could drive P-body accumulation upon heat stress? At least two targets that are transcribed upon heat stress, HSP70 and HSP90, are largely excluded from stress granules and are being translated (Anderson and Kedersha, 2008). Interestingly, Hsp90 directly regulates Ago2 function under stress conditions and targets it to P-bodies and stress granules and possibly accelerates or improves miRNA mediated gene silencing (Pare et al., 2009). Intriguingly, we recognized that in *edc-3* mutants, P-body formation upon heat stress was significantly enhanced compared to control animals (Figure 8G). Accumulation of P-bodies upon heat stress might be generally promoted by HSPs to differentially increase storage of specific, possibly expendable, mRNPs and maybe induce their degradation, while the formation of stress granules might be suppressed to maintain translation of essential heat stress resistance transcripts (see Figure 22).

Finally, we observed that loss of SKN-1 caused a robust increase of P-bodies in aged *edc-3* mutants, compared to wild type animals (Figure 14D), which points to a specific requirement of mRNP storage in this genetic background. Curiously, loss of EDC-3 triggers a hormesis response, which by itself does not cause significant alterations in P-body formation, even if counteracted by the ROS scavenger NAC (Figure 14D). The increase of P-body levels upon additional loss of SKN-1 is counteracted by NAC, and results in longer and healthier lifespan compared to control population (Figure 14C and 14D). It appears that alterations in P-body

formation upon oxidative stress differ from heat stress response. SKN-1 mediated activation of antioxidants might actively suppress P-body formation in *edc-3* mutant animals, but surely regulates ROS levels as previously suggested (Hunt et al., 2011). Alternatively, increased ROS could activate sensor kinases to regulate specific P-body components in a fashion similar to the yeast PKA activation upon glucose deprivation, which phosphorylates the P-body scaffolding factor Pat1, which prevents formation of larger aggregates but increases total number of smaller foci (Ramachandran et al., 2011). This scenario is congruent to our observations: Total P-body number in SKN-1/EDC-3 depleted animals is robustly increased and treatment with ROS scavenger NAC significantly decreases P-body levels but leaves their size unaffected (compare Figure 14D). Similar to glucose deprivation in yeast, regulated P-body size could be necessary during oxidative stress response in *C. elegans* to maintain the balance between mRNP storage, decay and translation (Figure 21; Ramachandran et al., 2011; Shah et al., 2012). However, more experimental efforts are necessary to decipher the potential mediator of this potential ROS/P-body signaling pathway that might interface with SKN-1 activation.

Based on our results we propose that transcriptional regulation through SKN-1 and HSF-1 differentially controls storage of mRNPs into P-bodies or stress granules upon different stress insult and during ageing. Loss of EDC-3 prolongs lifespan and increases accumulation of mRNPs in P-bodies, which suppresses translation, and in parallel might trigger mitohormesis. SKN-1 is activated via previously speculated pathways triggered by ROS and mediates oxidative stress response mechanisms (Ristow and Schmeisser, 2011). ROS could directly or indirectly regulate P-body size and storage in response to oxidative stress (Figure 21). Lifespan extension upon loss of EDC-3 also requires HSF-1 activity. Heat shock proteins suppress stress granule assembly during ageing, and actively store mRNPs in P-bodies upon heat stress insult. Additionally, HSF-1 regulates transcription and stability of eIF4E (IFE-2) and subsequently its role in mRNP transport, nuclear and cytoplasmic granulation and translation initiation (Figure 22). Whether these functions regulate ageing remains to be determined, also how nuclear granulation could be regulated by EDC-3. We determine that the observed processes act largely independent of DAF-16. Finally, we conclude that systematic accumulation of mRNPs in granules during ageing and stress contributes to a balance of general or specific transcript stability and turnover, which in turn influences protein synthesis (Figure 20).

Appendix:

Novel tools for microscopic 3D imaging

Abstract

We present a custom-made setup that combines Selective Plane Illumination Microscopy (SPIM) and Optical Projection Tomography (OPT) for rapid three-dimensional imaging. OPT eliminates the need for serial optical sectioning of specimens, required with conventional confocal microscopy, and allows for robust, high resolution fluorescence, as well as absorption imaging of whole specimens (compare Sharpe et al., 2002). The SPIM system is designed for high penetration depth, low photobleaching and high acquisition speeds when using fluorescently labeled specimens, enabling extended time-lapse *in vivo* experiments (compare Huisken et al., 2004). The setup permits to easily switch between SPIM and OPT and can be used to image fixed mammalian tissue, *Drosophila* embryos and live *C. elegans* animals.

We successfully applied OPT to image fluorescently labeled tissues and single neuronal cells, including axons, in live *C. elegans* (Rieckher et al., 2011). Further, we applied novel reconstruction algorithms to improve the resolution of OPT derived 3D images (Birk et al., 2010; Zhu et al., 2012). We recently developed a microfluidcs device for *C. elegans* that is designed for high-throughput *in vivo* imaging specifically through OPT and/or SPIM technology (compare Chronis et al., 2007). We implemented SPIM and obtained preliminary results for in-chip measurements. The system is now readily equipped to facilitate high-throughput imaging of *C. elegans* in longitudinal studies of gene expression during the process of ageing.

Imaging *C. elegans* through novel 3D microscopy techniques

Classical 3D imaging systems for *C. elegans* and their limitations

A fundamental advantage of *C. elegans* as a model organism is its transparency which allows deep point focussing through standard 2 dimensional (2D) microscopy techniques such as low-magnification stereomicroscopy, and high-magnification compound and confocal microscopy (Hope, 1999). However, there is need for 3D whole animal imaging in the nematode, which allows digital sectioning of a sample. This represents a useful tool to reveal the anatomical structure and to visualize gene expression patterns of transgenic animals. Optical sectioning techniques on *C. elegans* have been performed on the basis of serial-section reconstruction; laser scanning confocal microscopy (LSCM) and micro Magnetic Resonance Imaging (μMRI). Nevertheless, these techniques show limitations of applications in the nematode:

LSCM has the ability to produce in-focus 3D images of small specimens which is called optical sectioning. Images are acquired point-by-point and reconstructed, which also allows three-dimensional reconstructions of the sample. In LSCM, a laser beam passes through a light source aperture and objective lens focuses the light into a small area within the fluorescent specimen. The principle of the technique is that out-of-focus light is suppressed by passing through a pinhole, resulting in a sharp focused image. The use of a beam splitter allows only the laser light to pass to the photodetection device. Obtaining and digitally assembling images of various z axis planes (z stacks) through a specimen further permits the reconstruction of a 3D picture (Paddock, 1999). Confocal microscopy allows visualization and 3D reconstructions on subcellular level but is limited when it comes to whole-animal recording. In addition, confocal microscopy is solely based on fluorescence detection and not capable of imaging intrinsic or extrinsic absorption. In *C. elegans*, confocal miscroscopy, has found multiple use e.g. to visualize GFP and yellow fluorescent protein (YFP) labelled microtubule in vivo to study cell division (Kozlowski et al., 2007).

Another commonly used technique mainly for developmental studies in the nematode is 4D embryo imaging through a multifocal plane time-lapse video recording system (Hird, 1993). Multiple layers of the embryo are recorded through Differential Interference Contrast Microscopy (DICM, also called Nomarsky microscopy) in certain time intervals. The received information about positioning of single cells is manually represented in 4D, which is supported by standard used software such as SIMI BiocellTM. This allows improved cell lineage representations and precise studies of embryonic strategies such as pattern formation through cell sorting (Schnabel et al., 1997). These techniques have been further improved by fluorescently labelled nuclei which can be tracked more easily (Bao et al., 2006). Through the use of fluorescent labels the expression of certain genes can be followed up to the 350 cell stage of development and high-throughput methods have been applied (Bao et al., 2006; Hunt-Newbury et al., 2007). Nevertheless, this technique neither produces real 3D images nor allows in silico sectioning of the nematode.

The technique μMRI offers the possibility to view whole specimen and even gene expression patterns in vivo. A strong magnetic field is used to align the nuclear magnetization of hydrogen atoms of the sample resulting in a 3D image. Nevertheless, resolution and recording of fluorescence of the technique are strongly limited (Pautler and Fraser, 2003). The method proves to be inefficient to visualize *C. elegans* in satisfactory resolution.

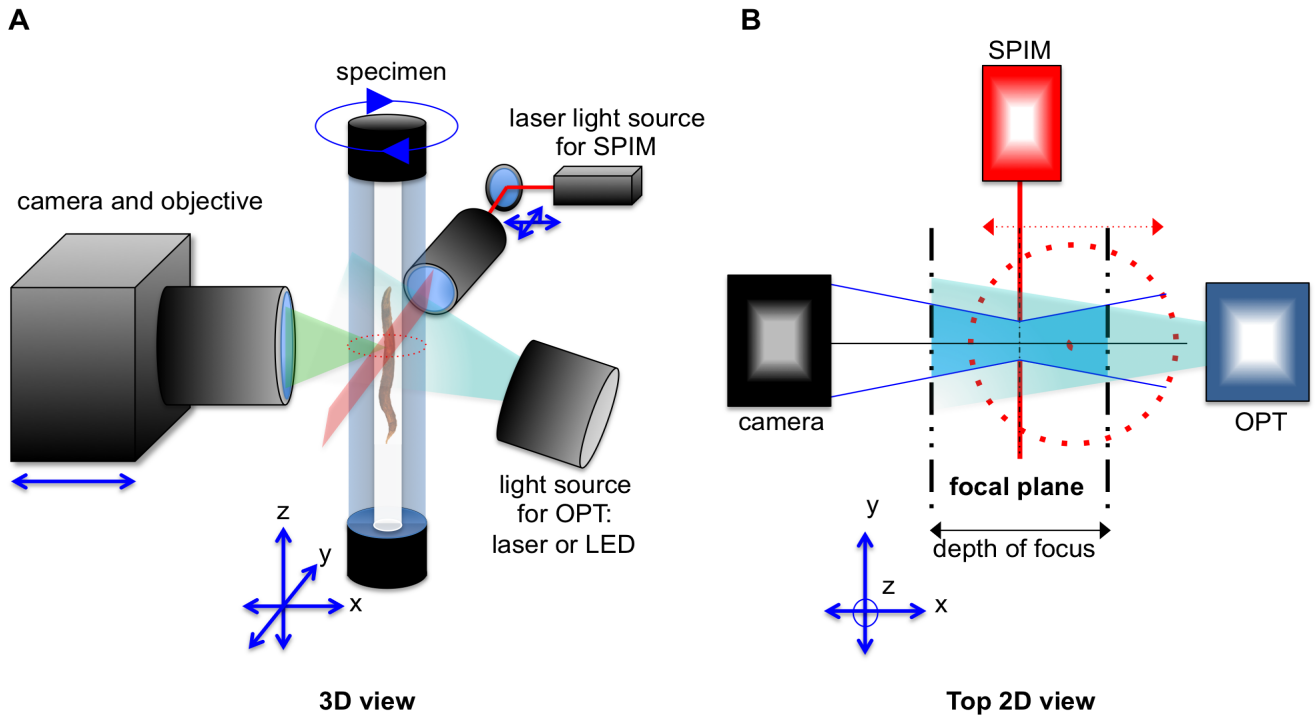

Figure 23: Representative scheme of combined SPIM and OPT setup and the principal of both techniques. **(A)** 3D imaging of in vivo cellular and molecular processes in the context of the whole organism is of high importance to study complex biological phenomena such as development and ageing. Both OPT and SPIM are recent techniques developed for rapid and high-resolution imaging. A camera-objective system is used to focus on the specimen immersed in a glass capillary. Light sources for SPIM are lasers of various wavelengths and the beam is focused to a light sheet through the specimen by a focal lens. OPT can potentially employ any laser or LED of the corresponding excitation light for the fluorophore or brightfield (see Materials and Methods for details). **(B)** OPT combines fluorescent, intrinsic and extrinsic absorption obtained from in-focus and out-of-focus imaging of the rotating specimen. SPIM is based on optical sectioning by illuminating the sample along a separate optical path orthogonal to the detection axis, optionally acquiring multi-angled image stacks by rotating the sample.

Selective Plane Illumination Microscopy (SPIM)

A powerful, relatively novel technique that makes *in vivo* optically sectioning throughout specimen up to several mm in size possible is SPIM: The technique offers optical sectioning, reduced fluorophore bleaching, fast, highly efficient image recording, and high depth penetration, especially when multiple imaging angles are combined. SPIM performs well in large samples such as fish or fly embryos, which can be observed in vivo for several days. The method is based on optical sectioning, similar to LSCM, in this case achieved through illuminating the sample along a separate optical path orthogonal to the detection axis (Huisken et al., 2004, compare Figure 23). The SPIM principles are universal and have been successfully applied using objective lenses with high magnification, covering sample sizes from 20 µm to 1 mm with isotropic resolutions from 5µm to 300 nm. Major disadvantage of SPIM is, as in LSCM, that absorption/brightfield information cannot be derived.

Since invention, SPIM has become applicable for various in vivo studies (Huisken, 2012). One application is the study of morphogen gradient dynamics of fluorescent Dorsal in Drosophila and activation of its target genes during embryonic development (Reeves et al., 2012). Another well-characterized target is cell lineage tracing in organogenesis and functional brain imaging of the zebra fish (Panier et al., 2013; Swoger et al., 2011). A recent application makes SPIM available for in vivo studies in *C. elegans*: The authors present an inverted SPIM (iSPIM) system that allows for coupled cell identity lineaging and neurodevelopmental imaging. Embryonic twitching makes live imaging of neurite outgrowth during neurolation

a difficult task, which was circumvented by application of iSPIM, e.g. to visualize ALA neurons as they circumnavigate the developing nerve ring (Wu et al., 2011). My collaborators and me have constructed a cost-effective SPIM setup, which is readily equipped to image multiple fluorophores and allows for *in vivo* imaging of *C. elegans* embryos and fully-grown adults (compare scheme of the setup in Figure 3, Materials an Methods).

Optical Projection Tomography (OPT)

Recently, a new method called optical projection tomography (OPT) has proven capability to produce rapid high resolution 3D visualization of small specimen of 1 to 10 mm in size (Sharpe, 2002; 2003). This technique fills the gap between µMRI and confocal microscopy. OPT is the optical equivalent of X-ray computed tomography (CT) scanning, where images of the attenuation coefficient or the emission distribution are obtained by applying an inverse Radon transform to back-propagate photons (Kalender, 2006). OPT uses projections from different angles perpendicular to the rotational axis of the specimen undergoing one full revolution. The use of standard convolution filtered back projection of each projection yields a reconstruction of all slices. Thereby 3D volumetric representation of the specimen including fluorescence patterns, intrinsic and extrinsic absorption or a combination of multiple channels is received (McGinty et al., 2008; Sharpe, 2004, compare Figure 23). OPT is already successfully implemented for 3D imaging of fixed chick and mouse embryos (Sharpe, 2002), plants (Lee et al., 2006), zebra fish (Bryson-Richardson et al., 2007; McGinty et al., 2011), Drosophila melanogaster (McGurk et al., 2007), and the developing human brain (Sarma et al., 2005).

Initially, OPT was mostly used on fixed specimens after optical clearing in order to reduce photon scattering. The advent of Mesoscopic Fluorescence Tomography (MFT) and fluorescence mediated tomography (FMT) allows efficient 3D imaging of live specimens, at mesoscopic or macroscopic scales (Ntziachristos et al., 2002; Vinegoni et al., 2007). However, the absence of effective microscopic OPT implementations precludes the use of OPT in vivo, for imaging anatomical features of sub-millimeter-sized model organisms with adequate resolution. My colleagues and me describe a tomographic setup which successfully meets the challenge of microscopic OPT and allows rapid and high-resolution imaging of whole specimens in vivo (Rieckher et al., 2011).

We present a simple and cost effective tomographic setup, which achieves fast 3D imaging of live *C. elegans* animals at single-cell resolution. The system is highly versatile and configurable for both absorption/brightfield and fluorescence imaging, with multiple chromophores and fluorophores. By post-acquisition filtering of residual sample movement and spurious drifts we have accomplished visualization of neuronal features, such as single axons and dendrites *in vivo* (Birk et al., 2010; Rieckher et al., 2011). We have combined the published OPT system with the novel SPIM setup, which allows for sequential recording of datasets of both techniques (compare scheme in Figure 3 and Figure 4 in Materials and Methods).

Microfluidic in 3D imaging

Recent advances in microfabrication technology permit the construction of well-controllable microchips with applications ranging from cell analysis to tissue engineering. In previous studies, microfluidic delivery systems have been used to trap and stimulate single cells and embryos. Several studies have extended the applications of microfluidics to in vivo *C. elegans* imaging. Microfluidic devices are available now for trapping and stimulating single worms while monitoring their behavior and neural function (Chronis, 2010; Chronis et al., 2007). Microfabrication of the worm chips is achieved through soft lithography, in which an elastomeric stamp with patterned relief structures on its surface is used to generate patterns in µm range (Xia and Whitesides, 1998). Molding of the chip is achieved by polydimethylsiloxane (PDMS)

application on fine structured silicone wafers, which is then attached to thin glass slides. Fluidic inlets and outlets allow loading and unloading of worms through attachable tubing systems (Chronis, 2010).

Microfluidics has found a wide range of use in imaging neuronal behavior such as response to mechanosensory, osmotic and calcium response, as well as microsurgery on single axons and regeneration processes, or development of single synapses (Allen et al., 2008; Chokshi et al., 2010; Chronis et al., 2007; Samara et al., 2010). Further, worm chips have been successfully implemented for high-throughput studies and automated on-chip subcellular microscopy, phenotyping, whole-animal sorting and screening in *C. elegans* (Chung et al., 2008; Rohde et al., 2007). Also, a low-resolution, lens-free optical tomographic system has been coupled to microfluidic devices, allowing for large-volume recording (Isikman et al., 2011). My colleagues and me have tackled the challenge to combine a novel microfluidics device with the previously developed OPT setup for high-throughput based on 3D imaging (Figure 5 in Materials and Methods). The same worm chips are also combined with our novel SPIM system and allow for efficient 3D visualization of fluorescent structures in *C. elegans*.

Novel tools for microscopic 3D imaging

Microscopic 3D imaging using OPT

We describe a tomographic setup which addresses the challenge of microscopic OPT and allows rapid and high-resolution imaging of whole specimens *in vivo* (Rieckher et al., 2011). The individual components of the system and their arrangement are outlined in Figure 3 and Figure 4. Nematodes are first immobilized in either the anesthetics levamisole or sodium azide, then transferred to halocarbon oil and finally mounted in a thin glass capillary, which is immersed in a chamber containing refractive index-matching fluid (see Materials and Methods). The capillary is attached to a rotation stage that allows precise positioning of the specimen for recording images from equidistant angles. To center the sample, the whole stage can be moved in all three dimensions through the stage controller, which in turn is controlled by customized software running on a computer (see Materials and Methods). Micrometric adjustment of the orientation and focusing of the specimen is facilitated by tilt controls on the rotation stage. The mounting stage is designed for easy coupling to microfluidics platforms, which have been developed for efficient manipulation and immobilization of nematodes (Chronis et al., 2007; Chung et al., 2008). Thus, processing of large numbers of individuals with negligible specimen perturbation can be attained. These features are particularly important when monitoring stochastic phenomena, where large animal populations are considered, as in the case of ageing studies, or when probabilistic and quantitative phenotypic traits are involved, as in spatio-temporal analysis of gene expression and comparative anatomy.

Two separate light sources are used for illumination of specimens. A white light LED source provides trans-illumination for absorption imaging. For fluorescence imaging, a range of different wave length-emitting LEDs can be utilized for epi-illumination, depending on the fluorophores to be excited

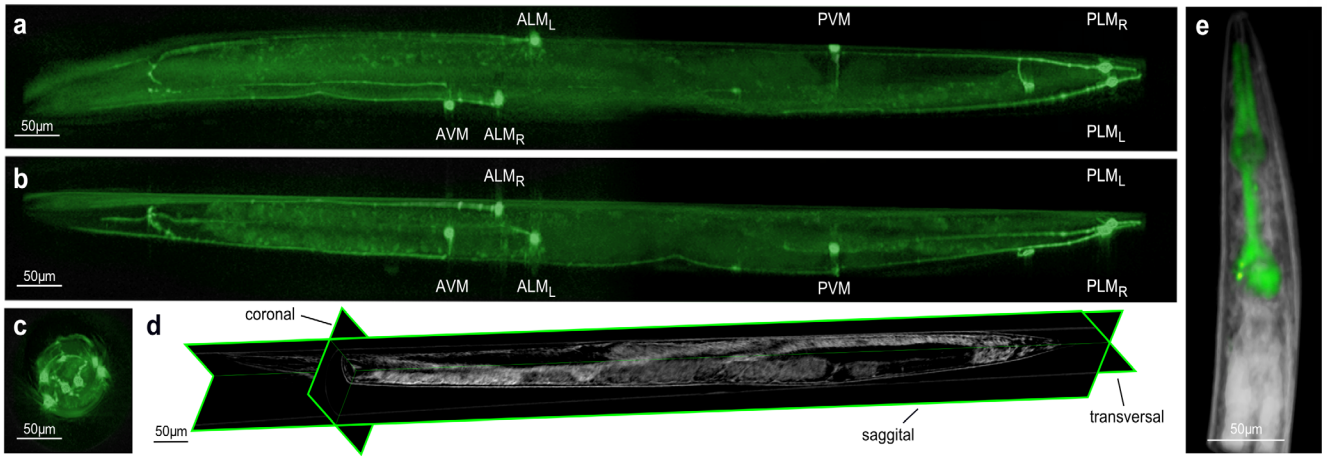

Figure 24: Tomographic reconstruction of wild type and transgenic C. elegans allows detailed analysis of anatomical features and fluorescence expression patterns. (a-c) Maximum intensity projections of a transgenic animal expressing GFP in mechanosensory neurons (see also Video 1). The three viewpoints, sagittal (a), transversal (b) and coronal (c) reveal the circuit of the 6 labeled mechanosensory neurons (ALML/R, AVM, PLML/R, PVM). **(d)** Assembled single slices of a 3D reconstruction of brightfield data, displaying the anatomy of *C. elegans*. Combined sagittal, transversal and coronal views allow visualization of structures such as intestine, pharynx, gonad and eggs. **(e)** Merged, brightfield and fluorescence tomographic reconstruction of the anterior part of *C. elegans*. Pharyngeal muscles expressing GFP are shown in green (see also Video 2). Size bar indicates 50µm.

in the specimen. Thus, the system can be readily adapted for imaging existing fluorescent marker proteins as well as endogenous fluorophores (autofluorescence) and fluorescent dyes used for staining various cellular components, both in vivo and after fixation of the specimens. Furthermore, several chromophores can be specifically imaged simultaneously, in addition to the fluorescence and anatomy (white light) modalities by using appropriate filter combinations in the trans-illumination light path. The OPT setup allows image registration at video rate, and is capable of measuring 500 projections in fewer than 5 minutes, dependent on intensity of the fluorescent signal. The white light data can be acquired in 1.5 min, including 500 projection images over 360°.

3D reconstructions of OPT data

A major challenge, which has hindered the use of OPT for microscopic imaging in vivo, is the residual random movement and drift of the sample during the course of observation, which becomes increasingly significant at higher magnifications required for microscopic OPT (Miao et al., 2009). By using landmarks in the organism, which are visible in all projection images, we correct for lateral movements of the sample. Additionally, we developed software, which compensates for slight non-circular motion of the rotation stage, by detecting changes in the predicted trajectories of the images consisting of data from a single line of CCD pixels for all angular measurements (sinograms) (Birk et al., 2010). Both correction algorithms are applied prior to data reconstruction (see Figure 4b, Materials and Methods). Filtered back projections of specimen images acquired at a number of equidistant angles are then used for 3D reconstruction. This processing enables visualizations of individual cells and cellular structures at high 3D resolution of about 2 µm, not previously possible with OPT.

We recently developed another novel method for motion correction in OPT, which is based on the Helgason-Ludwig consistency condition (HLCC). The method estimates object motion from projection data directly and does not require any other additional information, which results in a straightforward implementation. We decompose object movement into translation and rotation. Since finding the

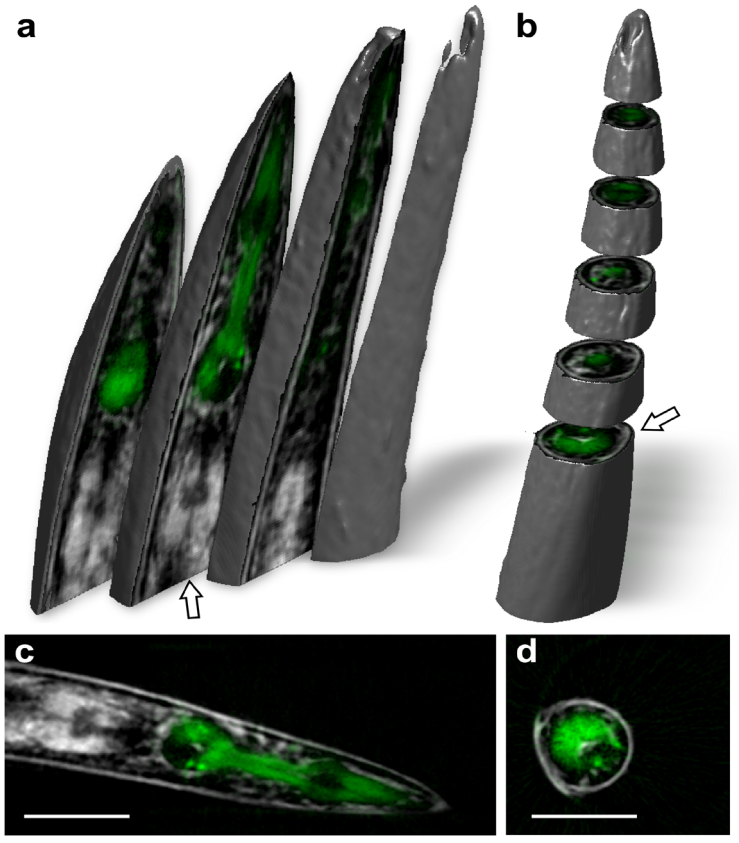

Figure 25: 3D rendering of the anterior part of the *C. elegans* body. (a, b) 3D visualizations of anterior body anatomy (see Video 3). Three transversal and five coronal sections are shown in (a) and (b), respectively. The 3D view allows detailed visualization and analysis of anatomical features, down to single cell level (see also Video 1 and Video 4). The process for generating 3D renderings is described in the Materials and Methods. (c, d) Two-dimensional, single slices in transversal and coronal planes, respectively, are shown (indicated by white arrows in (a) and (b) respectively). In all four panels, brightfield and fluorescence images are merged. Pharyngeal muscle cells expressing GFP are shown in green (see Video 2). Size bar indicates 50µm.

center of rotation accurately is critical in OPT, we also point out that the system's geometrical offset can be considered as object translation and therefore also calibrated through the translation estimation method (Shouping Zhu et al., 2012).

Imaging neurons and muscles through OPT

For experimental verification of the capacity for in vivo, high-resolution imaging by microscopic OPT, we used the in-house built tomographic system shown in Figure 3 and Figure 4 to image live transgenic *C. elegans* animals, carrying a green fluorescent protein (GFP) reporter fusion expressed specifically in only the 6 mechanosensory neurons of the nematode. These neurons extend processes that, in two sets of three, span the length of the animal (Figure 18a to 18c, see also Video 1 and Video 4). The three viewpoints shown in panels a-c (sagittal, transversal and coronal respectively) are depicted in Figure 24, for the corresponding white light data. Notwithstanding their diameter of approximately 2.7 µm, mechanosensory neuron processes are clearly visible, demonstrating the capacity of the system for highly sensitive 3D reconstruction at the level of living single cells, within the context of the whole organism. Such fine cellular features and anatomical details are not visible without sample movement correction, implemented on sinograms before reconstruction. Visualization and monitoring of alterations in individual neuronal axons is essential in the dissection of neuron degeneration and regeneration, two processes, which are extensively studied in *C. elegans* (Hall et al., 1997).

Reconstructed data derived from both absorption and fluorescence images can be combined to obtain anatomical information about gene expression patterns. This is illustrated in Figure 24e, which shows a merged brightfield and fluorescence reconstruction of pharyngeal muscle cells expressing GFP in the anterior part of the *C. elegans* body. In addition, as shown in Figure 25, accurate, in silico, 2D sectioning of the specimen as well as for volumetric 3D rendering of specific parts or of the entire animal is possible in this manner (compare Video 2 and Video 3). Coronal, sagittal and transversal sections through the specimen allow retrieval of precise anatomical information down to single cell level. The potential for high-resolution 3D fluorescence imaging coupled with absorption/brightfield-derived anatomical information is critical for analysis of gene expression using fluorescent reporter proteins, in addition to studies of biomolecule co-localization in the context of the whole organism, in vivo.

Moreover, the tomographic setup described here permits fast acquisition of imaging data, which in turn facilitates time-lapse OPT for spatio-temporal representation of changes in morphology, cell positioning, gene expression levels and molecular movement over extended periods of time, in vivo and through the entire animal (4D microscopy/imaging). This is becoming increasingly important for studies of development and ageing. Currently available conventional microscopy methodologies either do not allow, or are not optimized for such applications.

Recording worms with SPIM in a novel microfluidics device

We recently improved the above presented 3D microscopy setup to facilitate SPIM imaging (see Figure 3, Materials and Methods). To allow for SPIM imaging, we added a variety of lasers of different wavelengths, which focus their beams through a prism to create a light sheet that is directed on the specimen (Huisken et al., 2004). Data of the excited plane of the specimen are recorded by the perpendicular placed camera-lens system. The laser beams of the attached lasers can be focused directly on the sample, bypassing the prism (see scheme in Figure 3, Materials and Methods). The software that operates the setup has been updated. In principal, both OPT and SPIM can be applied sequentially to image the same specimen. Also, due to updated operation software, the speed of recording has been increased tremendously. Specimen can be

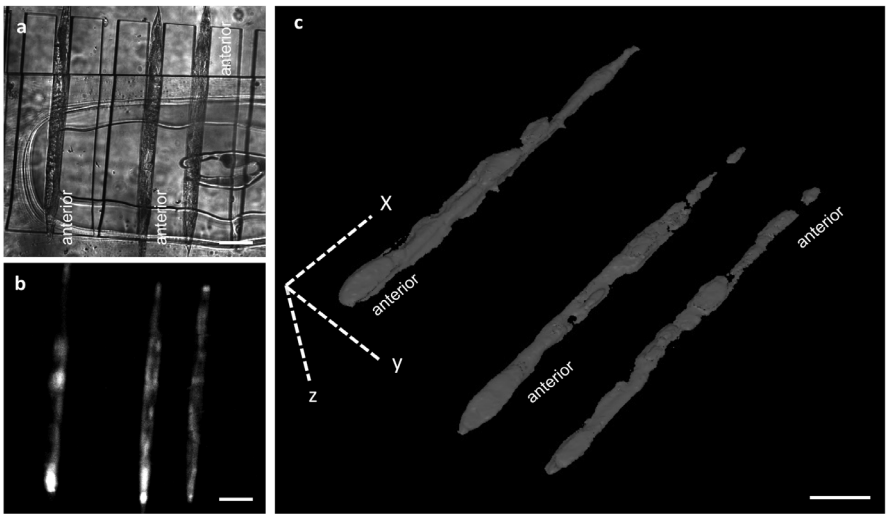

Figure 26: Preliminary results for SPIM based imaging of C. elegans in a microfluidics device. (a) Brightfield image of three animals loaded into the chip. **(b)** Maximum intensity projection of IFE-2::GFP fluorescence of the same worms. **(c)** 3D rendering via Fiji Volume Viewer of the fluorescent information. Signal is detected all along the animals with higher concentration and distribution in the head region (anterior).

scanned in a matter of seconds, depending on the desired resolution and excitation time. Therefore, the system now permits application for both SPIM and OPT recording.

The system is readily combined with a microfluidics device that permits high-throughput OPT and SPIM imaging of *C. elegans* (see Figure 5, Materials and Methods). We adopted previously published microfluidics techniques and designed a novel chip that allows convenient loading and *in vivo* imaging of up to 9 adult worms in parallel (Chronis et al., 2007). The final shape of the chip is cylindrical, which permits imaging from all angles, as beneficial for OPT, and is compatible with SPIM imaging. As for the procedure, animals are anaesthetized with levamisol, loaded into a tubing system that is attached to a syringe, which is then connected to the chip. While pumping the worms into the device, another syringe attached to the outlet applies suction and the animals are placed into chambers that hold them in position for rapid imaging. For unloading, suction/pressure is reversed and animals are recovered and can be grown under favorable conditions until the next imaging time point. This attachment to the microscopy system makes longitudinal imaging studies possible, which is important e.g. when studying changes in fluorescent expression during ageing.

We obtained preliminary data from the novel system that combines microfluidics technology with SPIM imaging. As a prove of principal, we decided to image multiple worms carrying IFE-2::GFP, which is ubiquitously expressed throughout the animals (compare confocal images in Figure 7A). As shown in Figure 26, we loaded several worms into conic chambers of our novel chip and performed rapid SPIM imaging. The ubiquitous fluorescent pattern was successfully detected and we applied simple, openly available reconstruction tools (Fiji, Volume Viewer, see Materials and Methods) to visualize the 3D signal distribution. We are currently applying and fine-tuning the system and experimental procedures. However, the preliminary results prove that the system is readily applicable for longitudinal high-throughput gene expression studies in *C. elegans*. We further note, that the present system is fully adaptable to image various fluorescent signals in other small model organisms.

In summary, we present a simple and cost effective setup that combines two novel imageing techniques SPIM and OPT, which achieve fast 3D imaging of live C. elegans animals at single-cell resolution. The system is highly versatile and configurable for both absorption/brightfield and fluorescence imaging via OPT, with multiple chromophores and fluorophores via SPIM and OPT. By post-acquisition filtering of residual sample movement and spurious drifts we have accomplished visualization of neuronal features, such as single axons and dendrites in vivo. This is not possible with other, previously described OPT implementations. Thus, the system is particularly suited for following neuron and axonal migration during development, as well as neurodegeneration, regeneration and other dynamic phenomena, at microscopic scale. We also note that the system can be adapted for other small model organisms such as Drosophila, other invertebrates, and small marine crustaceans, which have emerged as powerful models for evo-devo studies (Birk et al., 2010).

We have implemented a microfluidics device that allows high-throughput imaging of C. elegans via SPIM and OPT. This device, once fine adjusted for high-resolution imaging, will allow longitudinal gene expression studies by using the same group of individuals, rather than representative animals, for each time point in life. Combining SPIM and OPT data for reconstruction will be addressed in the future and will result in significantly improved quality of 3D images.

References

Alcedo, J., and Kenyon, C. (2004). Regulation of *C. elegans* Longevity by Specific Gustatory and Olfactory Neurons. Neuron 41, 45–55.

Allen, P.B., Sgro, A.E., Chao, D.L., Doepker, B.E., Scott Edgar, J., Shen, K., and Chiu, D.T. (2008). Single-synapse ablation and long-term imaging in live *C. elegans*. Journal of Neuroscience Methods 173, 20–26.

An, J.H., and Blackwell, T.K. (2003). SKN-1 links *C. elegans* mesendodermal specification to a conserved oxidative stress response. Genes and Development 17, 1882–1893.

Anderson, P., and Kedersha, N. (2002). Stressful initiations. Journal of Cell Science 115, 3227–3234.

Anderson, P., and Kedersha, N. (2006). RNA granules. Jcb 172, 803–808.

Anderson, P., and Kedersha, N. (2008). Stress granules: the Tao of RNA triage. Trends in Biochemical Sciences 33, 141–150.

Anderson, P., and Kedersha, N. (2009). RNA granules: post-transcriptional and epigenetic modulators of gene expression. Nat Rev Mol Cell Biol 10, 430–436.

ANDREI, M.A., INGELFINGER, D., HEINTZMANN, R., ACHSEL, T., RIVERA-POMAR, R., and LUHRMANN, R. (2005). A role for eIF4E and eIF4E-transporter in targeting mRNPs to mammalian processing bodies. Rna 11, 717–727.

Antebi, A. (2007). Genetics of Aging in Caenorhabditis elegans. PLoS Genet 3, e129.

Artal-Sanz, M., and Tavernarakis, N. (2009). Prohibitin couples diapause signalling to mitochondrial metabolism during ageing in *C. elegans*. Nature 461, 793–797.

Ashrafi, K., Chang, F.Y., Watts, J.L., Fraser, A.G., Kamath, R.S., Ahringer, J., and Ruvkun, G. (2003). Genome-wide RNAi analysis of Caenorhabditis elegans fat regulatory genes. Nature 421, 268–272.

Assouline, S., Culjkovic, B., Cocolakis, E., Rousseau, C., Beslu, N., Amri, A., Caplan, S., Leber, B., Roy, D.-C., Miller, W.H., et al. (2009). Molecular targeting of the oncogene eIF4E in acute myeloid leukemia (AML): a proof-of-principle clinical trial with ribavirin. Blood 114, 257–260.

Back, P., De Vos, W.H., Depuydt, G.G., Matthijssens, F., Vanfleteren, J.R., and Braeckman, B.P. (2012). Exploring real-time in vivo redox biology of developing and aging Caenorhabditis elegans. Free Radical Biology and Medicine 52, 850–859.

Balagopal, V., and Parker, R. (2009). Polysomes, P bodies and stress granules: states and fates of eukaryotic mRNAs. Current Opinion in Cell Biology 21, 403–408.

Bandiera, S., Rüberg, S., Girard, M., Cagnard, N., Hanein, S., Chrétien, D., Munnich, A., Lyonnet, S., and Henrion-Caude, A. (2011). Nuclear Outsourcing of RNA Interference Components to Human Mitochondria. Plos One 6, e20746.

Bao, Z., Murray, J.I., Boyle, T., Ooi, S.L., Sandel, M.J., and Waterston, R.H. (2006). Automated cell lineage tracing in Caenorhabditis elegans. Proc Natl Acad Sci USA 103, 2707–2712.

Barbee, S.A., Estes, P.S., Cziko, A.-M., Hillebrand, J., Luedeman, R.A., Coller, J.M., Johnson, N., Howlett, I.C., Geng, C., Ueda, R., et al. (2006). Staufen- and FMRP-containing neuronal RNPs are structurally and functionally related to somatic P bodies. Neuron 52, 997–1009.

Bargmann, C.I., and Avery, L. (1995). *C. elegans*: Modern Biological Analysis of an Organism. Methods in Cell Biology.

Beckham, C.J., and Parker, R. (2008). P Bodies, Stress Granules, and Viral Life Cycles. Cell Host & Microbe 3, 206–212.

Beelman, C.A., and Parker, R. (1995). Degradation of mRNA in eukaryotes. Cell 81, 179–183.

Bernstein, P., Peltz, S. W., & Ross, J. (1989). The poly(A)-poly(A)-binding protein complex is a major determi-

nant of mRNA stability in vitro. Molecular and Cellular Biology, 9(2), 659–670.

Bian, Z., Li, L.-M., Tang, R., Hou, D.-X., Chen, X., Zhang, C.-Y., and Zen, K. (2010). Identification of mouse liver mitochondria-associated miRNAs and their potential biological functions. Cell Res 20, 1076–1078.

Birk, U.J., Rieckher, M., Konstantinides, N., Darrell, A., Sarasa-Renedo, A., Meyer, H., Tavernarakis, N., and Ripoll, J. (2010). Correction for specimen movement and rotation errors for *in-vivo* Optical Projection Tomography. Biomed Opt Express 1, 87–96.

Bishop, N.A., and Guarente, L. (2007). Two neurons mediate diet-restriction-induced longevity in *C. elegans*. Nature 447, 545–549.

Bishop, N.A., and Yankner, T.L.B.A. (2010). Neural mechanisms of ageing and cognitive decline. Nature 1–7.

Bloch, D.B., Nobre, R.A., Bernstein, G.A., and YANG, W.-H. (2011). Identification and characterization of protein interactions in the mammalian mRNA processing body using a novel two-hybrid assay. Exp. Cell Res. 317, 2183–2199.

Blumenthal, J., Behar, L., Elliott, E., and Ginzburg, I. (2009). Dcp1a phosphorylation along neuronal development and stress. FEBS Letters 583, 197–201.

Blumenthal, T., Evans, D., Link, C.D., Guffanti, A., Lawson, D., Thierry-Mieg, J., Thierry-Mieg, D., Chiu, W.L., Duke, K., Kiraly, M., et al. (2002). A global analysis of Caenorhabditis elegans operons. Nature 417, 851–854.

Boag, P.R., Atalay, A., Robida, S., Reinke, V., and Blackwell, T.K. (2008). Protection of specific maternal messenger RNAs by the P body protein CGH-1 (Dhh1/RCK) during Caenorhabditis elegans oogenesis. Jcb 1–15.

Boag, P.R., Nakamura, A., and Blackwell, T.K. (2005). A conserved RNA-protein complex component involved in physiological germline apoptosis regulation in *C. elegans*. Development 132, 4975–4986.

Borden, K.L. (2011). Targeting the oncogene eIF4E in cancer: From the bench to clinical trials. Clin Invest Med 34, E315.

Bossé, G.D., Rüegger, S., Ow, M.C., Vasquez-Rifo, A., Rondeau, E.L., Ambros, V.R., Grosshans, H., and Simard, M.J. (2013). The Decapping Scavenger Enzyme DCS-1 Controls MicroRNA Levels in Caenorhabditis elegans. Molecular Cell.

Boyd, L., Guo, S., Levitan, D., Stinchcomb, D.T., and Kemphues, K.J. (1996). PAR-2 is asymmetrically distributed and promotes association of P granules and PAR-1 with the cortex in *C. elegans* embryos. Development 122, 3075–3084.

Braeckman, B.P. (2009). Intermediary metabolism. WormBook 1–24.

Brengues, M., and Parker, R. (2007). Accumulation of Polyadenylated mRNA, Pab1p, eIF4E, and eIF4G with P-Bodies in Saccharomyces cerevisiae. Molecular Biology of the Cell 1–11.

Brengues, M., Teixeira, D., and Parker, R. (2008). Movement of eukaryotic mRNAs between polysomes and cytoplasmic processing bodies. Science 1–9.

Brenner, S. (1974). The genetics of Caenorhabditis elegans. Genetics 77, 71–94.

Brown, C.E., Tarun, S.Z., Boeck, R., and Sachs, A.B. (1996). PAN3 encodes a subunit of the Pab1p-dependent poly(A) nuclease in Saccharomyces cerevisiae. Molecular and Cellular Biology

Bryson-Richardson, R.J., Berger, S., Schilling, T.F., Hall, T.E., Cole, N.J., Gibson, A.J., Sharpe, J., and Currie, P.D. (2007). FishNet: an online database of zebrafish anatomy. BMC Biology 5, 34.

Buchan, J.R., Muhlrad, D., and Parker, R. (2008). P bodies promote stress granule assembly in Saccharomyces cerevisiae. The Journal of Cell Biology 183, 441–455.

Buchan, J.R., and Parker, R. (2009). Eukaryotic Stress Granules: The Ins and Outs of Translation. Molecular Cell 36, 932–941.

Chatterjee, S., and Grosshans, H. (2009). Active turnover modulates mature microRNA activity in Caenorhabditis elegans. Nature 461, 546–549.

Chen, D., Pan, K.Z., Palter, J.E., and Kapahi, P. (2007). Longevity determined by developmental arrest genes in Caenorhabditis elegans. Aging Cell 6, 525–533.

Chiang, W.-C., Ching, T.-T., Lee, H.C., Mousigian, C., and Hsu, A.-L. (2012). HSF-1 regulators DDL-1/2 link insulin-like signaling to heat-shock responses and modulation of longevity. Cell 148, 322–334.

Chokshi, T.V., Bazopoulou, D., and Chronis, N. (2010). An automated microfluidic platform for calcium imaging of chemosensory neurons in Caenorhabditis elegans. Lab Chip 10, 2758–2763.

Chronis, N. (2010). Worm chips: Microtools for *C. elegans* biology. Lab Chip 10, 432.

Chronis, N., Zimmer, M., and Bargmann, C.I. (2007). Microfluidics for in vivo imaging of neuronal and behavioral activity in Caenorhabditis elegans. Nat Meth 4, 727–731.

Chung, K., Crane, M.M., and Lu, H. (2008). Automated on-chip rapid microscopy, phenotyping and sorting of *C. elegans*. Nat Meth 5, 637–643.

Coller, J., and Parker, R. (2004). Eukaryotic mRNA decapping. Annual Review of Biochemistry.

Collins, J.J., Huang, C., Hughes, S., and Kornfeld, K. (2008). The measurement and analysis of age-related changes in Caenorhabditis elegans. WormBook 1–21.

Cookson, M. R. (2011). Aging-RNA in development and disease. Wiley Interdisciplinary Reviews: RNA, 3(1), 133–143. doi:10.1002/wrna.109

Copeland, P.R., and Wormington, M. (2001). The mechanism and regulation of deadenylation: identification and characterization of Xenopus PARN. Rna.

Cougot, N., Bhattacharyya, S.N., Tapia-Arancibia, L., Bordonne, R., Filipowicz, W., Bertrand, E., and Rage, F. (2008). Dendrites of Mammalian Neurons Contain Specialized P-Body-Like Structures That Respond to Neuronal Activation. Journal of Neuroscience 28, 13793–13804.

Cougot N., van Dijk, E., Babajko, S., and Séraphin, B. (2004). “Cap-tabolism.” Trends in Biochemical Sciences 29, 436–444.

Coulson, A., Kozono, Y., Lutterbach, B., Shownkeen, R., Sulston, J., and Waterston, R. (1991). YACs and the *C. elegans* genome. Bioessays 13, 413–417.

Culjkovic, B., Topisirovic, I., and Borden, K.L. (2007). Controlling gene expression through RNA regulons: the role of the eukaryotic translation initiation factor eIF4E. Cell Cycle 6, 65–69.

Culjkovic, B., Topisirovic, I., Skrabanek, L., Ruiz-Gutierrez, M., and Borden, K.L. (2006). eIF4E is a central node of an RNA regulon that governs cellular proliferation. Journal of Cell Biology 1–12.

Culjkovic-Kraljacic, B., Baguet, A., Volpon, L., Amri, A., and Borden, K.L.B. (2012). The oncogene eIF4E reprograms the nuclear pore complex to promote mRNA export and oncogenic transformation. Cell Rep 2, 207–215.

Cypser, J., Henderson, S., and Tedesco, P. (2001). Relationship between increased longevity and stress resistance as assessed through gerontogene mutations in *Caenorhabditis elegans*. Experimental Gerontology

Dahm, R., Kiebler, M., and Macchi, P. (2007). RNA localisation in the nervous system. Semin. Cell Dev. Biol. 18, 216–223.

Dai, C., Whitesell, L., Rogers, A.B., and Lindquist, S. (2013). Heat Shock Factor 1 Is a Powerful Multifaceted Modifier of Carcinogenesis. Cell 1–14.

Dang, Y., Kedersha, N., Low, W.-K., Romo, D., Gorospe, M., Kaufman, R., Anderson, P., and Liu, J.O. (2006). Eukaryotic initiation factor 2alpha-independent pathway of stress granule induction by the natural product pateamine A. The Journal of Biological Chemistry 281, 32870–32878.

Decker, and Parker (2012). P-Bodies and Stress Granules: Possible Roles in the Control of Translation and mRNA Degradation. Perspectives in Biology 1–17.

Decker, C.J., Teixeira, D., and Parker, R. (2007). Edc3p and a glutamine/asparagine-rich domain of Lsm4p function in processing body assembly in Saccharomyces cerevisiae. Journal of Cell Biology 1–13.

Dillman, A. A., Hauser, D. N., Gibbs, J. R., Nalls, M. A., McCoy, M. K., Rudenko, I. N., et al. (2013). mRNA expression, splicing and editing in the embryonic and adult mouse cerebral cortex. Nature neuroscience, 1–9. doi:10.1038/nn.3332

Dimitriadi, M., and Hart, A.C. (2010). Neurodegenerative disorders: Insights from the nematode Caenorhabditis elegans. Neurobiology of Disease 40, 4–11.

Ding, L., Spencer, A., Morita, K., and Han, M. (2005). The developmental timing regulator AIN-1 interacts with miRISCs and may target the argonaute protein ALG-1 to cytoplasmic P bodies in *C. elegans*. Molecular Cell 19, 437–447.

Dong, S., Jacobson, A., and He, F. (2010). Degradation of YRA1 Pre-mRNA in the cytoplasm requires translational repression, multiple modular intronic elements, Edc3p, and Mex67p. Plos Biology 8, e1000360.

Dong, S., Li, C., Zenklusen, D., Singer, R.H., Jacobson, A., and He, F. (2007). YRA1 autoregulation requires nuclear export and cytoplasmic Edc3p-mediated degradation of its pre-mRNA. Molecular Cell 25, 559–573.

Dostie, J., Lejbkowicz, F., and Sonenberg, N. (1999). eIF4E interacts with a shuttling protein. Biochem. Cell Biol. 77, 391.

Draper, B.W., Mello, C.C., Bowerman, B., Hardin, J., and Priess, J.R. (1996). MEX-3 is a KH domain protein that regulates blastomere identity in early *C. elegans* embryos. Cell 87, 205–216.

Dunckley, T. (1999). The DCP2 protein is required for mRNA decapping in Saccharomyces cerevisiae and contains a functional MutT motif. Embo J 18, 5411–5422.

Durieux, J., Wolff, S., and Dillin, A. (2011). The Cell-Non-Autonomous Nature of Electron Transport Chain-Mediated Longevity. Cell.

Edbauer, D., Neilson, J.R., Foster, K.A., and Wang, C.F. (2010). Regulation of synaptic structure and function by FMRP-associated microRNAs miR-125b and miR-132. Neuron.

Eisinger-Mathason, T.S.K., Andrade, J., Groehler, A.L., Clark, D.E., Muratore-Schroeder, T.L., Pasic, L., Smith, J.A., Shabanowitz, J., Hunt, D.F., Macara, I.G., et al. (2008). Codependent functions of RSK2 and the apoptosis-promoting factor TIA-1 in stress granule assembly and cell survival. Molecular Cell 31, 722–736.

Ellis, H. (1986). Genetic control of programmed cell death in the nematode *C. elegans*. Cell 44, 817–829.

Erickson, S.L., and Lykke-Andersen, J. (2011). Cytoplasmic mRNP granules at a glance. Journal of Cell Science 124, 293–297.

Eulalio, A., Behm-Ansmant, I., Schweizer, D., and Izaurralde, E. (2007). P-Body Formation Is a Consequence, Not the Cause, of RNA-Mediated Gene Silencing. Molecular and Cellular Biology 1–12.

Eystathioy, T., Chan, E.K.L., Tenenbaum, S.A., Keene, J.D., Griffith, K., and Fritzler, M.J. (2002). A phosphorylated cytoplasmic autoantigen, GW182, associates with a unique population of human mRNAs within novel cytoplasmic speckles. Molecular Biology of the Cell 1–14.

Farny, N.G., Kedersha, N.L., and Silver, P.A. (2009). Metazoan stress granule assembly is mediated by P-eIF2alpha-dependent and -independent mechanisms. Rna 15, 1814–1821.

Felkai, S. (1999). CLK-1 controls respiration, behavior and aging in the nematode Caenorhabditis elegans. Embo J 18, 1783–1792.

Fenger-Grøn, M., Fillman, C., Norrild, B., and Lykke-Andersen, J. (2005). Multiple processing body factors and the ARE binding protein TTP activate mRNA decapping. Molecular Cell 20, 905–915.

Ferraiuolo, M.A. (2005). A role for the eIF4E-binding protein 4E-T in P-body formation and mRNA decay. The Journal of Cell Biology 170, 913–924.

Fortin, D.A., Srivastava, T., and Soderling, T.R. (2012). Structural modulation of dendritic spines during synaptic plasticity. Neuroscientist 18, 326–341.

Franks, T.M., and Lykke-Andersen, J. (2008). The Control of mRNA Decapping and P-Body Formation. Molecular Cell 32, 605–615.

Fromm, S.A., Truffault, V., Kamenz, J., Braun, J.E., Hoffmann, N.A., Izaurralde, E., and Sprangers, R. (2011). The structural basis of Edc3-and Scd6-mediated activation of the Dcp1: Dcp2 mRNA decapping complex. Embo J 31, 279–290.

Fuchs, S., Bundy, J.G., Davies, S.K., Viney, J.M., Swire, J.S., and Leroi, A.M. (2010). A metabolic signature of long life in Caenorhabditis elegans. BMC Biology 8, 14.

Fujimura, K., Katahira, J., Kano, F., Yoneda, Y., and Murata, M. (2009). Microscopic dissection of the process of stress granule assembly. Biochimica Et Biophysica Acta 1793, 1728–1737.

Gallo, M., and Riddle, D.L. (2010). 2010 Gallo and Riddle - Regulation of metabolism in *C. elegans* longevity. Journal of Biology 1–3.

Gallouzi, I.E., Brennan, C.M., Stenberg, M.G., Swanson, M.S., Eversole, A., Maizels, N., and Steitz, J.A. (2000). HuR binding to cytoplasmic mRNA is perturbed by heat shock. Proc Natl Acad Sci USA 97, 3073–3078.

Garneau, N.L., Wilusz, J., and Wilusz, C.J. (2007). The highways and byways of mRNA decay. Nat Rev Mol Cell Biol 8, 113–126.

Gems, D., and Partridge, L. (2008). Stress-Response Hormesis and Aging: “That which Does Not Kill Us Makes Us Stronger.” Cell Metabolism 7, 200–203.

Ghosh, D., and Seydoux, G. (2008). Inhibition of Transcription by the Caenorhabditis elegans Germline Protein PIE-1: Genetic Evidence for Distinct Mechanisms Targeting Initiation and Elongation. Genetics 178, 235–243.

Gilks, N., Kedersha, N., Ayodele, M., Shen, L., Stoecklin, G., Dember, L.M., and Anderson, P. (2004). Stress granule assembly is mediated by prion-like aggregation of TIA-1. Molecular Biology of the Cell 15, 5383–5398.

Goulet, I., Boisvenue, S., Mokas, S., Mazroui, R., and Côté, J. (2008). TDRD3, a novel Tudor domain-containing protein, localizes to cytoplasmic stress granules. Hum Mol Genet 17, 3055–3074.

Grousl, T., Ivanov, P., Frýdlová, I., Vasicová, P., Janda, F., Vojtová, J., Malínská, K., Malcová, I., Nováková, L., Janosková, D., et al. (2009). Robust heat shock induces eIF2alpha-phosphorylation-independent assembly of stress granules containing eIF3 and 40S ribosomal subunits in budding yeast, Saccharomyces cerevisiae. Journal of Cell Science 122, 2078–2088.

Guedes, S., and Priess, J.R. (1997). The *C. elegans* MEX-1 protein is present in germline blastomeres and is a P granule component. Development 124, 731-739

Hall, D.H., and Russell, R.L. (1991). The posterior nervous system of the nematode Caenorhabditis elegans: serial reconstruction of identified neurons and complete pattern of synaptic interactions. The Journal of Neuroscience.

Hall, D.H., Gu, G., García-Añoveros, J., Gong, L., Chalfie, M., and Driscoll, M. (1997). Neuropathology of Degenerative Cell Death in Caenorhabditis elegans.

Hammell, C.M., Lubin, I., Boag, P.R., Blackwell, T.K., and Ambros, V. (2009). nhl-2 Modulates microRNA activity in Caenorhabditis elegans. Cell 136, 926–938.

Hansen, M., Taubert, S., Crawford, D., Libina, N., Lee, S.-J., and Kenyon, C. (2007). Lifespan extension by conditions that inhibit translation in Caenorhabditis elegans. Aging Cell 6, 95–110.

Harigaya, Y., Jones, B.N., Muhlrad, D., Gross, J.D., and Parker, R. (2010). Identification and Analysis of the Interaction between Edc3 and Dcp2 in Saccharomyces cerevisiae. Molecular and Cellular Biology 30, 1446–1456.

Hariri, F., Arguello, M., Volpon, L., Culjkovic-Kraljacic, B., Holm Nielsen, T., Hiscott, J., Mann, K.K., and Borden, K.L.B. (2013). The eukaryotic translation initiation factor eIF4E is a direct transcriptional target of NF-κB and is aberrantly regulated in Acute Myeloid Leukemia. Leukemia.

Harman, D. (1992). Role of Free Radicals in Aging and Disease. Ann NY Acad Sci 673, 126–141.

Hertweck, M., Hoppe, T., and Baumeister, R. (2003). *C. elegans*, a model for aging with high-throughput capacity. Experimental Gerontology 38, 345–346.

Hipkiss, A.R. (2008). Error-protein metabolism and ageing. Biogerontology 10, 523–529.

Hird, S.N. (1993). Cortical and cytoplasmic flow polarity in early embryonic cells of Caenorhabditis elegans. The Journal of Cell Biology 121, 1343–1355.

Hirokawa, N. (2006). mRNA Transport in Dendrites: RNA Granules, Motors, and Tracks. The Journal of Neuroscience.

Hobert, O. (2003). Behavioral plasticity in *C. elegans*: paradigms, circuits, genes. Journal of Neurobiology 54, 203–223.

Honda, Y., and Honda, S. (1999). The *daf-2* gene network for longevity regulates oxidative stress resistance and Mn-superoxide dismutase gene expression in Caenorhabditis elegans. The FASEB Journal.

Hope, I.A. (1999). *C. elegans*: a practical approach. Oxford University Press.

Houseley, J., & Tollervey, D. (2009). The many pathways of RNA degradation. Cell, 136(4), 763–776. doi:10.1016/j.cell.2009.01.019

Houseley, J., LaCava, J., and Tollervey, D. (2006). RNA-quality control by the exosome. Nat Rev Mol Cell Biol 7, 529–539.

Hoyle, N.P., Castelli, L.M., Campbell, S.G., Holmes, L.E., and Ashe, M.P. (2007). Stress-dependent relocalization of translationally primed mRNPs to cytoplasmic granules that are kinetically and spatially distinct from P-bodies. The Journal of Cell Biology 179, 65–74.

Hsu, A.-L., Murphy, C.T., and Kenyon, C. (2003). Regulation of aging and age-related disease by DAF-16 and heat-shock factor. Science 300, 1142–1145.

Huang, L., Mollet, S., Souquere, S., Le Roy, F., Ernoult-Lange, M., Pierron, G., Dautry, F., and Weil, D. (2011). Mitochondria associate with P-bodies and modulate microRNA-mediated RNA interference. Journal of Biological Chemistry 286, 24219–24230.

Huisken, J. (2012). Slicing embryos gently with laser light sheets. Bioessays 34, 406–411.

Huisken, J., Swoger, J., Del Bene, F., Wittbrodt, J., and Stelzer, E.H.K. (2004). Optical sectioning deep inside live embryos by selective plane illumination microscopy. Science 305, 1007–1009.

Hunt, P.R., Son, T.G., Wilson, M.A., Yu, Q.-S., Wood, W.H., Zhang, Y., Becker, K.G., Greig, N.H., Mattson, M.P., Camandola, S., et al. (2011). Extension of Lifespan in *C. elegans* by Naphthoquinones That Act through Stress Hormesis Mechanisms. Plos One 6, e21922.

Hunt-Newbury, R., Viveiros, R., Johnsen, R., Mah, A., Anastas, D., Fang, L., Halfnight, E., Lee, D., Lin, J., Lorch, A., et al. (2007). High-throughput in vivo analysis of gene expression in Caenorhabditis elegans. Plos Biology 5, e237.

Hüttelmaier, S., Zenklusen, D., Lederer, M., Dictenberg, J., Lorenz, M., Meng, X., Bassell, G.J., Condeelis, J., and Singer, R.H. (2005). Spatial regulation of β-actin translation by Src-dependent phosphorylation of ZBP1. Nat Cell Biol 438, 512–515.

Impey, S., Davare, M., Lasiek, A., Fortin, D., and Ando, H. (2010). An activity-induced microRNA controls dendritic spine formation by regulating Rac1-PAK signaling. Molecular and Cellular Neuroscience.

Ingelfinger, D., Arndt-Jovin, D.J., LUHRMANN, R., and ACHSEL, T. (2002). The human LSm1-7 proteins colocalize with the mRNA-degrading enzymes Dcp1/2 and Xrnl in distinct cytoplasmic foci. Rna 8, 1489–1501.

Ishii, N., Fujii, M., Hartman, P.S., Tsuda, M., Yasuda, K., Senoo-Matsuda, N., Yanase, S., Ayusawa, D., and Suzuki, K. (1998). A mutation in succinate dehydrogenase cytochrome b causes oxidative stress and ageing in nematodes. Nature 394, 694–697.

Ishii, T., Miyazawa, M., and Ishii, P.S.H.N. (2011). Mitochondrial superoxide anion (O2•-) inducible “mev-1” animal models for aging research. BMB Reports 1–8.

Isikman, S.O., Bishara, W., Mavandadi, S., Yu, F.W., Feng, S., Lau, R., and Ozcan, A. (2011). Lens-free optical tomographic microscope with a large imaging volume on a chip. PNAS. Vol. 108, No.18.

Jakubowski, J., and Kornfeld, K. (1999). A Local, High-Density, Single-Nucleotide Polymorphism Map Used to Clone Caenorhabditis elegans cdf-1. Genetics.

Jeong, D.-E., Artan, M., Seo, K., and Lee, S.-J. (2012). Regulation of lifespan by chemosensory and thermosensory systems: findings in invertebrates and their implications in mammalian aging. Front Genet 3, 218.

Jones, A.R., Francis, R., and Schedl, T. (1996). GLD-1, a cytoplasmic protein essential for oocyte differentiation, shows stage-and sex-specific expression during Caenorhabditis elegans germline development. Developmental Biology 180, 165.

Jud, M.C., Czerwinski, M.J., Wood, M.P., Young, R.A., Gallo, C.M., Bickel, J.S., Petty, E.L., Mason, J.M., Little, B.A., Padilla, P.A., et al. (2008). Large P body-like RNPs form in *C. elegans* oocytes in response to arrested ovulation, heat shock, osmotic stress, and anoxia and are regulated by the major sperm protein pathway. Developmental Biology 318, 38–51.

Kahn, N.W., Rea, S.L., Moyle, S., Kell, A., and JOHNSON, T.E. (2008). Proteasomal dysfunction activates the transcription factor SKN-1 and produces a selective oxidative-stress response in Caenorhabditis elegans. Biochem. J. 409, 205.

Kak, A.C., and Slaney, M. (1988). Principles of Computerized Tomographic Imaging. IEEE.

Kalender, W.A. (2006). X-ray computed tomography. Phys. Med. Biol. 51, R29–R43.

Kamath, R.S., Fraser, A.G., Dong, Y., Poulin, G., Durbin, R., Gotta, M., Kanapin, A., Le Bot, N., Moreno, S., Sohrmann, M., et al. (2003). Systematic functional analysis of the Caenorhabditis elegans genome using RNAi. Nature 421, 231–237.

Kanazawa, T., Zappaterra, M.D., Hasegawa, A., Wright, A.P., Newman-Smith, E.D., Buttle, K.F., McDonald, K., Mannella, C.A., and van der Bliek, A.M. (2008). The *C. elegans* Opa1 Homologue EAT-3 Is Essential for Resistance to Free Radicals. PLoS Genet 4, e1000022.

Kauppinen, S., Greenberg, M.E., and Draguhn, A. (2009). A functional screen implicates microRNA-138-dependent regulation of the depalmitoylation enzyme APT1 in dendritic spine morphogenesis. Nature Cell ….

Kawasaki, I., Shim, Y.-H., Kirchner, J., Kaminker, J., Wood, W.B., and Strome, S. (1998). PGL-1, a predicted RNA-binding component of germ granules, is essential for fertility in *C. elegans*. Cell 1–11.

Kayser, E.-B., Morgan, P.G., and Sedensky, M.M. (1999). GAS-1: a mitochondrial protein controls sensitivity to volatile anesthetics in the nematode Caenorhabditis elegans. Anesthesiology 90, 545–554.

Kayser, E.-B., Morgan, P.G., Hoppel, C.L., and Sedensky, M.M. (2001). Mitochondrial expression and function of GAS-1 in Caenorhabditis elegans.

Kedersha, N., and Anderson, P. (2002). Stress granules: sites of mRNA triage that regulate mRNA stability and translatability. Biochemical Society

Kedersha, N., Cho, M.R., Li, W., Yacono, P.W., Chen, S., Gilks, N., Golan, D.E., and Anderson, P. (2000). Dynamic Shuttling of Tia-1 Accompanies the Recruitment of mRNA to Mammalian Stress Granules. The Journal of Cell Biology 151, 1257–1268.

Kedersha, N.L., Gupta, M., Li, W., Miller, I., and Anderson, P. (1999). RNA-binding proteins TIA-1 and TIAR link the phosphorylation of eIF-2α to the assembly of mammalian stress granules.

Kedersha, N., Stoecklin, G., Ayodele, M., Yacono, P., Lykke-Andersen, J., Fritzler, M.J., Scheuner, D., Kaufman, R.J., Golan, D.E., and Anderson, P. (2005). Stress granules and processing bodies are dynamically linked sites of mRNP remodeling. Jcb 169, 871–884.

Kenna, M., Stevens, A., McCammon, M., and Douglas, M.G. (1993). An essential yeast gene with homology to the exonuclease-encoding XRN1/KEM1 gene also encodes a protein with exoribonuclease activity.

Kenyon, C., and Apfeld, J. (1999). Regulation of lifespan by sensory perception in Caenorhabditis elegans. Nature 402, 804–809.

Kenyon, C.J. (2010). The genetics of ageing. Nature Reviews 1–9.

Kenyon, C., Chang, J., Gensch, E., Rudner, A., and Tabtlang, R. (2002). A *C. elegans* mutant that lives twice as long as wild type. Nature 1–4.

Kiebler, M.A., and Bassell, G.J. (2006). Neuronal RNA granules: movers and makers. Neuron 51, 685–690.

Kleemann, G.A., and Murphy, C.T. (2009). The endocrine regulation of aging in Caenorhabditis elegans. Molecular and Cellular Endocrinology 299, 51–57.

Kourtis, N., and Tavernarakis, N. (2011). Cellular stress response pathways and ageing: intricate molecular relationships. Embo J 30, 2520–2531.

Kozlowski, C., Srayko, M., and Nedelec, F. (2007). Cortical microtubule contacts position the spindle in *C. elegans* embryos. Cell 129, 499–510.

Köhrmann, M., Luo, M., Kaether, C., DesGroseillers, L., Dotti, C.G., and Kiebler, M.A. (1999). Microtubule-dependent recruitment of Staufen-green fluorescent protein into large RNA-containing granules and subsequent dendritic transport in living hippocampal neurons. Molecular Biology of the Cell 10, 2945–2953.

Krichevsky, A.M., and Kosik, K.S. (2001). Neuronal RNA GranulesA Link between RNA Localization and Stimulation-Dependent Translation. Neuron 32, 683–696.

Krol, J., Loedige, I., and Filipowicz, W. (2010). The widespread regulation of microRNA biogenesis, function and decay. Nat. Rev. Genet. 11, 597–610.

Kshirsagar, M., and Parker, R. (2004). Identification of Edc3p as an Enhancer of mRNA Decapping in Saccharomyces cerevisiae. Genetics 1–12.

Kumar, A., Gibbs, J. R., Beilina, A., Dillman, A., Kumaran, R., Trabzuni, D., et al. (2013). Age-associated changes in gene expression in human brain and isolated neurons. Neurobiology of aging, 34(4), 1199–1209. doi:10.1016/j.neurobiolaging.2012.10.021

Kuzuoglu-Öztürk, D., Huntzinger, E., Schmidt, S., and Izaurralde, E. (2012). The Caenorhabditis elegans GW182 protein AIN-1 interacts with PAB-1 and subunits of the PAN2-PAN3 and CCR4-NOT deadenylase complexes. Nucleic Acids Research 40, 5651–5665.

Kwon, S., Zhang, Y., and Matthias, P. (2007). The deacetylase HDAC6 is a novel critical component of stress granules involved in the stress response. Genes and Development 21, 3381–3394.

Lakowski, B., and Hekimi, S. (1998). The genetics of caloric restriction in Caenorhabditis elegans. Pnas 1–6.

Lall, S., Piano, F., and Davis, R.E. (2005). Caenorhabditis elegans Decapping Proteins: Localization and Functional Analysis of Dcp1, Dcp2, and DcpS during Embryogenesis. Molecular Biology of the Cell 1–11.

Larance, M., Rowland, A.F., Hoehn, K.L., Humphreys, D.T., Preiss, T., Guilhaus, M., and James, D.E. (2010). Global phosphoproteomics identifies a major role for AKT and 14-3-3 in regulating EDC3. Mol. Cell Proteomics 9, 682–694.

Larimer, F.W., Hsu, C.L., Maupin, M.K., and Stevens, A. (1992). Characterization of the XRN1 gene encoding a 5“→3” exoribonuclease: sequence data and analysis of disparate protein and mRNA levels of gene-disrupted yeast cells. Gene 120, 51–57.

Leacock, S.W., and Reinke, V. (2008). MEG-1 and MEG-2 Are Embryo-Specific P-Granule Components Required for Germline Development in Caenorhabditis elegans. Genetics 178, 295–306.

Lee, K., Avondo, J., Morrison, H., Blot, L., Stark, M., Sharpe, J., Bangham, A., and Coen, E. (2006). Visualizing Plant Development and Gene Expression in Three Dimensions Using Optical Projection Tomography. The Plant Cell, Vol. 18, 2145–2156.

Lee, S.-J., and Kenyon, C. (2009). Regulation of the longevity response to temperature by thermosensory neurons in Caenorhabditis elegans. Current Biology 19, 715–722.

Lenaz, G. (2001). The mitochondrial production of reactive oxygen species: mechanisms and implications in human pathology. IUBMB Life 52, 159–164.

Leung, A.K.L., Calabrese, J.M., and Sharp, P.A. (2006). Quantitative analysis of Argonaute protein reveals microRNA-dependent localization to stress granules. Proc Natl Acad Sci USA 103, 18125–18130.

Li, C., Wu, R.-C., Amazit, L., Tsai, S.Y., Tsai, M.-J., and O'Malley, B.W. (2007). Specific amino acid residues in the basic helix-loop-helix domain of SRC-3 are essential for its nuclear localization and proteasome-dependent turnover. Molecular and Cellular Biology 27, 1296–1308.

Li, W., Simarro, M., Kedersha, N., and Anderson, P. (2004). FAST is a survival protein that senses mitochondrial stress and modulates TIA-1-regulated changes in protein expression. Molecular and Cellular Biology 24, 10718–10732.

Libina, N., Berman, J.R., and Kenyon, A.C. (2003). Tissue-Specific Activities of *C. elegans* DAF-16 in the Regulation of Lifespan. Cell 1–14.

Lin, K. (1997). *daf-16*: An HNF-3/forkhead Family Member That Can Function to Double the Life-Span of Caenorhabditis elegans. Science 278, 1319–1322.

Ling, S.H.M., Decker, C.J., Walsh, M.A., She, M., Parker, R., and Song, H. (2008). Crystal Structure of Human Edc3 and Its Functional Implications. Molecular and Cellular Biology 1–12.

Loschi, M., Leishman, C.C., Berardone, N., and Boccaccio, G.L. (2009). Dynein and kinesin regulate stress-granule and P-body dynamics. Journal of Cell Science 1–10.

Lykke-Andersen, J. (2002). Identification of a Human Decapping Complex Associated with hUpf Proteins in Nonsense-Mediated Decay. Molecular and Cellular Biology.

Maduro, D.P. (1995). Identification and Cloning of Unc-119, a Gene Expressed in the Caenorhabditis Elegans Nervous System. Genetics 141, 977.

Ma, X.M., and Blenis, J. (2009). Molecular mechanisms of mTOR-mediated translational control. Nat Rev Mol Cell Biol 10, 307–318.

Mamane, Y., Petroulakis, E., Rong, L., Yoshida, K., Ler, L.W., and Sonenberg, N. (2004). eIF4E – from translation to transformation. Oncogene 23, 3172–3179.

Matsumoto, K., Minami, M., Shinozaki, F., Suzuki, Y., Abe, K., Zenno, S., Matsumoto, S., and Minami, Y. (2011). Hsp90 is involved in the formation of P-bodies and stress granules. Biochemical and Biophysical Research Communications 407, 720–724.

Mazroui, R., Di Marco, S., Kaufman, R.J., and Gallouzi, I.-E. (2007). Inhibition of the ubiquitin-proteasome system induces stress granule formation. Molecular Biology of the Cell 18, 2603–2618.

Mazroui, R., Sukarieh, R., Bordeleau, M.-E., Kaufman, R.J., Northcote, P., Tanaka, J., Gallouzi, I., and Pelletier, J. (2006). Inhibition of ribosome recruitment induces stress granule formation independently of eukaryotic initiation factor 2alpha phosphorylation. Molecular Biology of the Cell 17, 4212–4219.

McGinty, J., Tahir, K.B., Laine, R., Talbot, C.B., Dunsby, C., Neil, M.A.A., Quintana, L., Swoger, J., Sharpe, J., and French, P.M.W. (2008). Fluorescence lifetime optical projection tomography. J Biophotonics 1, 390–394.

McGinty, J., Taylor, H.B., Chen, L., Bugeon, L., Lamb, J.R., Dallman, M.J., and French, P.M.W. (2011). In vivo fluorescence lifetime optical projection tomography. Biomed Opt Express 2, 1340–1350.

McGurk, L., Morrison, H., Keegan, L.P., Sharpe, J., and O'Connell, M.A. (2007). Three-Dimensional Imaging of Drosophila melanogaster. Plos One 2, e834.

Mello, C.C., and Conte, D. (2004). Revealing the world of RNA interference. Nat Cell Biol 431, 338–342.

Miao, Q., Rahn, J.R., Tourovskaia, A., Meyer, M.G., Neumann, T., Nelson, A.C., and Seibel, E.J. (2009). Dual-modal three-dimensional imaging of single cells with isometric high resolution using an optical projection tomography microscope. J. Biomed. Opt. 14, 064035.

Mokas, S., Mills, J.R., Garreau, C., Fournier, M.J., Robert, F., Arya, P., Kaufman, R.J., Pelletier, J., and Mazroui, R. (2009). Uncoupling Stress Granule Assembly and Translation Initiation Inhibition. Molecular Biology of the Cell 20, 2673–2683.

Montero, H., Rojas, M., Arias, C.F., and López, S. (2008). Rotavirus Infection Induces the Phosphorylation of eIF2alpha but Prevents the Formation of Stress Granules. Journal of Virology 82, 1065–1065.

Mori, I. (1999). GENETICS OF CHEMOTAXIS AND THERMOTAXIS IN THE NEMATODE CAENORHABDITIS ELEGANS. Annu Rev Genet 33, 399–422.

Murakami, S. (2007). Caenorhabditis elegans as a model system to study aging of learning and memory. Mol. Neurobiol. 35, 85–94.

Müller-McNicoll, M., and Neugebauer, K.M. (2013). How cells get the message: dynamic assembly and function of mRNA–protein complexes. Nat. Rev. Genet. 1–13.

Narasimhan, S.D., Yen, K., and Tissenbaum, H.A. (2009). Converging Pathways in Lifespan Regulation. Current Biology 19, R657–R666.

Narayanaswamy, R., Levy, M., Tsechansky, M., Stovall, G.M., O'Connell, J.D., Mirrielees, J., Ellington, A.D., and Marcotte, E.M. (2009). Widespread reorganization of metabolic enzymes into reversible assemblies upon nutrient starvation. Pnas 106, 10147–10152.

Natalizio, B.J., and Wente, S.R. (2013). Postage for the messenger: designating routes for nuclear mRNA export. Trends in Cell Biology 1–9.

Navarro, R.E., and Blackwell, T.K. (2005). Requirement for P granules and meiosis for accumulation of the germline RNA helicase CGH-1. Genesis 1–9.

Nissan, T., Rajyaguru, P., She, M., Song, H., and Parker, R. (2010). Decapping Activators in Saccharomyces cerevisiae Act by Multiple Mechanisms. Molecular Cell 39, 773–783.

Noble, S.L., Allen, B.L., Goh, L.K., Nordick, K., and Evans, T.C. (2008). Maternal mRNAs are regulated by diverse P body-related mRNP granules during early Caenorhabditis elegans development. The Journal of Cell Biology 182, 559–572.

Ntziachristos, V., Tung, C.-H., Bremer, C., and Weissleder, R. (2002). Fluorescence molecular tomography resolves protease activity in vivo. Nat. Med. 8, 757–760.

NYKAMP, K., LEE, M.-H., and KIMBLE, J. (2009). *C. elegans* La-related protein, LARP-1, localizes to germline P bodies and attenuates Ras-MAPK signaling during oogenesis. Rna 1–12.

O'Connell, J.D., Zhao, A., Ellington, A.D., and Marcotte, E.M. (2012). Dynamic Reorganization of Metabolic Enzymes into Intracellular Bodies. Annual Review of Cell and Developmental Biology, Vol. 28: 89-111.

Oeffinger, M., and Zenklusen, D. (2012). To the pore and through the pore: a story of mRNA export kinetics. Biochimica Et Biophysica Acta 1819, 494–506.

Ohn, T., Kedersha, N., Hickman, T., Tisdale, S., and Anderson, P. (2008). A functional RNAi screen links O-GlcNAc modification of ribosomal proteins to stress granule and processing body assembly. Nat Cell Biol 10, 1224–1231.

Olsen, A. (2006). Using Caenorhabditis elegans as a Model for Aging and Age-Related Diseases. Ann NY Acad Sci 1067, 120–128.

Opyrchal, M., Anderson, J.R., Sokoloski, K.J., Wilusz, C.J., and Wilusz, J. (2005). A cell-free mRNA stability assay reveals conservation of the enzymes and mechanisms of mRNA decay between mosquito and mammalian cell lines. Insect Biochem. Mol. Biol. 35, 1321–1334.

Paddock, S.W. (1999). Confocal laser scanning microscopy. BioTechniques 27, 992–6–998–1002–1004.

Pan, C.-L., Peng, C.-Y., Chen, C.-H., and McIntire, S. (2011). Genetic analysis of age-dependent defects of the Caenorhabditis elegans touch receptor neurons. Pnas 108, 9274–9279.

Pan, K.Z., Palter, J.E., Rogers, A.N., Olsen, A., Chen, D., LITHGOW, G.J., and Kapahi, P. (2007). Inhibition of mRNA translation extends lifespan in Caenorhabditis elegans. Aging Cell 6, 111–119.

Panier, T., Romano, S.A., Olive, R., Pietri, T., Sumbre, G., Candelier, R., and Debrégeas, G. (2013). Fast functional imaging of multiple brain regions in intact zebrafish larvae using Selective Plane Illumination Mi-

croscopy. Front Neural Circuits 7, 65.

Pare, J.M., Tahbaz, N., López-Orozco, J., LaPointe, P., Lasko, P., and Hobman, T.C. (2009). Hsp90 regulates the function of argonaute 2 and its recruitment to stress granules and P-bodies. Molecular Biology of the Cell 20, 3273–3284.

Park, S.-K., Tedesco, P.M., and Johnson, T.E. (2009). Oxidative stress and longevity in Caenorhabditis elegans as mediated by SKN-1. Aging Cell 8, 258–269.

Pautler, R.G., and Fraser, S.E. (2003). The year(s) of the contrast agent – micro-MRI in the new millennium. Current Opinion in Immunology 15, 385–392.

Peng, C.-Y., Chen, C.-H., Hsu, J.-M., and Pan, C.-L. (2011). *C. elegans* model of neuronal aging. Communicative & Integrative Biology 4, 696–698.

Pilkington, G.R., and Parker, R. (2008). Pat1 Contains Distinct Functional Domains That Promote P-Body Assembly and Activation of Decapping. Molecular and Cellular Biology 28, 1298–1312.

Rajyaguru, P., and Parker, R. (2009). CGH-1 and the control of maternal mRNAs. Trends in Cell Biology 19, 24–28.

Ramachandran, V., Shah, K.H., and Herman, P.K. (2011). The cAMP-dependent protein kinase signaling pathway is a key regulator of P body foci formation. Molecular Cell 43, 973–981.

Rattan, S.I.S. (2010). Synthesis, Modification and Turnover of Proteins during Aging. In Protein Metabolism and Homeostasis in Aging, (Boston, MA: Springer US), pp. 1–13.

Reeves, G.T., Trisnadi, N., Truong, T.V., Nahmad, M., Katz, S., and Stathopoulos, A. (2012). Dorsal-Ventral Gene Expression in the Drosophila Embryo Reflects the Dynamics and Precision of the Dorsal Nuclear Gradient. Developmental Cell 22, 544–557.

Reines, D. (2012). Decapping Goes Nuclear. Molecular Cell 46, 311–324.

Riddle, D.L., Blumenthal, T., Meyer, B.J., Priess, J.R., Riddle, D.L., Blumenthal, T., Meyer, B.J., and Priess, J.R. (1997). Introduction to *C. elegans* (Cold Spring Harbor (NY): Cold Spring Harbor Laboratory Press).

Rieckher, M., Birk, U.J., Meyer, H., Ripoll, J., and Tavernarakis, N. (2011). Microscopic optical projection tomography in vivo. Plos One 6, e18963.

Rieckher, M., Kourtis, N., Pasparaki, A., and Tavernarakis, N. (2009). Transgenesis in Caenorhabditis elegans. In Methods in Molecular Biology, (Totowa, NJ: Humana Press), pp. 21–39.

Ripoll, J., and Ntziachristos, V. (2004). IMAGING SCATTERING MEDIA FROM A DISTANCE: THEORY AND APPLICATIONS OF NONCONTACT OPTICAL TOMOGRAPHY. Mod. Phys. Lett. B 18, 1403–1431.

Ristow, M., and Schmeisser, S. (2011). Extending life span by increasing oxidative stress. Free Radical Biology and Medicine 51, 327–336.

Robert, V.J.P. (2005). Chromatin and RNAi factors protect the *C. elegans* germline against repetitive sequences. Genes and Development 19, 782–787.

Rohde, C.B., Zeng, F., Gonzalez-Rubio, R., Angel, M., and Yanik, M.F. (2007). Microfluidic system for on-chip high-throughput whole-animal sorting and screening at subcellular resolution. Proceedings of the ….

Rong, L., Livingstone, M., Sukarieh, R., Petroulakis, E., Gingras, A.-C., Crosby, K., Smith, B., Polakiewicz, R.D., Pelletier, J., Ferraiuolo, M.A., et al. (2008). Control of eIF4E cellular localization by eIF4E-binding proteins, 4E-BPs. Rna 14, 1318–1327.

Ross CA, Poirier MA (2005) Opinion: what is the role of protein aggregation in neurodegeneration? Nat Rev Mol Cell Biol 6: 891–898

Salinas, L.S., Maldonado, E., Macías-Silva, M., Blackwell, T.K., and Navarro, R.E. (2007). The DEAD box RNA helicase VBH-1 is required for germ cell function in *C. elegans*. Genesis 45, 533–546.

Samara, C., Rohde, C.B., Gilleland, C.L., Norton, S., Haggarty, S.J., and Yanik, M.F. (2010). Large-scale in vivo femtosecond laser neurosurgery screen reveals small-molecule enhancer of regeneration. Pnas 107,

18342–18347.

Sanduja, S., Blanco, F.F., and Dixon, D.A. (2010). The roles of TTP and BRF proteins in regulated mRNA decay. WIREs RNA 2, 42–57.

Sarma, S., Kerwin, J., Puelles, L., Scott, M., Strachan, T., Feng, G., Sharpe, J., Davidson, D., Baldock, R., and Lindsay, S. (2005). 3D modelling, gene expression mapping and post-mapping image analysis in the developing human brain. Brain Research Bulletin 66, 449–453.

Scheckel, C., Gaidatzis, D., Wright, J.E., and Ciosk, R. (2012). Genome-wide analysis of GLD-1-mediated mRNA regulation suggests a role in mRNA storage. PLoS Genet 8, e1002742.

Schedl, J.K. (1988). Fog-2, a Germ-Line-Specific Sex Determination Gene Required for Hermaphrodite Spermatogenesis in Caenorhabditis Elegans. Genetics 119, 43.

Shamovsky, I., Ivannikov, M., Kandel, E.S., Gershon, D., and Nudler, E. (2006). RNA-mediated response to heat shock in mammalian cells. Nature 440, 556–560.

Schisa, J.A., Pitt, J.N., and Priess, J.R. (2001). Analysis of RNA associated with P granules in germ cells of *C. elegans* adults. Development 1–12.

Schmitz, C., Kinge, P., and Hutter, H. (2007). Axon guidance genes identified in a large-scale RNAi screen using the RNAi-hypersensitive *Caenorhabditis elegans* strain *nre-1(hd20);lin-15b(hd126)*. Proc Natl Acad Sci USA 104, 834–839.

Schnabel, R., Hutter, H., Moerman, D., and Schnabel, H. (1997). Assessing Normal Embryogenesis inCaenorhabditis elegansUsing a 4D Microscope: Variability of Development and Regional Specification. Developmental Biology 184, 234–265.

Schnabel, R., Weigner, C., Hutter, H., Feichtinger, R., and Schnabel, H. (1996). mex-1 and the general partitioning of cell fate in the early*C. elegans* embryo. Mechanisms of Development 54, 133–147.

Schratt, G. (2009). microRNAs at the synapse. Nat Rev Neurosci 10, 842–849.

Schratt, G.M., Tuebing, F., Nigh, E.A., Kane, C.G., Sabatini, M.E., Kiebler, M., and Greenberg, M.E. (2006). A brain-specific microRNA regulates dendritic spine development. Nature 439, 283–289.

Schwartz, D.C., and Parker, R. (1999). Mutations in translation initiation factors lead to increased rates of deadenylation and decapping of mRNAs in Saccharomyces cerevisiae. Molecular and Cellular Biology 19, 5247–5256.

Schwartz, D.C., and Parker, R. (2000). mRNA Decapping in Yeast Requires Dissociation of the Cap Binding Protein, Eukaryotic Translation Initiation Factor 4E. Molecular and Cellular Biology.

Sengupta, M.S., Low, W.Y., Patterson, J.R., Kim, H.M., Traven, A., Beilharz, T.H., Colaiacovo, M.P., Schisa, J.A., and Boag, P.R. (2013). ifet-1 is a broad-scale translational repressor required for normal P granule formation in *C. elegans*. Journal of Cell Science 126, 850–859.

Shah, K.H., Zhang, B., Ramachandran, V., and Herman, P.K. (2012). Processing body and stress granule assembly occur by independent and differentially regulated pathways in S. cerevisiae. Genetics 1–49.

Shan, J., Munro, T.P., Barbarese, E., Carson, J.H., and Smith, R. (2003). A molecular mechanism for mRNA trafficking in neuronal dendrites. Journal of Neuroscience 23, 8859–8866.

Sharpe, J. (2002). Optical Projection Tomography as a Tool for 3D Microscopy and Gene Expression Studies. Science 296, 541–545.

Sharpe, J. (2003). Optical projection tomography as a new tool for studying embryo anatomy. Journal of Anatomy 202, 175–181.

Sharpe, J. (2004). OPTICAL PROJECTION TOMOGRAPHY. Annu. Rev. Biomed. Eng. 6, 209–228.

Sheth, U., and Parker, R. (2003). Decapping and Decay of Messenger RNA Occur in Cytoplasmic Processing Bodies. Science 300, 805–808.

Sheth, U., Pitt, J., Dennis, S., and Priess, J.R. (2010). Perinuclear P granules are the principal sites of mRNA

export in adult *C. elegans* germ cells. Development 137, 1305–1314.

Shimada, M., and Kawahara, H. (2002). Novel family of CCCH-type zinc-finger proteins, MOE-1,-2 and-3, participates in *C. elegans* oocyte maturation. Genes to Cells 7, 933–947.

Shouping Zhu, Di Dong, Birk, U.J., Rieckher, M., Tavernarakis, N., Xiaochao Qu, Jimin Liang, Jie Tian, and Ripoll, J. (2012). Automated Motion Correction for In Vivo Optical Projection Tomography. IEEE Trans Med Imaging 31, 1358–1371.

Simarro, M., Mauger, D., Rhee, K., Pujana, M.A., Kedersha, N.L., Yamasaki, S., Cusick, M.E., Vidal, M., Garcia-Blanco, M.A., and Anderson, P. (2007). Fas-activated serine/threonine phosphoprotein (FAST) is a regulator of alternative splicing. Proc Natl Acad Sci USA 104, 11370–11375.

Simmer, F., Moorman, C., van der Linden, A.M., Kuijk, E., van den Berghe, P.V.E., Kamath, R.S., Fraser, A.G., Ahringer, J., and Plasterk, R.H.A. (2003). Genome-wide RNAi of *C. elegans* using the hypersensitive rrf-3 strain reveals novel gene functions. Plos Biology 1, E12.

Spike, C.A., Bader, J., Reinke, V., and Strome, S. (2008a). DEPS-1 promotes P-granule assembly and RNA interference in *C. elegans* germ cells. Development 135, 983–993.

Spike, C., Meyer, N., Racen, E., Orsborn, A., Kirchner, J., Kuznicki, K., Yee, C., Bennett, K., and Strome, S. (2008b). Genetic Analysis of the Caenorhabditis elegans GLH Family of P-Granule Proteins. Genetics 178, 1973–1987.

Squirrell, J.M., Eggers, Z.T., Luedke, N., Saari, B., Grimson, A., Lyons, G.E., Anderson, P., and White, J.G. (2005). CAR-1, a Protein That Localizes with the mRNA Decapping Component DCAP-1, Is Required for Cytokinesis and ER Organization in Caenorhabditis elegans Embryos. Molecular Biology of the Cell 1–9.

Steffen, K.K., MacKay, V.L., Kerr, E.O., Tsuchiya, M., Hu, D., Fox, L.A., Dang, N., Johnston, E.D., Oakes, J.A., Tchao, B.N., et al. (2008). Yeast Life Span Extension by Depletion of 60S Ribosomal Subunits Is Mediated by Gcn4. Cell 133, 292–302.

Stoecklin, G., Stubbs, T., Kedersha, N., Wax, S., Rigby, W.F., Blackwell, T.K., and Anderson, P. (2004). MK2-induced tristetraprolin:14-3-3 complexes prevent stress granule association and ARE-mRNA decay. Embo J 23, 1313–1324.

Stöhr, N., Lederer, M., Reinke, C., Meyer, S., Hatzfeld, M., Singer, R.H., and Hüttelmaier, S. (2006). ZBP1 regulates mRNA stability during cellular stress. Jcb 175, 527–534.

Strome, S., & Wood, W. B. (1982). Immunofluorescence visualization of germ-line-specific cytoplasmic granules in embryos, larvae, and adults of Caenorhabditis elegans. Proceedings of the National Academy of Sciences of the United States of America, 79(5), 1558–1562.

Strome, S., and Wood, W.B. (1983). Generation of asymmetry and segregation of germ-line granules in early *C. elegans* embryos. Cell 35, 15–25.

Subramaniam, K., and Seydoux, G. (1999). nos-1 and nos-2, two genes related to Drosophila nanos, regulate primordial germ cell development and survival in Caenorhabditis elegans. Development 1–11.

Sulston, J.E., Schierenberg, E., White, J.G., and Thomson, J.N. (1983). The embryonic cell lineage of the nematode Caenorhabditis elegans. Developmental Biology 100, 64–119.

Sun, Y., Yang, P., Zhang, Y., Bao, X., Li, J., Hou, W., Yao, X., Han, J., and Zhang, H. (2011). A genome-wide RNAi screen identifies genes regulating the formation of P bodies in *C. elegans* and their functions in NMD and RNAi. Protein Cell 2, 918–939.

Suswam, E.A., Li, Y.Y., Mahtani, H., and King, P.H. (2005). Novel DNA-binding properties of the RNA-binding protein TIAR. Nucleic Acids Research.

Suzuki, Y., Minami, M., Suzuki, M., Abe, K., Zenno, S., Tsujimoto, M., Matsumoto, K., and Minami, Y. (2009). The Hsp90 inhibitor geldanamycin abrogates colocalization of eIF4E and eIF4E-transporter into stress granules and association of eIF4E with eIF4G. Journal of Biological Chemistry 284, 35597–35604.

Swisher, K.D., and Parker, R. (2010). Localization to, and Effects of Pbp1, Pbp4, Lsm12, Dhh1, and Pab1 on

Stress Granules in Saccharomyces cerevisiae. Plos One.

Swoger, J., Muzzopappa, M., López-Schier, H., and Sharpe, J. (2011). 4D retrospective lineage tracing using SPIM for zebrafish organogenesis studies. J Biophotonics 4, 122–134.

Syntichaki, P., Troulinaki, K., and Tavernarakis, N. (2007). eIF4E function in somatic cells modulates ageing in Caenorhabditis elegans. Nature 445, 922–926.

Tank, E.M.H., Rodgers, K.E., and Kenyon, C. (2011). Spontaneous Age-Related Neurite Branching in Caenorhabditis elegans. Journal of Neuroscience 31, 9279–9288.

Tavernarakis, N., and Driscoll, M. (2002). Caloric restriction and lifespan: a role for protein turnover? Mechanisms of Ageing and Development 123, 215–229.

Tavernarakis, N., Wang, S.L., Dorovkov, M., Ryazanov, A., and Driscoll, M. (2000). Heritable and inducible genetic interference by double-stranded RNA encoded by transgenes. Nat Genet 24, 180–183.

Tavernarakis, N. (2008). Ageing and the regulation of protein synthesis: a balancing act? Trends in Cell Biology 1–8.

Teixeira, D., Sheth, U., VALENCIA-SANCHEZ, M.A., Brengues, M., and Parker, R. (2005). Processing bodies require RNA for assembly and contain nontranslating mRNAs. Rna 1–12.

Tenenhaus, C., Schubert, C., and Seydoux, G. (1998). Genetic Requirements for PIE-1 Localization and Inhibition of Gene Expression in the Embryonic Germ Lineage ofCaenorhabditis elegans. Developmental Biology 200, 212–224.

Tharun, S. (2009). Lsm1-7-Pat1 complex - A link between 3 and 5-ends in mRNA decay. RNA Biology 1–5.

Tharun, S., He, W., Mayes, A.E., Lennertz, P., and Parker, J.D.B.R. (2000). Yeast Sm-like proteins function in mRNA decapping and decay. Nature 1–4.

Topisirovic, I., Siddiqui, N., Lapointe, V.L., Trost, M., Thibault, P., Bangeranye, C., Piñol-Roma, S., and Borden, K.L.B. (2009). Molecular dissection of the eukaryotic initiation factor 4E (eIF4E) export-competent RNP. Embo J 28, 1087–1098.

Toth, M.L., Melentijevic, I., Shah, L., Bhatia, A., Lu, K., Talwar, A., Naji, H., Ibanez-Ventoso, C., Ghose, P., Jevince, A., et al. (2012). Neurite sprouting and synapse deterioration in the aging Caenorhabditis elegans nervous system. Journal of Neuroscience 32, 8778–8790.

Tritschler, F., Braun, J.E., Eulalio, A., Truffault, V., Izaurralde, E., and Weichenrieder, O. (2010). Structural Basis for the Mutually Exclusive Anchoring of P Body Components EDC3 and Tral to the DEAD Box Protein DDX6/Me31B. Molecular Cell 33, 661–668.

Tritschler, F., Eulalio, A., Truffault, V., Hartmann, M.D., Helms, S., Schmidt, S., Coles, M., Izaurralde, E., and Weichenrieder, O. (2007). A Divergent Sm Fold in EDC3 Proteins Mediates DCP1 Binding and P-Body Targeting. Molecular and Cellular Biology 1–12.

Troulinaki, K., and Tavernarakis, N. (2011). Endocytosis and intracellular trafficking contribute to necrotic neurodegeneration in *C. elegans*. Embo J 31, 654–666.

Tudisca, V., Recouvreux, V., Moreno, S., Boy-Marcotte, E., Jacquet, M., and Portela, P. (2010). Differential localization to cytoplasm, nucleus or P-bodies of yeast PKA subunits under different growth conditions. European Journal of Cell Biology 89, 339–348.

Tullet, J.M.A., Hertweck, M., An, J.H., Baker, J., Hwang, J.Y., Liu, S., Oliveira, R.P., Baumeister, R., and Blackwell, T.K. (2008). Direct Inhibition of the Longevity-Promoting Factor SKN-1 by Insulin-like Signaling in *C. elegans*. Cell 132, 1025–1038.

Updike, D., and Strome, S. (2010). P granule assembly and function in Caenorhabditis elegans germ cells. J. Androl. 31, 53–60.

Vellai, T., Takács-Vellai, K., Zhang, Y., Kovacs, A.L., Orosz, L., and Muller, F. (2003). Genetics: influence of TOR kinase on lifespan in *C. elegans*. Nature 426, 620.

Vinegoni, C., Pitsouli, C., Razansky, D., Perrimon, N., and Ntziachristos, V. (2007). In vivo imaging of Drosophila melanogaster pupae with mesoscopic fluorescence tomography. Nat Meth 5, 45–47.

Voronina, E., Seydoux, G., Sassone-Corsi, P., and Nagamori, I. (2011). RNA granules in germ cells. Cold Spring Harb Perspect Biol 3.

Walhout, A.J., Boulton, S.J., and Vidal, M. (2000). Yeast two-hybrid systems and protein interaction mapping projects for yeast and worm. Yeast 17, 88–94.

Wang, G., and Reinke, V. (2008). A *C. elegans* Piwi, PRG-1, Regulates 21U-RNAs during Spermatogenesis. Current Biology 18, 861–867.

Wang, J., Robida-Stubbs, S., Tulleta, J.M.A., Rual, J.-F.O., Vidal, M., and Blackwell, T.K. (2010). RNAi Screening Implicates a SKN-1–Dependent Transcriptional Response in Stress Resistance and Longevity Deriving from Translation Inhibition. PLoS Genet 1–17.

Waterston, R., and Sulston, J. (1995). The genome of *Caenorhabditis elegans*. Proc Natl Acad Sci USA 92, 10836–10840.

White, J.G., Southgate, E., Thomson, J.N., and Brenner, S. (1976). The structure of the ventral nerve cord of *Caenorhabditis elegans*.

White, J.P., and Lloyd, R.E. (2012). Regulation of stress granules in virus systems. Trends in Microbiology 20, 175–183.

Wiederhold, K., and Passmore, L.A. (2010). Cytoplasmic deadenylation: regulation of mRNA fate. Biochem. Soc. Trans 38, 1531.

Wilczynska, A., Aigueperse, C., Kress, M., Dautry, F., and Weil, D. (2005). The translational regulator CPEB1 provides a link between dcp1 bodies and stress granules. Journal of Cell Science 118, 981–992.

Wong, D., Bazopoulou, D., Pujol, N., Tavernarakis, N., and Ewbank, J.J. (2007). Genome-wide investigation reveals pathogen-specific and shared signatures in the response of Caenorhabditis elegans to infection. Genome Biology 8, R194.

Wu, Y., Ghitani, A., Christensen, R., Santella, A., Du, Z., Rondeau, G., Bao, Z., Colón-Ramos, D., and Shroff, H. (2011). Inverted selective plane illumination microscopy (iSPIM) enables coupled cell identity lineaging and neurodevelopmental imaging in Caenorhabditis elegans. Proc Natl Acad Sci USA 108, 17708–17713.

Xia, Y., and Whitesides, G.M. (1998). SOFT LITHOGRAPHY. Annu. Rev. Mater. Sci. 28, 153–184.

Yamashita, A., Chang, T.-C., Yamashita, Y., Zhu, W., Zhong, Z., Chen, C.-Y.A., and Shyu, A.-B. (2005). Concerted action of poly(A) nucleases and decapping enzyme in mammalian mRNA turnover. Nature Structural and Molecular Biology 12, 1054–1063.

Yang, F., Peng, Y., Murray, E.L., Otsuka, Y., Kedersha, N., and Schoenberg, D.R. (2006). Polysome-bound endonuclease PMR1 is targeted to stress granules via stress-specific binding to TIA-1. Molecular and Cellular Biology 26, 8803–8813.

Yang, W., and Hekimi, S. (2010). A Mitochondrial Superoxide Signal Triggers Increased Longevity in Caenorhabditis elegans. Plos Biology 8, e1000556.

Yu, C., York, B., Wang, S., Feng, Q., Xu, J., and O'Malley, B.W. (2007). An essential function of the SRC-3 coactivator in suppression of cytokine mRNA translation and inflammatory response. Molecular Cell 25, 765–778.

Zalfa, F., ACHSEL, T., and Bagni, C. (2006). mRNPs, polysomes or granules: FMRP in neuronal protein synthesis. Current Opinion in Neurobiology 16, 265–269.

Zeitelhofer, M., Karra, D., Macchi, P., Tolino, M., Thomas, S., Schwarz, M., Kiebler, M., and Dahm, R. (2008a). Dynamic Interaction between P-Bodies and Transport Ribonucleoprotein Particles in Dendrites of Mature Hippocampal Neurons. Journal of Neuroscience 28, 7555–7562.

Zeitelhofer, M., Macchi, P., and Dahm, R. (2008b). Perplexing bodies - The putative roles of P-bodies in neurons. RNA Biology 1–5.

Zhang, H.L., Pan, F., Hong, D., Shenoy, S.M., Singer, R.H., and Bassell, G.J. (2003). Active Transport of the Survival Motor Neuron Protein and the Role of Exon-7 in Cytoplasmic Localization. The Journal of ….

Zhang, L., Ding, L., Cheung, T.H., Dong, M.-Q., Chen, J., Sewell, A.K., Liu, X., Yates 3rd, J.R., and Han, M. (2007). Systematic identification of *C. elegans* miRISC proteins, miRNAs, and mRNA targets by their interactions with GW182 proteins AIN-1 and AIN-2. Molecular Cell 28, 598.

Zhang, P., Judy, M., Lee, S.-J., and Kenyon, C. (2013). Direct and Indirect Gene Regulation by a Life-Extending FOXO Protein in *C. elegans*: Roles for GATA Factors and Lipid Gene Regulators. Cell Metabolism 17, 85–100.

Zhang, T., Delestienne, N., Huez, G., Kruys, V., and Gueydan, C. (2005). Identification of the sequence determinants mediating the nucleo-cytoplasmic shuttling of TIAR and TIA-1 RNA-binding proteins.

Zhang, Y., Shao, Z., Zhai, Z., Shen, C., and Powell-Coffman, J.A. (2009). PLOS ONE: The HIF-1 Hypoxia-Inducible Factor Modulates Lifespan in *C. elegans*. Plos One.

Zhu, H., Hasman, R. A., Barron, V. A., Luo, G., & Lou, H. (2006). A nuclear function of Hu proteins as neuron-specific alternative RNA processing regulators. Molecular Biology of the Cell, 17(12), 5105–5114. doi:10.1091/mbc.E06-02-0099

Zid, B.M., Rogers, A.N., Katewa, S.D., Vargas, M.A., Kolipinski, M.C., Lu, T.A., Benzer, S., and Kapahi, P. (2009). 4E-BP Extends Lifespan upon Dietary Restriction by Enhancing Mitochondrial Activity in Drosophila. Cell 139, 149–160.


Age is an issue of mind over matter.
If you don't mind, it doesn't matter.
Mark Twain
Komos beach, Crete